OCS Study
BOEMRE 2010-046

Multicomponent and Multifrequency Seismic for Assessment of Fluid-Gas Expulsion Geology and Gas-Hydrate Deposits: Gulf of Mexico

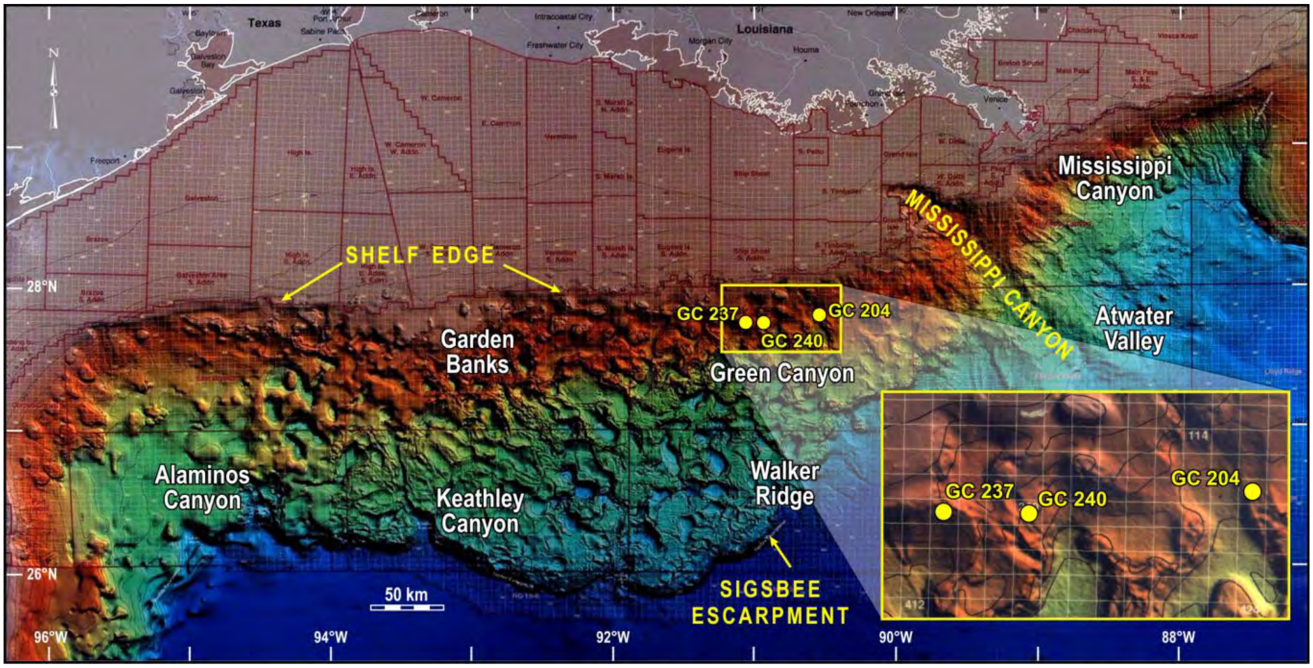

U.S. Department of the Interior
Bureau of Ocean Energy Management,
Regulation and Enforcement
Gulf of Mexico OCS Region

OCS Study
BOEMRE 2010-046

Multicomponent and Mutifrequency Seismic for Assessment of Fluid-Gas Expulsion Geology and Gas-Hydrate Deposits: Gulf of Mexico Hydrates

Authors

B.A. Hardage
H.H. Roberts

Prepared under BOEMRE Cooperative Agreement
1435-01-05-CA-39076 (M05AC12295)
by
Louisiana State University
Coastal Marine Institute
Baton Rouge, Louisiana 70803

Published by

U.S. Department of the Interior
Bureau of Ocean Energy Management, Regulation and Enforcement
Gulf of Mexico OCS Region

New Orleans
December 2010

DISCLAIMER

This report was prepared under contract between the Bureau of Ocean Energy Management, Regulation and Enforcement (BOEMRE), and the Coastal Marine Institute at Louisiana State University. This report has been technically reviewed by the BOEMRE, and it has been approved for publication. Approval does not signify that the contents necessarily reflect the views and policies of BOEMRE, nor does mention of trade names or commercial products constitute endorsement or recommendation for use. It is, however, exempt from review and compliance with the BOEMRE editorial standards.

REPORT AVAILABILITY

This report is available only in compact disc format from the Bureau of Ocean Energy Management, Regulation and Enforcement, Gulf of Mexico OCS Region, at a charge of $15.00, by referencing OCS Study BOEMRE 2010-046. The report may be downloaded from the BOEMRE website through the Environmental Studies Program Information System (ESPIS). You will be able to obtain this report also from the National technical Information Service in the near future. Here are the addresses. You may also inspect copies at selected Federal Depository Libraries.

Bureau of Ocean Energy Management,
Regulation and Enforcement
Gulf of Mexico OCS Region
Public Information Office(MS 5034)
1201 Elmwood Park Boulevard
New Orleans, Louisiana 70123-2394
Telephone requests may be placed at
(504) 736-2519, 1-800-200-GULF, or
Rush Orders: 1-800-553-6847
Fax: (504) 736-2620

U.S. Department of Commerce
National Technical Information Service
5285 Port Royal Road
Springfield, Virginia 22161
Phone: (703) 605-6040
Fax: (703) 605-6900
Email: bookstore@ntis.gov

CITATION

Suggested citation:

Hardage, B.A. and H.H. Roberts. 2010. Multicomponent and multifrequency seismic for assessment of fluid-gas expulsion geology and gas-hydrate deposits: Gulf of Mexico. U. S. Dept. of the Interior, Bureau of Ocean Energy Management, Regulation and Enforcement, Gulf of Mexico OCS Region, New Orleans, LA. OCS Study BOEMRE 2010-046. 112 pp.

ABOUT THE COVER

A computer-enhanced multibeam bathymetry image of the northern Gulf of Mexico continental slope illustrating the complex surface morphology representing intraslope basins where sediments have accumulated to great thicknesses separated by rough-appearing salt –supported domes and ridges.

ACKNOWLEDGMENTS

We primarily acknowledge the Minerals Management Service (MMS) for financial support of this study which focuses a new seismic data set (4C-OBS) data) on the interpretation of gas hydrate-bearing strata. The 4C-OBC seismic data were provided for this research by WesternGeco under the present contract and Cooperative Agreement between MMS and the Coastal Studies Institute at Louisiana State University (Cooperative Agreement Number M05AC12295). C&C Technologies was subcontracted to provide AUV data along 4C-OBC lines and over critical study sites. Manned submersible time over GC 204 and GC 237 was provided by both MMS, NOAA-NURP, The Louisiana Education Quality Support Fund, and the Gulf of Mexico Hydrate Research Consortium at the University of Mississippi over the span of several projects.

TABLE OF CONTENTS

LIST OF FIGURES

LIST OF TABLES

1. INTRODUCTION

The northern Gulf of Mexico continental slope is a well-documented province where fluids and gases migrate to the modern seafloor at numerous sites. Many of these sites are accompanied by exposed gas hydrate deposits. Migration pathways and gas hydrates have been difficult to image because of the presence of bubble-phase gas and very complex geology (the product of a dynamic interaction between sedimentary loading and salt deformation). In the complex geology of the northern Gulf's hydrate stability zone there are very few reflection events that can be interpreted as bottom simulating reflectors (BSRs). These BSR's generally represent the phase change between gas hydrate and free gas at the base of the hydrate stability zone, but they are difficult to identify in existing p-wave seismic data sets from the northern Gulf. In simple geologic settings, BSRs clearly cut across subsurface stratigraphy. However, as the geologic complexity of the subsurface increases, BSRs become more difficult to identify and trace. Even though the entire continental slope is covered with high quality 3D-seismic, migration pathways for fluids and gases, as well as gas hydrates, are not well-imaged and details of these features have generally alluded geoscientists.

This study provides an unparalleled research opportunity to employ a new multi-component seismic data set collected from across a large area of the northern Gulf of Mexico's upper continental slope (to a depth of 1000 m). These data were acquired to provide a new imaging capability. WesternGeco has collected the long offset multi-component seismic data (four-component ocean bottom cable seismic, 4C-OBC) from which both shear wave and conventional compressional wave (p-wave) data can be derived. Not only will this long offset 4C-OBC data allow deeper imaging within the sediment column, but the c-wave data (up-going SV shear wave created by p-to-SV mode conversion) made possible with this acquisition strategy images through gas and image different stratal surfaces and boundaries, unlike standard p-wave data. In addition, lithofacies data, as well as shear moduli and bulk moduli, can be calculated from 4C-OBC data. We therefore consider this research to be a great opportunity to image migration pathways from the deep subsurface and to provide stratal information that can help define the base of the hydrate stability zone and properties of sediments invaded by gas hydrate. Analysis of 4C-OBC data also provides us with a means to assess c-wave data, with a focus on cross-over information that may be important for interpreting p-wave data of various frequency contents (8-100 Hz 3D-seismic to 2-8 kHz). Three test sites were established, based on relative fluid-gas expulsion rates: slow flux, intermediate flux, and rapid flux. These qualitative classes of flux rate are based on geologic response at the modern seafloor. The three study sites are located in the Green Canyon lease area in lease blocks 204, 237, and 240 (Figure 1). Seismic profiles with three different frequency contents were collected along common track-lines across each experimental site. One of these three seismic types was 4C-OBC data. The others are standard exploration-scale 3D-seismic and much higher frequency "chirp sonar" subbottom data. The c-wave data from the 4C-OBC data provide valuable new insight critical for resource evaluation in the case of gas hydrates and imaging of fault systems necessary for constructing realistic numerical models of fluid and gas migration from the deep subsurface. In addition, critical geologic differences between slow flux to rapid flux settings may be revealed. Linking very high resolution images of the shallow subsurface using AUV and chirp technology with the 4C-OBC data is one goal of this investigation.

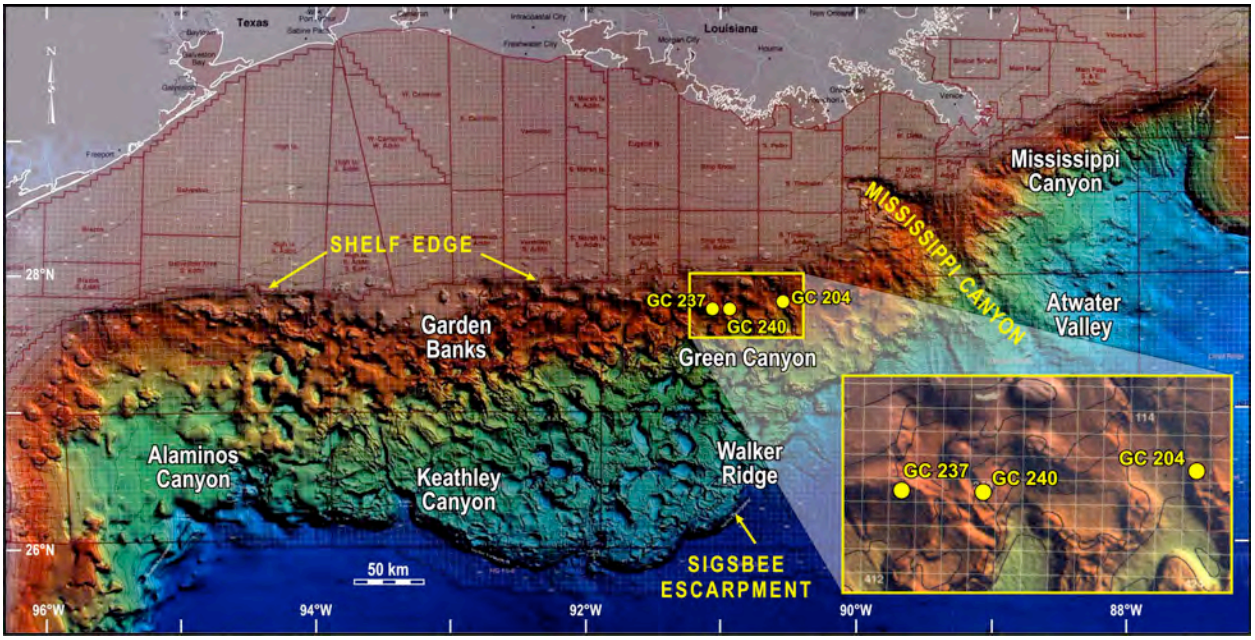

Figure 1. A computer-enhanced multibeam bathymetry image of the northern Gulf of Mexico continental slope illustrating the complex surface morphology representing intraslope basins (smooth areas) where sediments have accumulated to great thicknesses separated by rough-appearing salt-supported domes and ridges. The three study sites in the Green Canyon lease area (GC 204, GC 237, and GC 240) are shown both on the large-scale image and in the enlarged inset that illustrates local seafloor topography associated with each site.

The use of 4C-OBC data for the study of gas hydrates in conjunction with other sources of seismic data associated with this study has led to a variety of scientific papers by the authors and their associates including (a) defining the “seismic target;” (b) geologic expressions of gas hydrate at or near the seafloor; and, (c) rock physics of hydrate-bearing sediments. These published papers, which are largely the products of research conducted under the canopy of this MMS-sponsored project, are summarized in this final report, and included in this report as Appendices A-F.

This report discusses the unique value of multicomponent seismic data to study and interpret detailed shallow subsurface geology, including the seismic characteristics and rock physics of gas hydrate-bearing strata in this part of the sedimentary section. When processed using the special techniques described in this report, PP (compressional) and PS (converted-shear) images derived from 4C-OBC data are nearly comparable to images generated from much higher frequency and higher resolution seismic sources such as “chirp sonar,” a dataset used in this study and acquired by an autonomous underwater vehicle (AUV).

Autonomous Underwater Vehicle (AUV) technology has become invaluable for studying deep-water seafloor properties. An AUV system uses inertial guidance to steer an unmanned, self-propelled vehicle along a preselected route at a height of about 50 m above the seafloor. Navigation accuracy is precise, with deviations from a preprogrammed profile on the order of 1 or 2 m over a traverse of one lease block (4,800 m; 3 mi). AUV data consist of side-scan sonar, multibeam bathymetry, and chirp-sonar profiles. These datasets are commonly used by industry for geohazards assessments and site evaluations of production platforms and pipelines. Chirp-sonar data were important in this study because these profiles provided high-resolution P-P images of seafloor strata to sub-seafloor depths of approximately 50 m. Approximately 80 km of AUV data were amassed across the project study areas. Because one of our research objectives was to compare the relative merits of multi-frequency seismic data and multicomponent seismic data to study deep-water hydrate systems, these AUV profiles were juxtaposed to 4-component ocean-bottom-cable (4C OBC) profiles where low-frequency (10-200 Hz) seismic data and converted-shear (P-SV) seismic data could be compared with high-frequency (1-10 kHz) AUV compressional-wave (P-P) data and with low-frequency (10-200 Hz) OBC P-P data (Appendix B). All datasets were focused on building a better understanding of gas hydrate deposits in Gulf of Mexico sediments and the geologic characteristics of the gas hydrate stability zone.

Maps illustrating where AUV and OBC profiles traversed the two primary study sites (GC 204 and GC 237) and our secondary site (GC 240) are displayed as Figure 2. An important research finding was that low-frequency (10-150 Hz) OBC P-SV data resolved an interface that was sometimes less than 1 m below the seafloor in the vicinity of these two deep-water expulsion features; whereas, high-frequency (1-10 kHz) AUV P-P data generated only 40 meters above the seafloor often did not image this horizon. Examples of these data behaviors are shown by horizons labeled A, B, C, D on the profiles displayed in the following section of this report. As shown by these data, low-frequency, surface-source OBC P-SV data resolve some near-seafloor geologic features local to expulsion features (for example, horizon A) better than do high-frequency, near-seafloor-source AUV P-P data, which is an important technology demonstration.

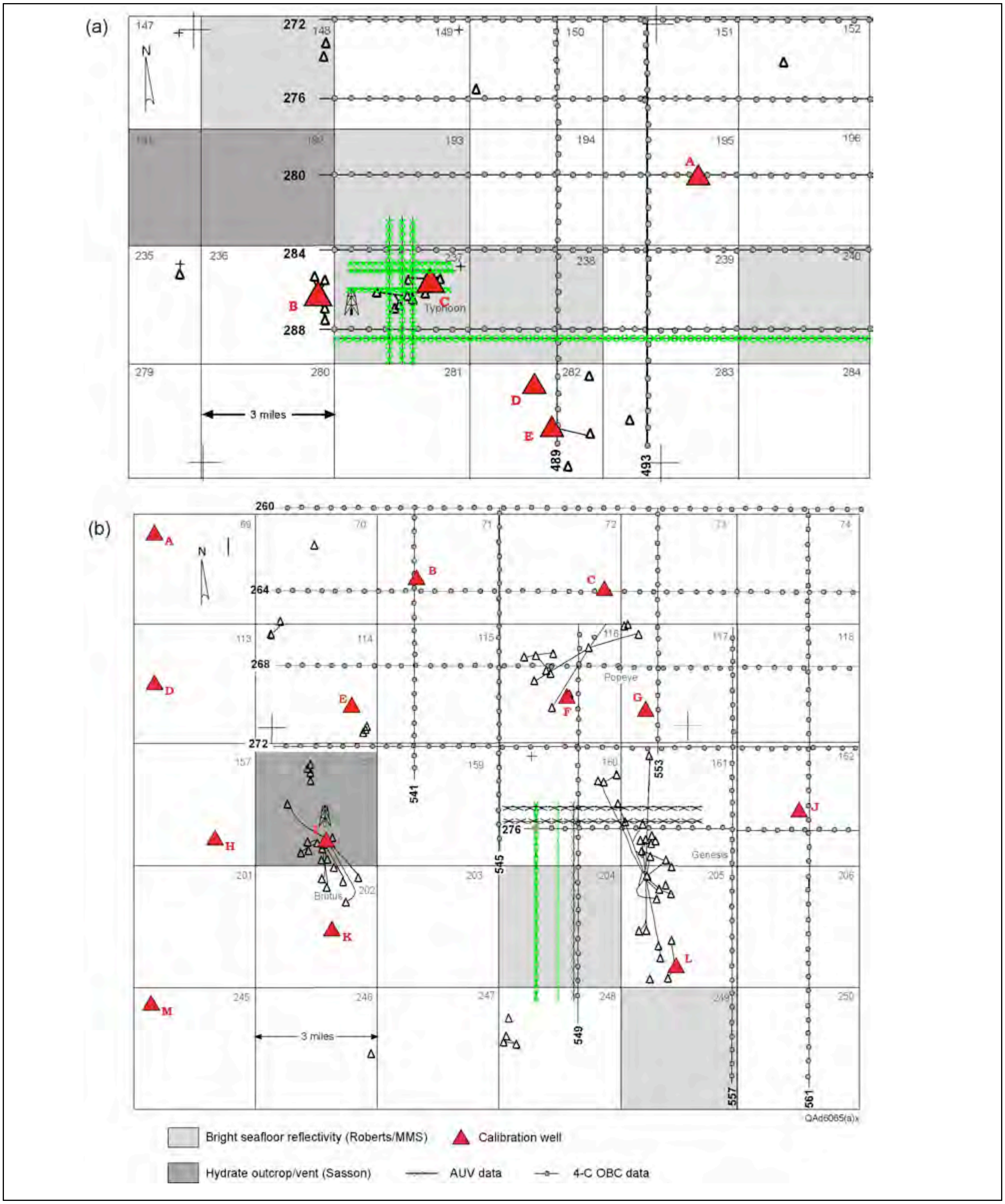

Figure 2. Locations of AUV and OBC profiles used in the project. (a) Typhoon Field area. (b) Genesis Field area. Expulsion features are present in Typhoon-area Blocks 237 and 240 (a) and in Genesis-area Block 204 (b).

2. GEOLOGIC FRAMEWORK

The data collection sites for this project are in the Green Canyon lease area of the upper continental slope opposite the state of Louisiana. Our geologic knowledge of this region, as well as the rest of the continental slope, is largely a result of data collected in support of the search for and production of hydrocarbons. Deep water data collection significantly advanced when the petroleum industry moved onto the Gulf's continental slope in the 1970s. The oil and gas industry has assembled an enormous database of high quality 3D-seismic grids, well data, and high resolution acoustic data used for pipeline and geohazards studies. No other deepwater area in today's oceans has the density of data coverage to compare with the northern Gulf of Mexico. In the case of 3D-seismic data, the continental slope is almost totally covered from the slope off the east Texas coast at the western extreme to DeSoto Canyon at the eastern boundary. The computer enhanced multibeam image of Figure 1 illustrates the complex morphology of the slope surface shaped by salt deformation as a product of sediment loading. The resultant regional morphology of the seafloor is that of rather smooth intraslope basins bordered by rough and relatively high relief ridges and domes supported by salt in the shallow subsurface.

Evolution of the slope's surface geology and present morphology is related to the history of allochthonous salt, faults, and the development of intraslope sedimentary basins. Seismic profiles and well data (various types of well logs and associated micropaleontological data) provide the main elements to evaluate the evolving depositional environments, sedimentary facies, and salt characteristics. Some authors have produced sequential structural restorations from these types of data sets (Worrall and Snelson 1989; Diegel et al. 1995; Peel et al. 1995; Rowan 1995; and McBride 1995). Such reconstructions help explain the evolution of salt structures coincident with sedimentation. This recently developed understanding of the dynamic changes that have taken place through time to give us the present slope configuration is possible because of improved seismic imaging technology (Ratcliff 1993), better physical modeling of salt-sediment systems (Vendeville and Jackson 1992), and the application of sequential restoration (McBride 1996). Such innovative and new-generation work on the slope has shown us that tabular allochthonous salt sheets and nappes are not new to the slope, but have occurred previously and have undergone various stages of deformation and evacuation (Diegel and Cook 1990). The emplacement and eventual evacuation of allochthonous salt appears to vary spatially and temporally throughout the northern Gulf of Mexico basin. No single model for salt movement can explain the array of salt geometries presently imaged in the subsurface. However, it is clear that original salt geometries and the manner in which they interact dictate the positions of later minibasins, remnant salt diapirs, extensional growth faults, contractional structures, and strike-slip deformations (McBride 1996). It is clear that this framework, provided by salt deformation and sediment loading, is the template for understanding the complexities of the modern seafloor and the pathways for fluid and gas migration from the deep subsurface.

In addition to the 3D-seismic data that led to the understanding of the slope's subsurface geology and regional surface morphology, higher resolution data sets have provided a detailed view of the modern sea floor. These data sets have been acquired for engineering and regulatory purposes related to choosing drilling sites, pipeline routes, platform locations, and for identifying potential geohazards. High resolution subbottom profiles, side-scan sonar swaths, and multibeam bathymetry are the key data sets used for engineering and geohazards purposes. These data have revealed a spectrum of smaller and lower relief features superimposed on the slope's regional morphology of domes, ridges, and basins. The smaller class of features is of a scale not easily imaged by 3D-seimsic data. Unlike regional 3D-seismic grids, higher resolution data sets are local in extent, and data sets may be separated by great distances, making it difficult to link features to formative processes. However, the widespread coverage of 3D-seismic data along with regional multibeam bathymetry puts the slope's seafloor complexity into a regionally consistent framework for analysis.

Using a combination of high-resolution acoustic data and 3D-seismic data, a wide variety of sea floor features have been identified, including submarine landslides and slumps, mud volcanoes and mud flows, hardgrounds, mounded carbonates, salt outcrops, brine pools and seeps, and outcropping gas hydrates. Of great importance, finding gas hydrate and associated chemosynthetic communities at or very near the sea floor identifies areas where hydrocarbons are being transported from the subsurface to the sediment-water interface. The most useful seismic property for selecting areas of fluid and gas expulsion at the modern sea floor has been ocean bottom reflectivity determined with 3D-seismic data. Strength and phase of the seafloor reflector are important characteristics that help identify areas of hydrocarbon seepage or more rapid venting in the continental slope environment (Roberts et al. 1992a; Roberts et al. 2006, Appendix A). The rate at which fluids and gas are delivered to the modern sea floor is important to the geological and biological response, and therefore the surface reflectivity, recorded in the 3D-seismic data. As outlined by Roberts and Carney (1997) and Roberts (2001), slow delivery settings promote significant mineralization of the sea floor and shallow subsurface while rapid delivery settings result in mudflows and the accretion of mud volcanoes. Biologically, sedentary animals that typically inhabit hydrocarbon seep sites, such as tubeworms and mussels, cannot survive the rapid sedimentation associated with rapid delivery settings. So, slower flux and more specifically intermediate flux environments are supportive of these chemosynthetic organisms.

While hard bottom areas can occur in association with slow flux to rapid flux hydrocarbon delivery settings, slow and intermediate flux environments are typically characterized by authigenic carbonates in the form of nodular masses in surrounding sediments, blocks, slabs, and mounds. These carbonates are ^{13}C-depleted and are composed of Mg-calcite, aragonite, and sometimes dolomite (Ritger et al. 1987; Ferrell and Aharon 1994; Roberts et al. 1992b). On 3D-seismic surface amplitude (reflectivity) data, areas with abundant hard bottoms provide very high amplitude response and positive polarity of the surface reflector. This response is in contrast to rapid flux areas that are characterized by recently deposited "soft" sediment that frequently is gas-charged, resulting in low reflectivity of the sea floor and negative polarity of the surface reflector.

Identifying of sites of fluid-gas expulsion is important to this study because investigations of the seafloor at these sites using manned submersibles and ROVs have shown that gas hydrate is commonly exposed at the sediment-water interface of intermediate flux rate sites. That is, at sites where the delivery of hydrocarbon gas and perhaps crude oil is not extremely slow or fast enough to export heat and sometimes sediments from the subsurface. Addition of heat may violate the stability conditions under which gas hydrate forms at any given water depth on the slope. It is clear on 3D-seismic profiles that the base of the hydrate stability zone, defined by a bottom simulating reflector (BSR), is deflected upward around the hydrocarbon migration pathway. This pathway is defined by an acoustically opaque zone or “chimney” that extends from the deep subsurface to the ocean bottom. In many cases, there is a bathymetric response at this intersection point in the form of a mound or complex of mounds. Gas hydrate is frequently observed outcropping on the sea floor at such locations (McDonald et al. 1994). At these sites the BSR is deflected upward and either coincides or nearly coincides with the sea floor. In our study, defining the base of the hydrate stability zone by recognition of a BSR on seismic data or by calculations based on gas composition, temperature, and pressure is important to define zones of hydrate occurrence above this stratigraphic horizon.

3. STUDY SITE SELECTION

Three sites were selected for investigation based on their fluid and gas expulsion geology, sea floor reflectivity on 3D-seismic data, coincidence with the 4C-OBC data collection grid, and proximity to oil fields where well data are available to "calibrate" seismic properties of the subsurface (Figures 1 and 2). All three of these sites fall in the Green Canyon lease area where both deep-water fields and oil and gas seeps are numerous. All three sites are on the flanks of an intraslope basin where salt is common in the shallow subsurface and numerous faults provide access for deep subsurface fluids and gases to the modern sea floor. The three study sites are in Green Canyon Block 204 (GC 204), Green Canyon Block 237 (GC 237), and Green Canyon Block 240 (GC 240) (Figure 2). The GC 204 site is next to Chevron's Genesis Field in GC 205, which has numerous wells and geotechnical borings that comprise a database useful to this project. One north-south oriented 4C-OBC line runs through this block and the expulsion features in it. The other key site is in GC 237. BHP Billiton's Typhoon Field is in the northeast corner of this block, and associated well and geotechnical boring data from the Typhoon Field support our interpretations of shallow subsurface geology and the possible presence of gas hydrate. Our evaluation of the subsurface comes from analysis of 4C-OBC data plus high resolution chirp subbottom profiles acquired by AUV. Within the AUV data collection grid, key AUV data were acquired along the 4C-OBC lines. Only the GC 240 site has no supporting oil field data in the vicinity of the fluid-gas expulsion anomaly. For this reason our discussion is focused primarily on the GC 204 and GC 237 sites.

Figure 2 illustrates that two east-west trending 4C-OBC lines cross GC 237, one to the north of the anomaly and the Typhoon production site and one to the south. This figure also shows the considerable coverage of high resolution (chirp sonar) subbottom profile data at this site. Figure 3 illustrates the location of the GC 237 anomaly in relation to the 4C-OBC lines. This surface reflectivity anomaly was identified on 3D-seismic surface amplitude data and investigated with three manned submersible dives that confirmed the presence of surficial gas hydrate at this site. The principal feature of interest appears as a circular anomaly. Within the confines of the anomaly, both zones of high and low sea floor reflectivity are present as determined from the 3D-seismic surface amplitude data (Figure 3). Onsite investigation of this area using the Johnson Sea-Link manned submersible revealed highly variable sea floor conditions, such as authigenic carbonate hardgrounds, large upturned carbonate blocks, and scattered chemosynthetic communities of tubeworms and mussels (Figures 3A, B). At the center of the anomaly area were two closely spaced sites of fluidized mud extrusion. These extrusion sites corresponded to low reflectivity areas within the overall anomaly as determined on the 3D-seismic surface amplitude data. One of these features was a spectacular mud volcano rising over 10 m above the surrounding seafloor. The surface of this feature was covered with white flow patterns resulting from barium-rich fluids that precipitated barite on the mound flanks (Figure 3C). Several active gas seeps were observed at the top and on the flanks of the mound. Sampling revealed the presence of gas hydrate beneath the surface sediments.

Surrounding the low reflectivity of the mud volcano areas are scattered high reflectivity zones related to extensive regions of hard bottom composed of authigenic carbonates. Many of the carbonate blocks surrounding the mud extrusion sites are upturned, suggesting local expansion and uplift of the sea floor, perhaps in conjunction with the near-surface formation of gas hydrate. Around and between these carbonate blocks are small communities of tubeworms and mussels. A region of brine seepage occurs along the western margin of the overall surface reflectivity anomaly.

In terms of surficial geology, GC 204 is much more complex than GC 237 (Appendix A). The 3D-seismic surface amplitude (reflectivity) map of Figure 4 illustrates this complexity. Our 4C-OBC line runs through an area in the southeastern part of the block where several circular expulsion centers are defined by low reflectivity. Another major expulsion site is located at the north-northwestern block boundary. Surrounding these expulsion centers are areas of high

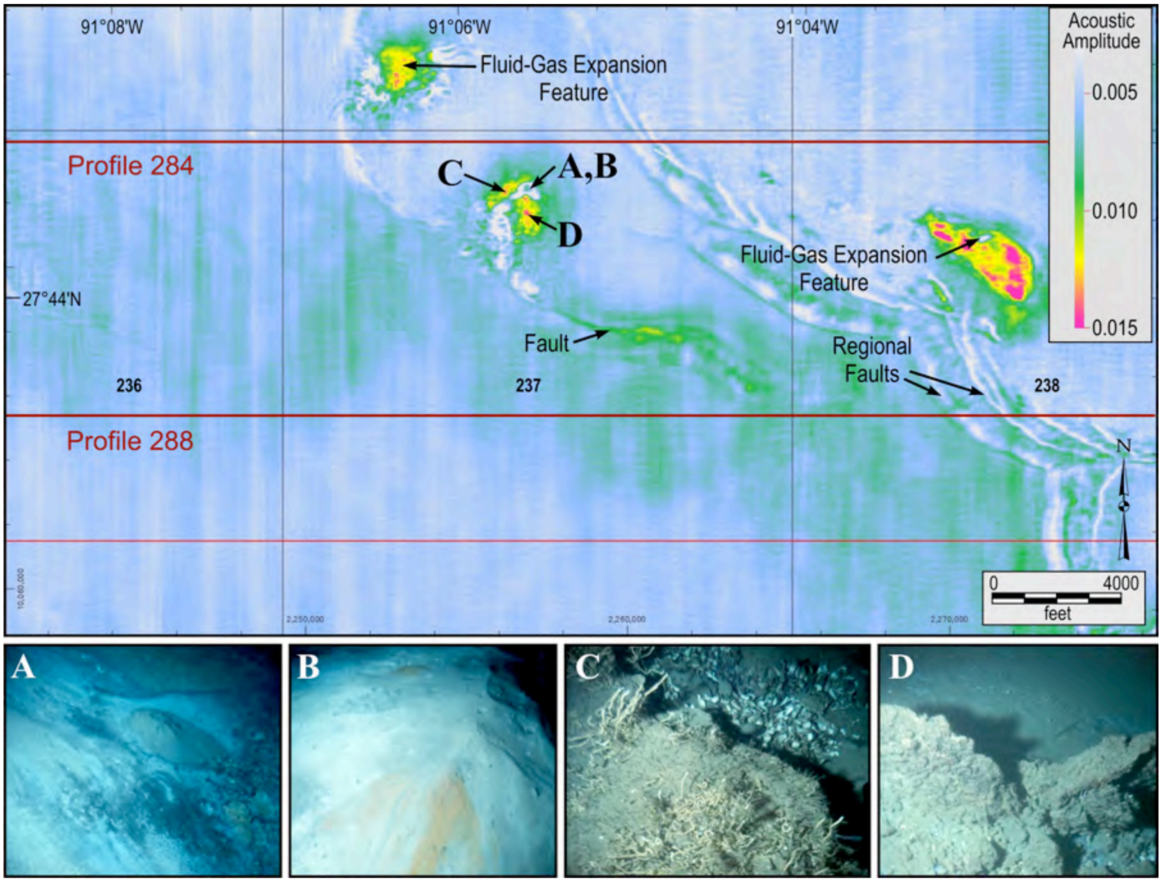

Figure 3. Seafloor reflectivity map constructed from towed-cable 3D-seismic data shows a well-defined expulsion area in GC 237. Both high-reflectivity (red, yellow) and low-reflectivity (blue, white) areas are a part of this complex fluid-gas expulsion area. Low-reflectivity sites represent zones of fluidized sediment expulsion resulting in the creation of mud volcanoes. Extruded sediment and associated fluids have a high barium content. (A) This picture shows barite (white areas) on the flank of the mud volcano. (B) The high-reflectivity areas represent carbonate hardgrounds and slabs. Many of the carbonate slabs surrounding the mud volcano area upturned like the one in this photograph. (C) The chemosynthetic communities of tubeworms and mussels are localized and tend to occur between and around the carbonate blocks and slabs. The lines shown in red (Profile 284 and Profile 288) are tracklines along which 4C-OBC data were collected.

reflectivity that represent regions of hard bottom. The most striking surface features in Figure 4 are long mudflows originating from the major expulsion centers located on bathymetric highs with complex seafloor around them. Manned submersible observations indicate that theexpulsion centers are still active but at a level much lower than in the past when the long mud flows developed. Escaping gas and some evidence of localized fluidized sediment expulsion were observed. In towed–cable seismic profiles, the subsurface area beneath the cluster of expulsion sites is represented by an acoustically amorphous zone, assumed to be the principal fluid-gas migration pathway. It is clear from the surficial geology of GC 204 that this area has experienced extrusions of large volumes of fluidized sediment. The timing for the major expulsion events that developed the long mud flow patterns seen in Figure 4 is unknown. The expulsion activity has obviously slowed to its present near-dormant state. On the high ground around the extrusion sites, the modern seafloor is irregular because of the presence of authigenic carbonate slabs, blocks, and low-relief mounds (Figure 4A). These hardbottom features contain clam and mussel shells that have been cemented by carbonates precipitated as a by-product of microbial oxidation of hydrocarbons. Surrounding the outcropping carbonates are densely populated shell beds composed of lucinid-vesycomyid clams and, to a lesser extent, mussels. Although localized living mussels and clams are present, most of the shell beds do not represent living communities. The combination of carbonates and shell beds creates significant seafloor reflectivity, as represented by 3D-seismic data (Figure 4).

In contrast to the carbonate hardgrounds of the areas surrounding the extrusion sites, it is logical to assume that the fine-grained sediments comprising the mud flows have low reflectivity. However, Figure 4 indicates that these features actually have moderate to high acoustic amplitudes, similar to the hardground areas surrounding the active expulsion sites. The reason for this acoustic response is the presence of numerous clam shells on the surface and perhaps in the shallow subsurface of the flow (Figure 4B). Lucinid-vesycomyid clams exploit hydrogen sulfide produced by microbial communities that metabolize hydrocarbons incorporated in the muds. Once the hydrogen sulfide is depleted, the clams die, leaving a bed of shells. With subsequent mud flows, new clam populations develop. It is reasonable to assume that the high reflectivity of some mud flows is caused by the accumulation of numerous stacks of these shell horizons. In addition, nodular authigenic carbonates also form in the mudflows, which also promote high reflectivity. Our study focused on areas local to a fluid-gas expulsion feature located near Typhoon field (GC 237) and a second expulsion feature close to Genesis field (GC 205) where supporting well data was available. Unfortunately, the third site, GC 240, has no adjacent oil/gas field or associated supporting data. This site was therefore not analyzed in the same detail as the other two study sites (Figure 5).

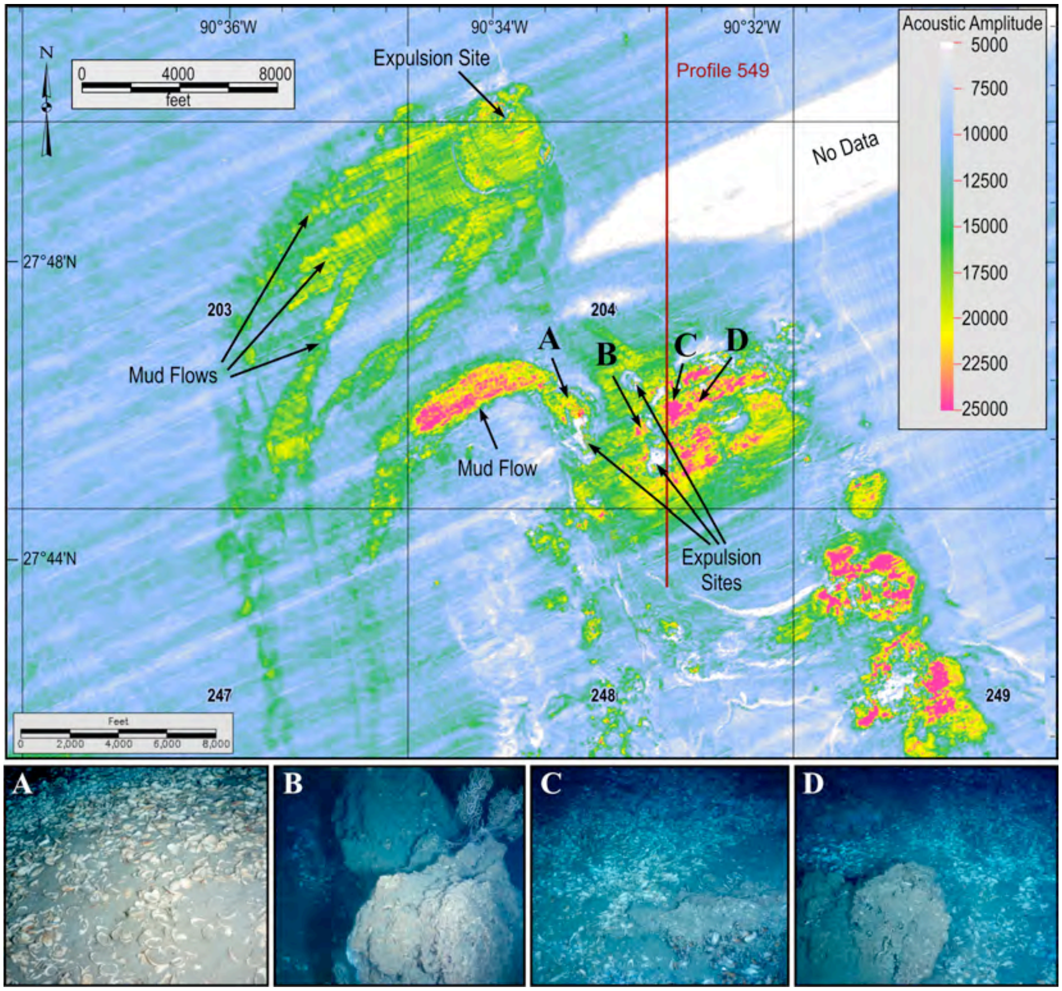

Figure 4. Within the region of GC 204, numerous expulsion centers and associated mud flows are defined by towed-cable, 3D-seismic, seafloor reflectivity data. Both the areas near the expulsion site and parts of the mud flows exhibit high reflectivity (red and yellow). (A) The high-amplitude areas surrounding the expulsion sites are zones of cemented seafloor with living mussel and clam beds. Large blocks of carbonate-cemented mussel shells and clam shells are typical of these areas. Tube worms are not present. (B) Mud flows have high reflectivity primarily because of dense seafloor accumulations of clam shells. Populations of lucinid-vesycomyid clams develop on new flows containing hydrocarbons. After exploiting hydrogen sulfide, a product of microbial oxidation of hydrocarbons, the community dies and leaves a carpet of shells on the surface. New flows provide another trophic resource for development of another community of clams. The large reflection amplitudes observed on towed-cable, 3D-seismic seafloor reflectivity data are assumed to be associated with multiple stratigraphic horizons of these clam shells. (C) This photograph illustrates the surface density of clam shells. Authigenic carbonate nodules and cements in the extruded muds also add to the seismic reflectivity.

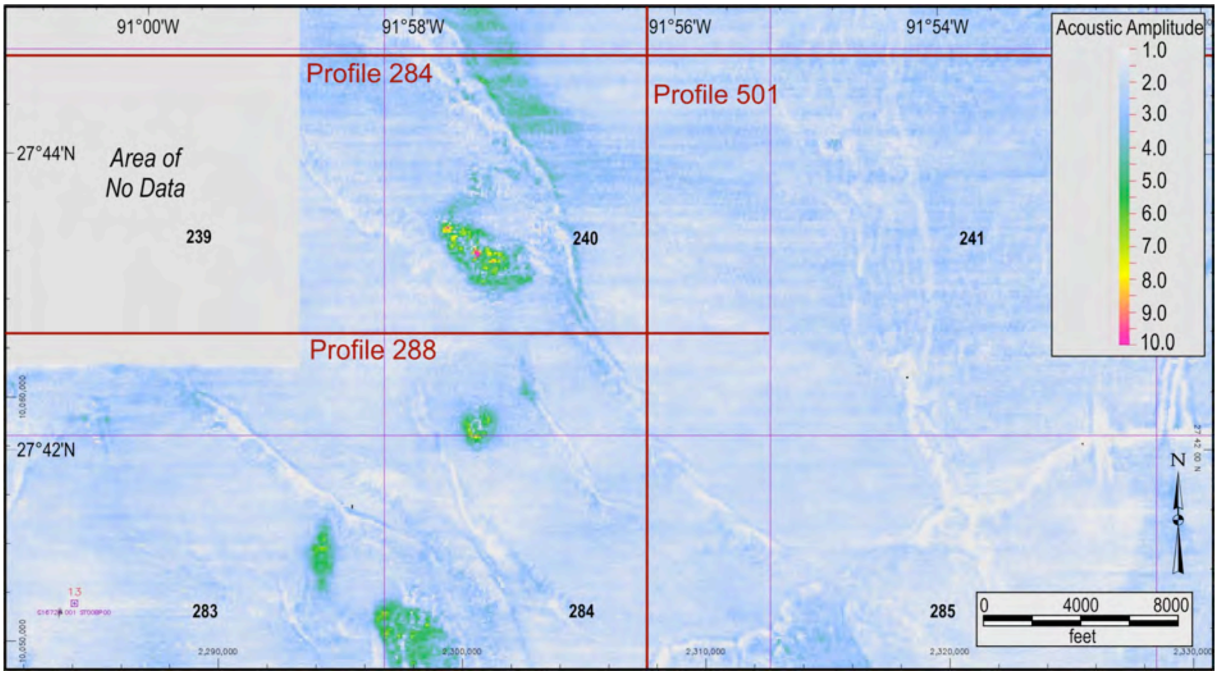

Figure 5. This 3D-seismic surface reflectivity map of the GC 240 expulsion feature suggests that this area is characterized by abundant hard bottoms, probably authigenic carbonates as were found in GC 237 and GC 204. However, no submersible or ROV data exist for this site to be used for "calibration" of the reflectivity data. Seismic profiles indicate a clear migration pathway from the deep subsurface to this site.

4. COMPARISONS OF AUV P-P AND OBC P-SV IMAGES

Our research has demonstrated that low-frequency (10-200 Hz) converted-shear (P-SV) images constructed from 4-component ocean-bottom-cable (4C OBC) seismic data provide a spatial resolution of near-seafloor geology equivalent to, and sometimes better than, the resolution achieved with high-frequency (1-10 kHz) AUV data. We consider this research finding to be an important application for studying deep-water hydrate systems that needs to be shared with the international hydrate research community. The methodology we developed to create P-P and P-SV images from deep-water 4C OBC data has been published (Backus et al. 2006; Appendix B) and was selected by the Society of Exploration Geophysicists as “The Best Paper in THE LEADING EDGE” during 2006 publication year, which is testimony that peers have high regard for the research done in our deep-water hydrate studies. Rather than re-describe the data-processing procedure in this report, we add a pdf version of the published paper as Appendix B. Our gas hydrate papers published in the special issue of THE LEADING EDGE are presented in Appendices A-F.

In our comparisons of high-frequency AUV P-P data and low-frequency air-gun-generated P-SV data, we found that OBC P-SV data often resolved an interface (such as the one labeled A on Figure 6 (top) that is within 1 m of the seafloor; whereas, AUV P-P data along several profiles do not image this horizon (Figure 6, bottom). Low-frequency (10-200 Hz) OBC P-SV data thus often resolve some near-seafloor geologic features better than do high-frequency (1–10 kHz) AUV P-P data—an important project finding and demonstration. The reason for this superb resolution of OBC P-SV data is that the low values of V_S velocity in the shallowest seafloor strata, coupled with the fundamental equation

(1) $\;{}_{SV} = V_S/f$,

that links wavelength ( ), velocity (V), and frequency (f), cause most of the SV wavelengths ($_{SV}$) to be less than 1 m. A second equation of importance is

(2) $V_P/V_S = 2(\;T_{PS}/\;T_{PP}) - 1$

which relates the V_P/V_S velocity ratio across a sub-seafloor layer to the P-SV time thickness (T_{PS}) and P-P time thickness (T_{PP}) measured across that layer. Applying this equation to the depth-equivalent horizons exhibited on Figure 6 shows that the V_P/V_S ratios across the shallowest near-seafloor layering are (a) seafloor to B is 45 to 48; (b) seafloor to C is 38 to 40; and, (c) C to D is 18 to 20.

We found that the V_P velocity from the seafloor to horizon D (12 to 24 m below the seafloor) varied from 1430 to 1550 m/s; consequently, these velocity ratios result in V_S values that range from 30 to 75 m/s across the sub-seafloor interval extending to depth D. The image comparisons illustrated on Figure 6 are typical of the AUV P-P and OBC P-SV image properties along all of the AUV profiles that we studied in this project.

The OBC profile 264 across the Genesis Field area (Figure 2) is shown on Figure 7 to illustrate depth-equivalent geology in P-P and P-SV image spaces across our study areas. This profile is important because it traverses two calibration wells (Well B and Well C). Log data acquired in these wells span part of the hydrate stability zone at each well location. The resistivity-log measurements across these hydrate-stability intervals are important calibration data used in our estimations of hydrate concentration.

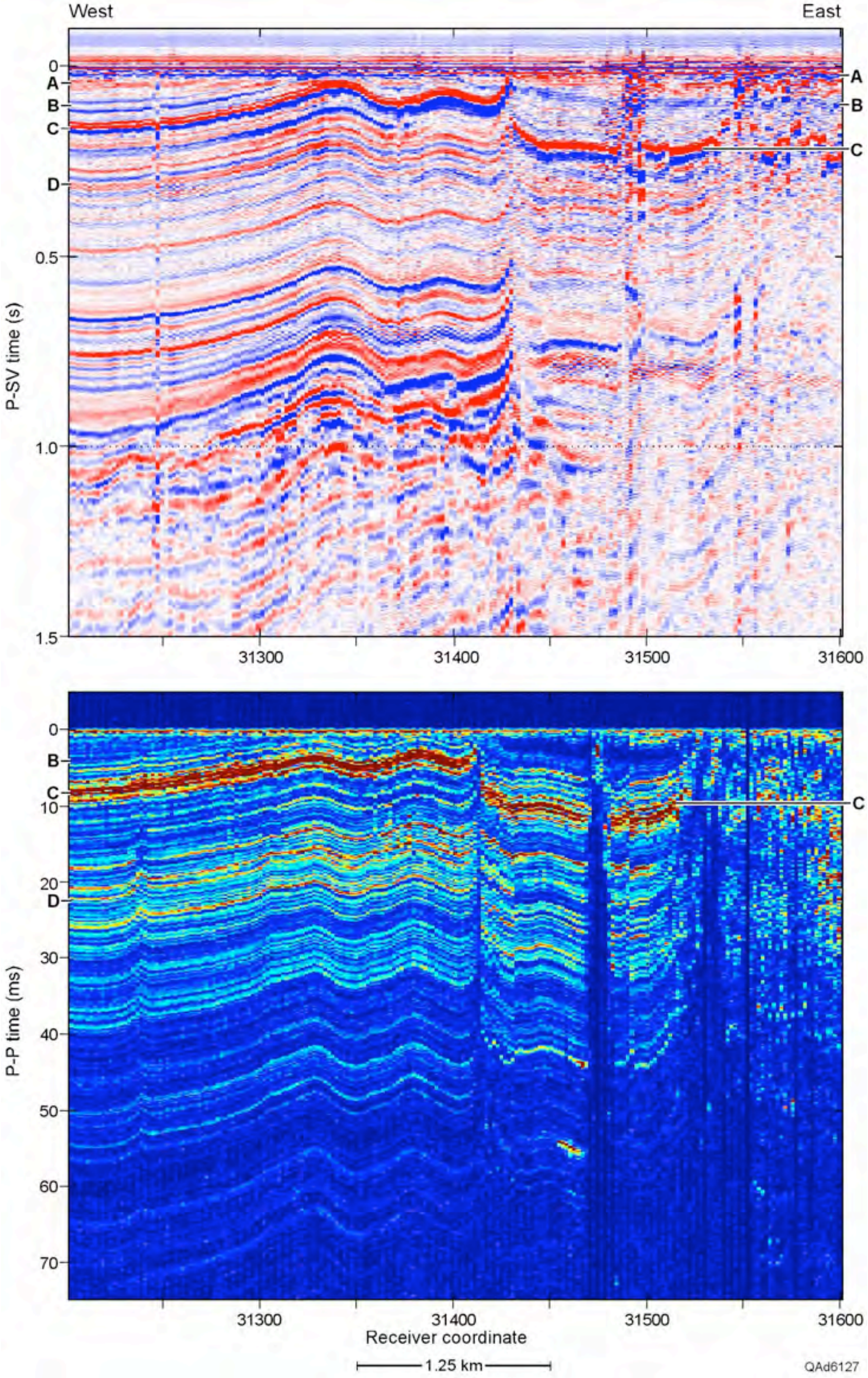

Figure 6. (Top) Interpreted OBC P-SV image. (Bottom) Interpreted AUV P-P image. Depth-equivalent P-SV and P-P reflections are labeled A to D. Unit A is not imaged by the AUV data.

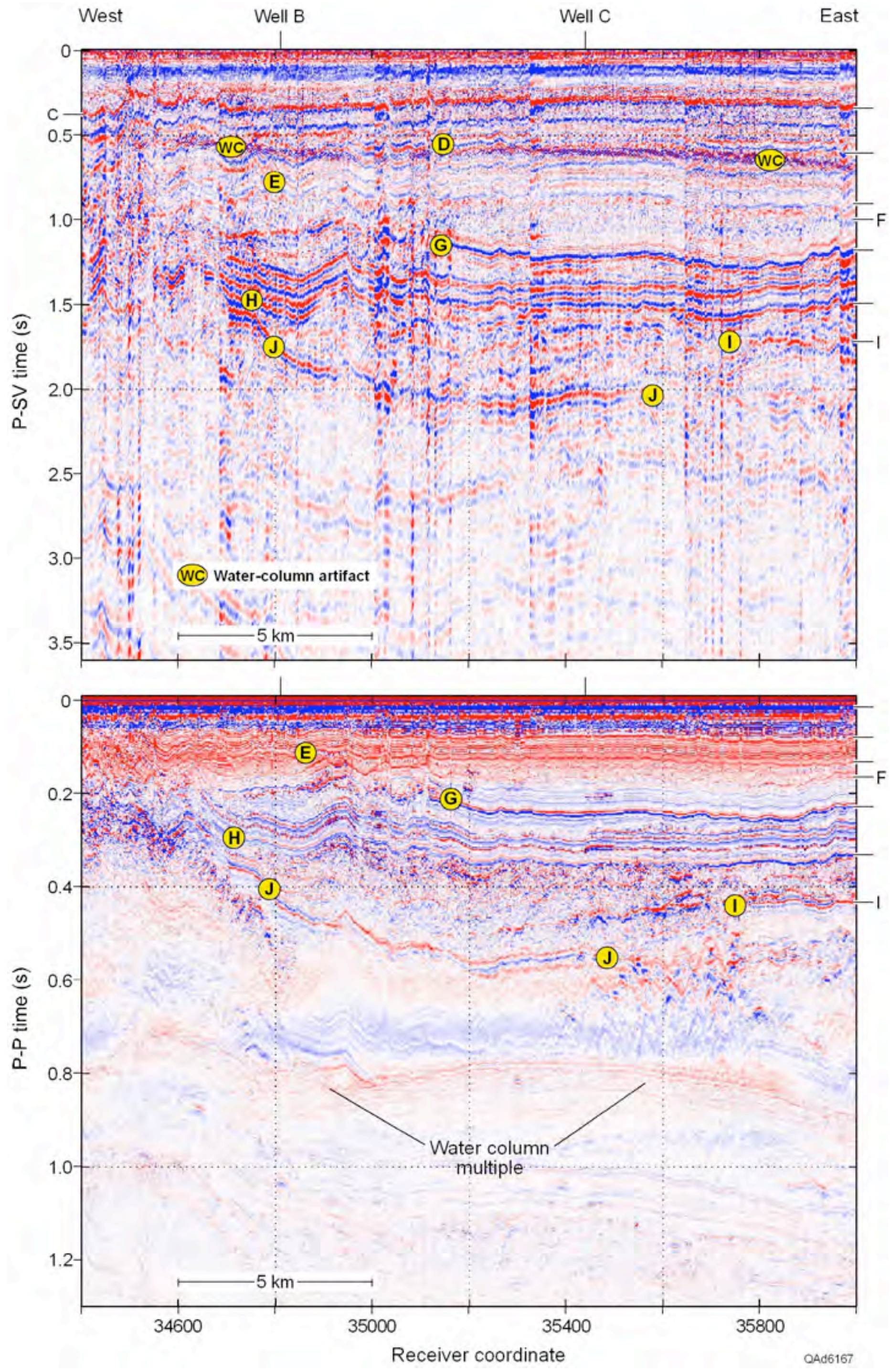

Figure 7. Interpreted P-SV (top) and P-P (bottom) images along OBC profile 264, Genesis area. Depth-equivalent horizons are labeled. P-SV horizons C and D correspond to their equivalents on Figure 6.

5. RAYTRACING TO DETERMINE LAYER VELOCITIES

The P-P and P-SV images along each OBC profile were interpreted to determine which sub-seafloor P-SV reflection even between the seafloor and the base of the hydrate stability zone (BHSZ) were depth-quivalent to selected P-P reflections across the same sub-seafloor depth interval. The depth-equivalent P-P and P-SV horizons shown on Figure 7 were determined by interpreter logic, not by mathematical rigor. We consider interpreted horizons such as these to be "tentatively" depth-equivalent. In order to reliably estimate hydrate concentration by using seismic interval velocities across sub-seafloor layers, we applied numerical analysis to interpreted horizons to determine if each pair of "tentative" depth-equivalent P-P and P-SV is truly depth-equivalent. If not, other reflection events must be selected to establish depth-equivalency. Thus a major part of this study was developing and implementing a raytracing procedure with the following components:

1. create a system of sub-seafloor layers with defined thicknesses and with specified V_P and V_S velocities;
2. calculate travel times along P-P and P-SV reflected raypaths through this velocity layering from a large number of sea-level source stations to a defined seafloor receiver station;
3. compare these calculated raytrace reflection times to actual times of the P-P and P-SV reflections that were interpreted to be depth equivalent at that receiver station; and.
4. adjust layer thicknesses and V_P and V_S interval velocities until raytrace times and actual times for each layer interface converge to acceptable agreement.

At selected seafloor receiver stations distributed across the OBC grid of 2-D profiles, the earth-layer construction process was performed to build depth-equivalent P-P and P-SV horizons and continuous velocity layering along each line of profile. Velocity Layer 1 (and depth-equivalent layer 1) started at the seafloor and extended to the shallowest interpretable P-P reflection. Velocity Layers 2, 3, and 4 (and depth-equivalent layers 2, 3, 4) extended to successively deeper seafloor depths until a Velocity Layer N (and depth-equivalent layer N) was created that extended deeper than the BHSZ boundary.

A computer screen display of a velocity raytrace analysis done at one seafloor receiver station is exhibited as Figure 8. This type of raytrace analysis was done using common-receiver gathers of P-P and P-SV reflectivity traces that were transformed to the reduced-time domain where the time origin T = 0 at each source-offset coordinate was the direct-arrival time at which the downgoing illuminating P wavefield arrives at the seafloor receiver station. In the example in Figure 8, five depth-equivalent pairs of P-P and P-SV horizons are shown overlaying the P-P and P-SV reflectivity gathers. Reflection travel times are calculated downward from a large number of source stations to each layer interface and then upward to the seafloor receiver along refracted raypaths that pass through the velocity layering (shown on the right). These raytrace times are then compared to the "tentative" depth-equivalent P-P and P-SV reflections to determine if reflections from the layer interfaces (right panel) are the horizons marked on the data displays (left and center panels).

A principal advantage of this raytrace-based velocity-analysis strategy is that velocity layers are defined as a function of depth below the seafloor. As a result, seismic-based V_P and V_S interval velocities can be depth correlated with depth-based well-log data, such as resistivity logs. These raytrace analyses were done at intervals of 250 meters along each OBC profile.

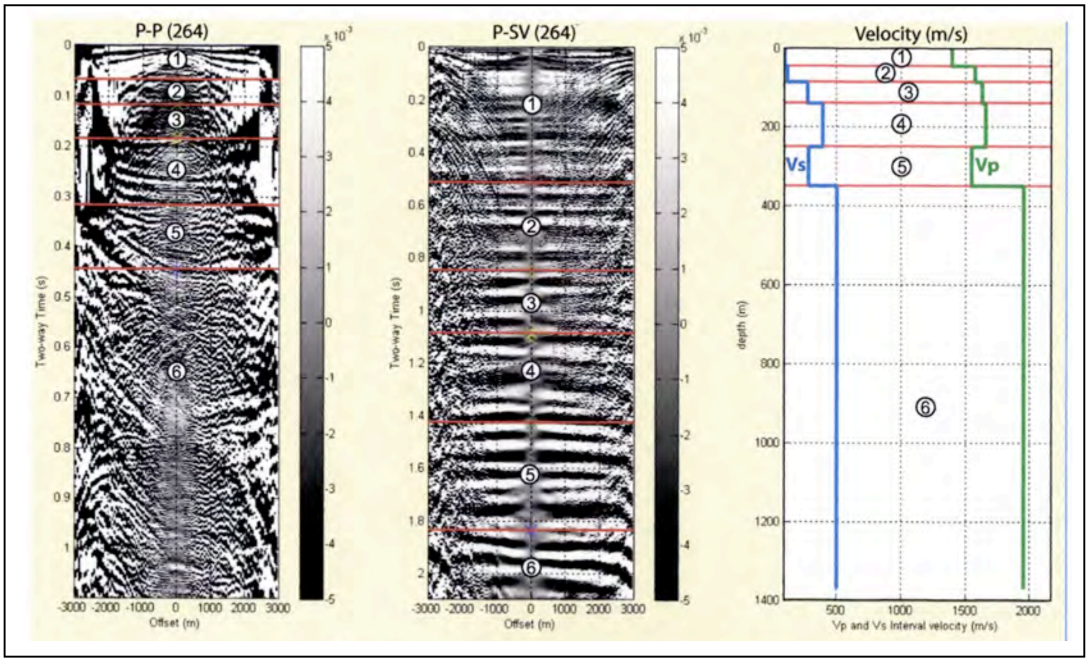

Figure 8. Raytrace-based velocity analysis at calibration Well B, OBC profile 264, Genesis Field area. (Right) 6-layer V_P and V_S model at receiver station 34811, the well location. (Center) OBC P-SV receiver gather shows “flatness” of P-SV reflections associated with layer interface horizons when time shifts determined by raytracing are applied to all offset traces. (Left) OBC P-P receiver gather showing reflections associated with interface horizons after raytraced time shifts are applied.

6. INTEGRATION OF RESISTIVITY, VELOCITY, AND SEISMIC DATA

The resistivity and velocity profiles at calibration wells B and C will now be correlated to the P-P and P-SV images along OBC profile 264 (Figure 7) to demonstrate how a joint-inversion of hydrate concentration was estimated at calibration wells. Data comparisons are shown first at Well C where a layer-velocity model was adjusted to match the P-P and P-SV image-time axes at the well location (Figure 9). This correlation process allows depth-based data to be compared against time-based seismic velocities. Figure 9 shows that each Earth-velocity layer correlates with a distinct seismic facies unit in both P-P image space and in P-SV image space. The V_P and V_S velocity profiles increase in unison from the seafloor to the base of Layer 3, and then the P and SV velocities change in opposing directions across the lower portion of the hydrate stability zone (Layers 4 and 5).

Three estimates of the base of the gas hydrate stability zone (labeled BHSZ(90%), BHSZ(R), BHSZ(V)) are marked on each seismic profile (Figure 9). These horizons have the following meanings:

a. BHSZ(90%): The depth of the base of the hydrate stability zone for a natural gas chemistry having 90.4 % methane, which was calculated by Milkov and Sassen (2001) for the gas hydrate system in nearby Block GC185.
b. BHSZ(R): The depth of a decrease in formation resistivity that is "close to" the depth of horizon BHSZ(90%) and that appears to be a logical choice for the base of the gas hydrate stability zone when examining resistivity log data acquired in the calibration well.
c. BHSZ(V): The depth of a decrease in V_P velocity that is "close to" the depth of horizon BHSZ(90%) and that appears to be a logical choice for the onset of free-gas trapped below the base of stable gas hydrate, as defined by seismic V_P interval velocities.

It is important to note that the V_P velocity profile at Well C (Figure 9) exhibits an increasing trend in magnitude through Layer 4 and then undergoes a velocity reversal in Layer 5. All of the resistivity data associated with the interpreted gas hydrate stability zone are confined to velocity Layer 5. The position of the BHSZ(R) horizon shown on the figure is "interpreted" as the resistivity break at a depth of 1430 ft below the seafloor. A tentative dilemma presented by this data-correlation exercise is that formation resistivity increases in Layer 5, indicating increased gas hydrate content in that layer; whereas, the P-wave velocity decreases, which indicates decreased (or absent) hydrate content. *We thus have opposing interpretations: resistivity data imply gas hydrate is present in Layer 5, but velocity data indicate hydrate is absent.*

We conclude the increased formation resistivity in velocity Layer 5 is caused by free gas, not by gas hydrate. This interpretation of the resistivity log brings the resistivity data and velocity data at calibration well C into agreement because the decrease in V_P velocity in Layer 5 is also

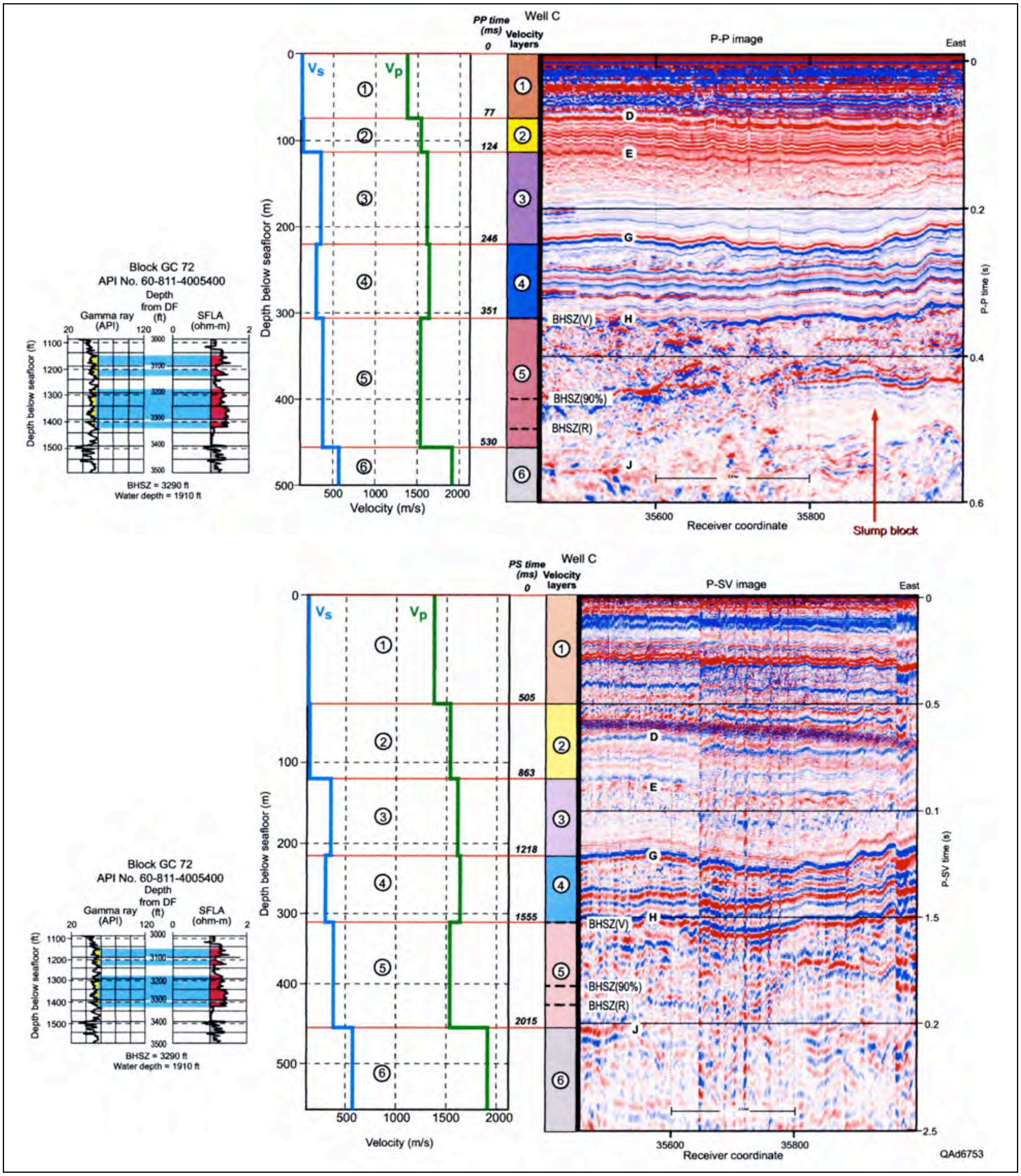

Figure 9. Integration of V_P and V_S velocity analysis at Well C with (top) P-P seismic data along OBC profile 264 (Genesis Field) and (bottom) P-SV seismic data. Horizon BHSZ(R) is the base of the hydrate stability zone interpreted from the resistivity log. Horizon BHSZ(V) is the adjusted position of the BHSZ based on velocity behavior.

consistent with the presence of free gas. From this logic, we readjust the base of gas hydrate stability at Well C upward to depth BHSZ(V), the base of velocity Layer 4 where the reversal in V_P velocity begins.

The integration of resistivity, velocity, and 4C seismic data at Well B is shown in Figure 10, using the information developed at Well C that resistivity-log behavior across velocity Layer 5 is caused by free gas, not by gas hydrate. Again, depth BHSZ(V), where there is a reversal in the magnitude of the V_P interval velocity, appears to be the proper choice of the base of stable gas hydrate.

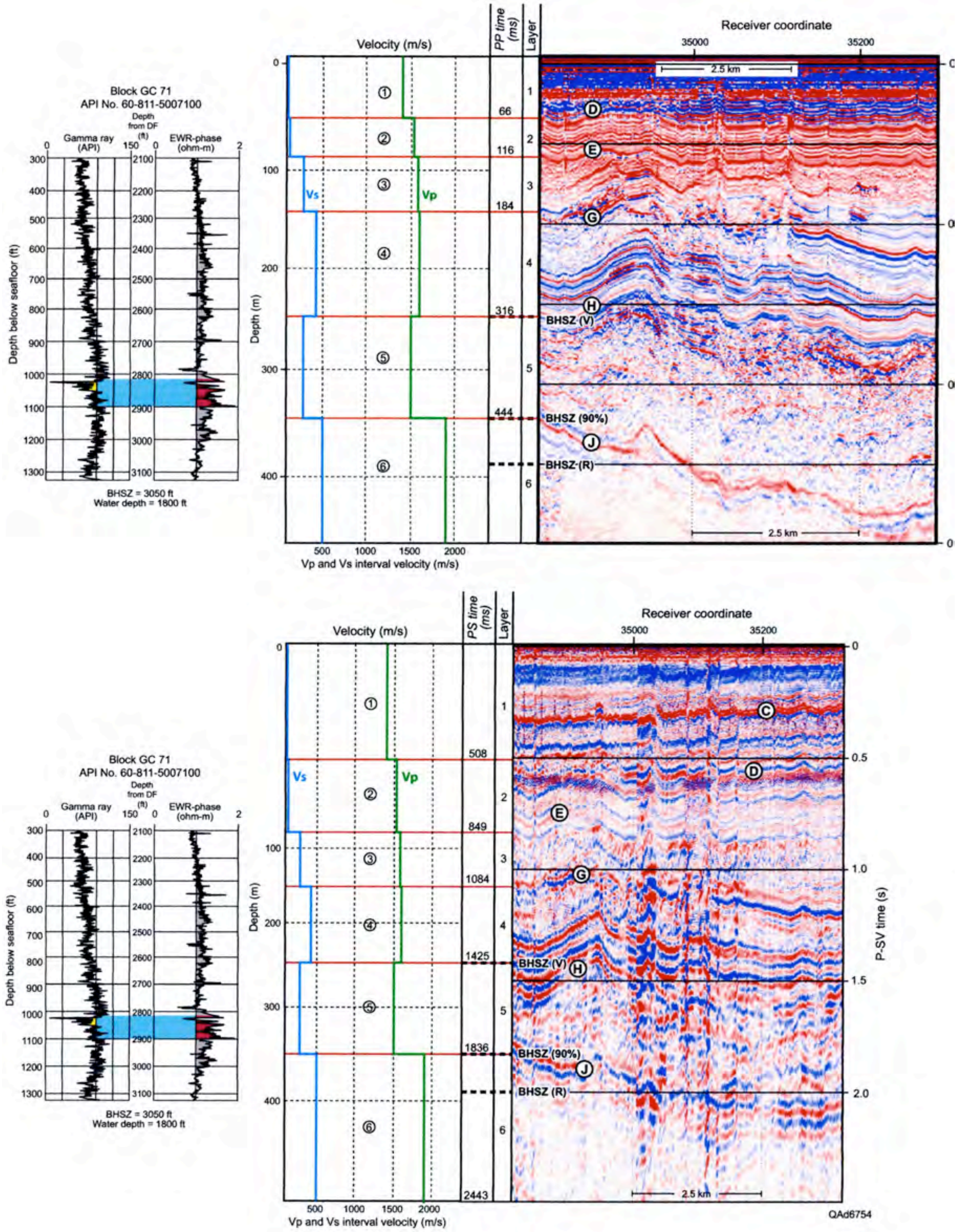

Figure 10. Integration of Vp and Vs velocity analysis at Well B with (a) P-P seismic data along OBC profile 264 (Genesis Field) and (b) P-SV seismic data. Horizon BHSZ(R) is the base of the hydrate stability zone interpreted from the resistivity log. Horizon BRSZ(V) is the adjusted position of BHSZ based on velocity behavior.

7. JOINT INVERSION OF RESISTIVITY AND VELOCITY: THEORY

The relation between gas hydrate concentration and resistivity of strata containing hydrates is non-unique and uncertain. Similarly, any relationship between hydrate concentration and seismic propagation velocity in sediment containing gas hydrate is also uncertain and non-unique. Sources of these uncertainties are related to (a) data-measurement errors; (b) inability to define accurate mineral fractions that exist in the sediment that host hydrate; (c) poor understanding of whether hydrate is distributed among sediment grains as a disseminated material or as a layered material (either vertical or horizontal layering); (d) unexpected spatial variability of rock properties; and, (e) inadequate understanding of numerous other physical conditions and processes associated with hydrate systems.

By combining different types of gas hydrate-dependent geophysical information, particularly velocity estimates and formation-resistivity measurements, predictions of gas hydrate concentration can be constrained, and the uncertainty of predictions can be reduced (Figure 7). To take advantage of this principle, we developed a method for predicting gas hydrate concentration that is based on stochastic simulations and on two rock-physics theories: one theory relates hydrate concentration to formation resistivity (R), and the second relates seismic V_P and V_S velocities to hydrate concentration. The fundamental theory of the rock physics modeling that describes how seismic velocity relates to hydrate concentration is described in Appendix C.

In applying our joint-inversion methodology, we account for the uncertainty of every parameter that enters into the calculation of hydrate concentration in our analytical models. These rock physics theories are described in a paper published in the AAPG Hedberg Conference on Natural Gas Hydrates (Sava and Hardage 2008).

Our approach to predicting gas hydrate concentration is based on the concept that all of the parameters used in our rock physics elastic modeling and in our applications of the Archie Equation are uncertain. The language of probability theory enables us to quantify this uncertainty and to combine various types of information, such as velocity data and resistivity data, into a joint inversion for gas hydrate concentration. To implement a joint-inversion technique, each parameter in our rock-physics elastic modeling and in our formulation of the Archie Equation is expressed as a probability density function (PDF). The PDFs used in this joint inversion are either Gaussian distributions or uniform distributions. Gaussian distributions are used when the expected value for the model parameter is known (Figure 11). The mean of the Gaussian function is the expected value of the parameter; the standard deviation defines the uncertainty associated with this expected parameter value. Gaussian PDFs are used in numerous research fields to express measurement uncertainty in data. In our methodology, we use Gaussian PDFs to describe data provided by porosity logs, resistivity logs, gamma-ray logs, sonic and dipole-sonic logs, and seismic-based velocities.

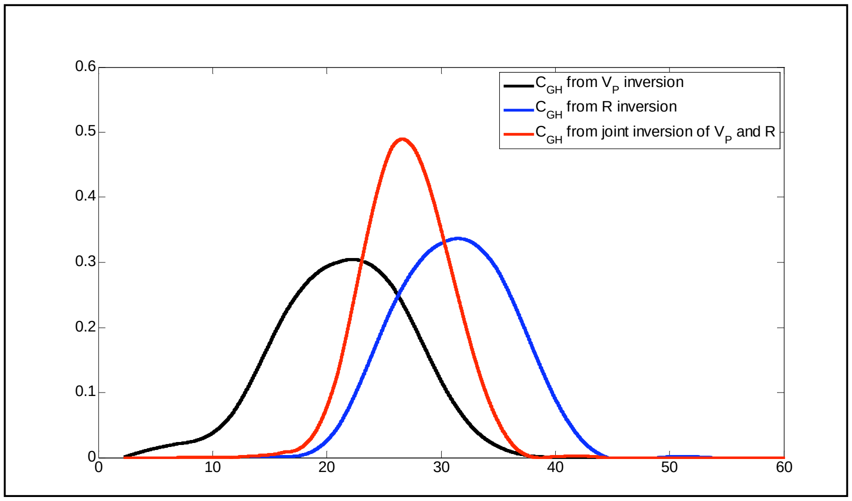

Figure 11. Idealized posterior PDF of gas hydrate concentration at a random sub-seafloor depth location based on the inversion of seismic V_P velocity (black curve), inversion of formation resistivity R (blue curve), and joint inversion of V_P and R (red curve). Joint inversion constrains the hydrate estimate and reduces the uncertainty of the estimate.

In contrast to a Gaussian distribution, a uniform distribution is used when the value of a parameter is not known but the range of variability for the parameter can be defined. A uniform distribution assumes that within the range of variability being considered, any value of the described parameter is equally probable.

The type of PDF that we use for the parameters needed in our joint inversion are assigned as follows:

a. Gaussian distribution: porosity ( ); clay fraction (V_{cl}); bulk and shear moduli for quartz, clay, and brine (K_q, K_{cl}, K_w, G_q, G_{cl}); density of brine, quartz, and clay ($_w$, $_q$, $_{cl}$); effective pressure (P_{eff}); coordination number (C); cementation exponent (m); geometrical factor (a); and pore-fluid resistivity (R_w).

b. Uniform distribution: hydrate concentration (c_{gh}); bulk and shear moduli of hydrate (K_{gh}, G_{gh}); hydrate density ($_{gh}$); critical porosity ($_c$); saturation exponent (n); and resistivity of clay mineral (R_{cl}).

Our probabilistic approach to estimating hydrate concentration is based on the concept that all parameters used in the inversion are described by PDFs that allow us to account for the natural variability in the elastic properties of the mineral, gas hydrate, and fluid constituents of seafloor sediments, as well as for the variability in brine resistivity, cementation exponent, clay mineral resistivity, and other petrophysical parameters required for a joint inversion of resistivity and seismic velocity to hydrate concentration.

It is important to note that probability density functions for parameters (e.g., porosity, effective pressure, mineralogy, coordination number, cementation exponent, geometric factor, and resistivity of brine) that are needed in an inversion for gas hydrate concentration vary with depth. In our method, we update the PDFs for these parameters at each depth coordinate, with these updates based on depth variations of parameters observed from geotechnical borings at

Typhoon and Genesis Fields and on parameter behavior determined *a priori* (reasoning based on theoretical deduction, not on observation).

At each depth coordinate we model the joint theoretical relations between hydrate concentration c_{gh} (the model parameter we are calculating) and the resistivity R and seismic propagation velocity (both V_P and V_S) of sub-seafloor strata (representing the observed parameters). We refer to the parameters involved in our rock physics elastic modeling and in our Archie Equation (corrected for clay) as common parameters. There are three of these common parameters: porosity ( ), gas hydrate concentration (c_{gh}), and fraction volume of clay (V_{cl}). Clay fraction is estimated from local gamma-ray logs. We use a Monte Carlo procedure to draw values for common parameters and V_{cl} from their associated PDFs and then compute the corresponding velocity and resistivity values using Monte Carlo draws from the PDFs for each of the model parameters that are required for calculating gas hydrate concentration.

In this fashion we obtain many possible realizations of the functions relating hydrate concentration, resistivity, and seismic propagation velocity. This joint relation is non-unique, uncertain, and can be expressed mathematically as a probability density function in three-dimensional (c_{gh}, V_P, R) data space (or in (c_{gh}, V_S, R) data space). This 3-D joint-theoretical PDF, which we will denote as (c_{gh}, V_P, R), changes with depth and defines the correlation (and the inherent uncertainty) between gas hydrate concentration and the velocity and resistivity properties of gas hydrate-bearing sediments. We emphasize V_P velocities rather than V_S velocities in our inversion.

To estimate gas hydrate concentration using seismic and resistivity data, we implement a Bayesian approach formulated in the context of an inverse problem, as proposed by Tarantola (1987). First, we express our prior information about hydrate concentration (information obtained before analyzing any seismic or resistivity data) as a PDF. We denote this prior PDF as ${}_M(c_{gh})$, where subscript M stands for "model" parameter. In our study, this prior PDF is assumed to be a uniform distribution over all physically possible values for the hydrate pore-space fraction, meaning we allow this uniform distribution to range from 0 to 100%.

Second, we combine this prior PDF of hydrate concentration, ${}_M(c_{gh})$, with information provided by seismic and resistivity measurements at calibration wells. Our prior information and any information obtained from seismic and resistivity data are assumed to be statistically independent. This assumption allows the prior joint PDF that combines gas hydrate concentration and data, (c_{gh},V_P,R), to be written as

$$(3) \qquad (c_{gh},V_P,R) = {}_M(c_{gh}). \quad {}_D(V_P). \quad {}_D(R).$$

In this equation, subscript D stands for data, and ${}_D(V_P)$ and ${}_D(R)$ are Gaussian PDFs that account, respectively, for measurement uncertainties in the seismic P-wave data and resistivity log data we use in our gas hydrate inversion. Our assumption of statistical independence between seismic and resistivity measurements is logical because velocity and resistivity data are obtained at different calendar times and with different field procedures and equipment.

Third, we use Tarantola's (1987) strategy that states that the posterior PDF combining gas hydrate concentration and data, (c_{gh},V_P, R), is proportional to the prior joint PDF for hydrate concentration and data, (c_{gh}, V_P, R), multiplied by the joint theoretical PDF, (c_{gh}, V_P, R), which we derive using stochastic rock physics modeling. Therefore, we can write:

(4)) $(c_{gh},V_P, R) = (c_{gh}, V_P,R) \,.\, (c_{gh}, V_P, R)$.

From this posterior joint PDF, (c_{gh},V_P, R), we derive what is called the marginal distribution of hydrate concentration, $_M(c_{gh})$, by integrating the posterior joint PDF over velocity and resistivity data space. This marginal distribution, $_M(c_{gh})$, represents the posterior PDF for gas hydrate concentration in the pore space of the host sediment, and the mean of this distribution is the parameter that we display along our OBC profiles to represent the amount of in-place gas hydrate.

At each calibration well, we apply this Bayesian inversion procedure to estimate the posterior PDF of gas hydrate concentration, using both local seismic velocity values and local resistivity-log data in the inversion. This estimation utilizes the theoretical joint PDF, (c_{gh}, V_P, R), that we derive using rock-physics stochastic modeling. When we leave a calibration well and calculate hydrate concentration along an OBC profile, our hydrate estimate is expressed at each depth location along the OBC line as a posterior PDF that involves only V_P velocities. We define the mean value of this posterior PDF as the expected value for gas hydrate concentration at each OBC line coordinate. In addition we produce a measure of the uncertainty associated with this estimate of gas hydrate concentration—the standard deviation of the posterior PDF.

Example of Joint Inversion of Resistivity and Velocity

The gas hydrate prediction concepts described in the preceding section were used to create joint-inversion estimates of hydrate concentration at selected calibration wells. The input data for these inversions were the resistivity log acquired in the calibration well and the seismic-based V_P and V_S interval velocities determined from raytrace modeling of OBC seismic data local to each well. We assumed that load-bearing gas hydrate was the correct gas hydrate-sediment morphology to use to describe relationships between gas hydrate concentration and seismic velocity. Our rock physics theory allows other gas hydrate-sediment morphologies to be considered when necessary. Using this load-bearing-gas hydrate assumption, the estimation of gas hydrate concentration at Well B, Genesis Field (see Figure 2 for well location), is illustrated on Figure 12.

The function labeled NC on the data panels of this figure defines the effect of normal compaction on the rock property that is illustrated in each panel. This normal-compaction effect is calculated for a mixture of 95% clay and 5% quartz grains that is 100% brine saturation. The near-seafloor porosity dependence used in the normal-compaction calculation was extracted from lab measurements of water content of near-seafloor cores and submerged unit weight of near-seafloor samples as reported in seafloor geotechnical reports available at Typhoon and Genesis fields. The depth-dependent increase in V_P and V_S velocities caused by normal compaction was calculated using Walton's theory (Walton 1987) and assuming:

(a) the numerical values for elastic moduli K and G and for bulk density assigned to clay, quartz, and brine are the values listed in Table 1;
(b) the coordination number C needed in the Walton theory ranges from 1 at the seafloor to 13 at a sub-seafloor depth of 1,400 meters; and,
(c) hydrostatic pore pressure equals the columnar weight of brine having the density defined in Table 1.

Intervals above the BHSZ boundary where both velocity and resistivity have values greater than those associated with normal compaction are assumed to be zones of hydrate concentration. Using this normal-compaction behavior as one constraint for our joint inversion, the mean value of the probability distribution function (PDF) in Figure 12b indicates that hydrate occupies approximately 14% of the pore space in the local vicinity of Well B. The standard deviation of the PDF indicates the uncertainty of this estimate is ±2.6 percentage points.

Table 1.

Parameters Used in Rock Physics Modeling

Constituent	**Bulk Modulus**	**Shear Modulus**	**Density**
quartz	37 GPa	44 GPa	2650 kg/m3
clay	25 GPa	9 GPa	2550 kg/m3
brine	2.29 GPa	0 GPa	1005 kg/m3
gas hydrate	7.14 GPa	2.4 GPa	910 kg/m3

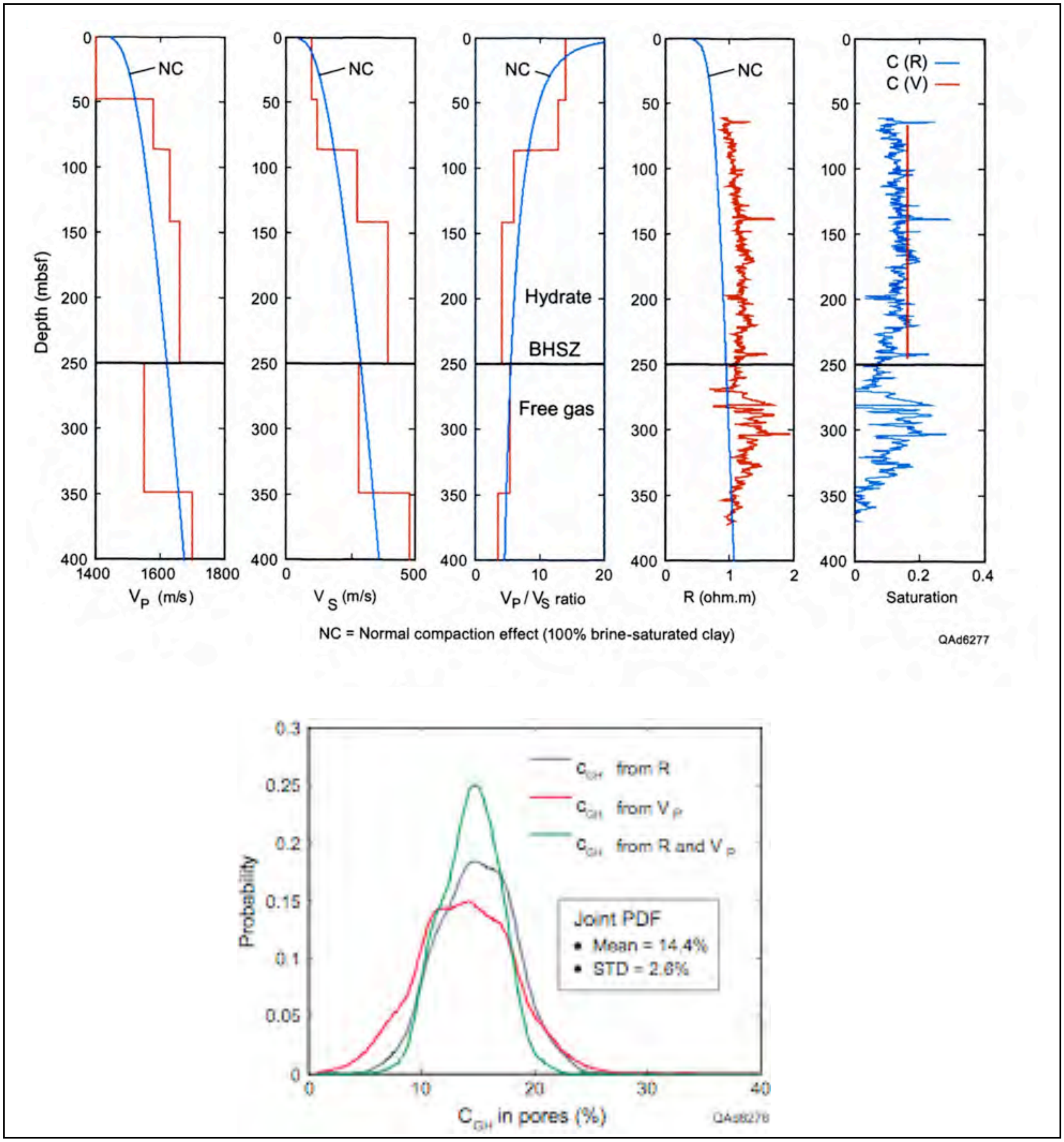

Figure 12. (Top) Seismic-based V_P and V_S interval velocities, resistivity log, and their respective estimates of hydrate concentration at Well B, Genesis Field. The BHSZ boundary is defined as the top of the layer where V_P velocity exhibits a reversal in magnitude. The increase in resistivity below the BHSZ boundary is caused by free gas. (Bottom) Joint inversion of resistivity and V_P velocity indicates hydrate occupies 14.4% of the pore space (mean value of the PDF). The estimation error is ±2.6 percentage points (standard deviation of the PDF).

8. 2-D PROFILES OF VELOCITY LAYERING

After performing joint inversions such as those illustrated on Figure 12 at several calibration wells, we determined an optimal function that could be used to relate hydrate concentration to seismic-based V_P velocity at OBC line coordinates between calibration wells. The input data for this velocity-based gas hydrate estimation were 2-D profiles of V_P layer velocities determined by raytrace analysis of common-receiver gathers (see Figure 8). These raytrace analyses were done at intervals of 10 receiver stations (250 m) along each OBC profile. Examples of the type of 2-D velocity layer models that we created along each OBC profile are exhibited on Figures 13 and 14. Note on Figure 13 (top) that a possible BHSZ horizon is marked along the northern half of the OBC profile.

2-D Profiles of Hydrate Concentration

Relationships between V_P velocity and hydrate concentration developed at calibration wells were applied to the V_P velocity layer models constructed along each OBC profile. The inversion results for the velocity layering along profile 549 are displayed on Figures 13 and 14.

Because the normal compaction curve NC has a dynamic depth variation across Velocity Layer 1 immediately below the seafloor (Figure 12) and no log data were available across this shallowest layer to confirm the effect of compaction on velocity, we assigned a constant, near-zero gas hydrate concentration to Layer 1 and focused our hydrate estimation on velocity Layer 2 and deeper layers that extended down to the BHSZ horizon. Our velocity analyses did not indicate a velocity magnitude in Layer 1 anywhere across the OBC profile grid that implied gas hydrate was present in this shallowest layer.

Calculated hydrate concentrations exhibit considerable lateral spatial variation within each velocity layer and even greater vertical variability from layer to layer. The maximum gas hydrate concentration found along these two particular OBC profiles were local areas where gas hydrate occupied a little more than 30% of the pore space of the host sediment.

We found that hydrate is pervasive across the Green Canyon areas we studied at concentrations that ranged up to one-third of the available pore space of the host sediment. In most areas, the hydrate fraction was in the range of 10 to 20% of the available pore space. We determined that a free-gas layer immediately underlies the base of the gas hydrate stability zone across the entirety of our study area. This free-gas zone is revealed by a reduction in V_P velocity determined by our high-resolution raytrace modeling technique. The amount of free gas in this zone was not estimated, but we expect the layer has a gas saturation of only a few percentage points. Domenico (1976) has demonstrated that a small amount of free gas can produce a significant reduction in V_P velocity. This free-gas zone is not easily distinguished from a hydrate-bearing zone when examining resistivity logs available across the area. We found that the observed increase in log resistivity related to free gas can be confused with a resistivity increase caused by gas hydrate. Thus, interpreting the thickness of the gas hydrate stability zone from resistivity logs alone can add to an overestimation of the thickness of stable gas hydrate and of the amount of gas hydrate that is present.

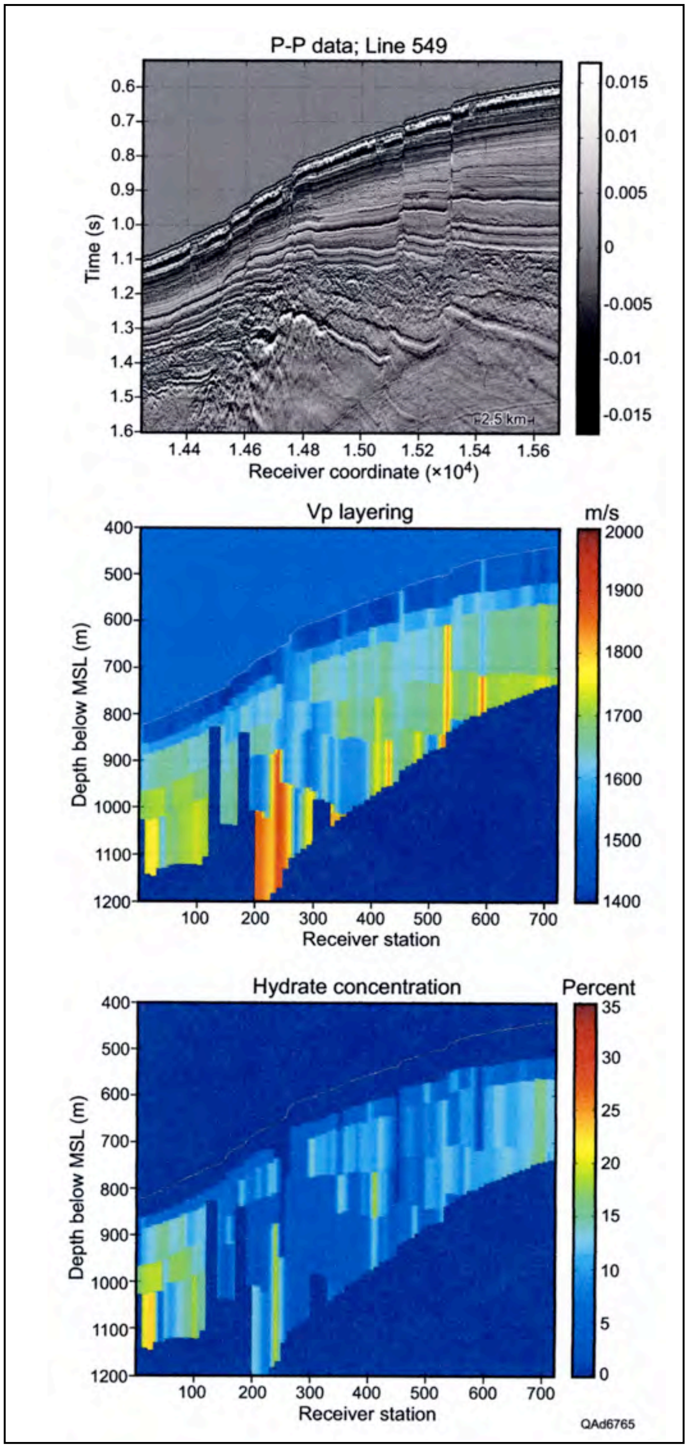

Figure 13. (Top) P-P image along OBC profile 549, Genesis area (Figure 2b). The dashed horizon marks a possible BSR position. (Center) V_P velocity layering. (Bottom) Estimated hydrate concentration. Along each OBC profile, the BHSZ boundary was defined as the shallower of either (1) the depth of the onset of a reversal in V_P magnitude (such as documented on Figures 9 and 10), or (2) the depth of the thermal-based constraint for 90% methane hydrate published by Milkov and Sassen (2001). If we noticed any indication of a BSR boundary, such as that noted on Figure 13a, we used that evidence to define the base of the hydrate stability zone.

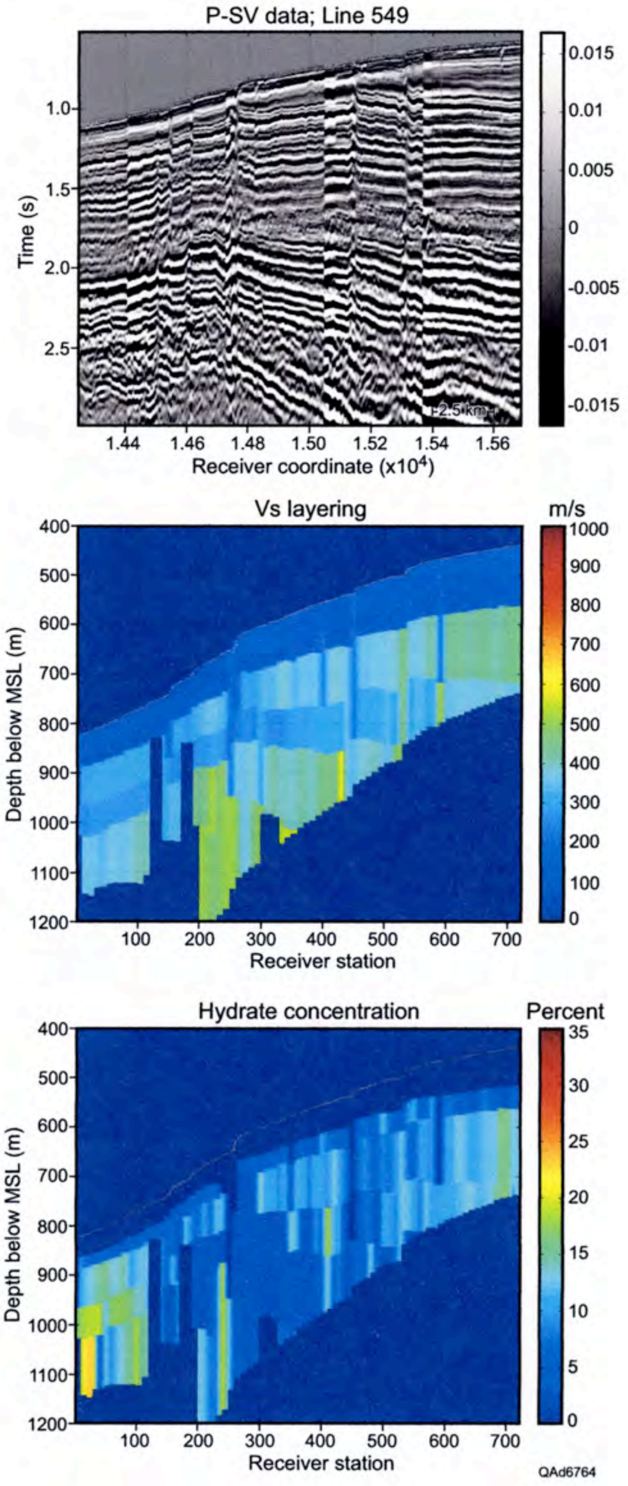

Figure 14. (Top) P-SV image along OBC profile 549, Genesis area (Figure 2b). (Center) V_S velocity layering. (Bottom) Estimated hydrate concentration.

9. MAPPING THE AMOUNT OF IN SITU HYDRATE

To determine the amount of in situ hydrate existing within the interval extending from the seafloor to the BHSZ boundary, we multiplied our seismic-based hydrate concentrations (expressed as the fraction of occupied pore space) by each layer thickness and layer porosity and summed these products to create an estimate of total in-place hydrate. The methodology is illustrated on Figure 15. The sub-seafloor strata along each OBC profile were segregated into narrow strips having dimensions of 250 m in the inline direction and 1 m in the crossline direction. The inline dimension of 250 m was the distance between adjacent velocity analysis points where we determined the thickness and interval velocity of each interpreted sub-seafloor Earth layer. Hydrate concentration within each layer of each 250 m^2 strip was estimated using the inversion procedure illustrated on Figure 12. Layer velocities were the hydrate-sensitive parameter used along each OBC profile after values of inversion parameters were optimized by doing joint inversion of velocity and resistivity at local calibration wells.

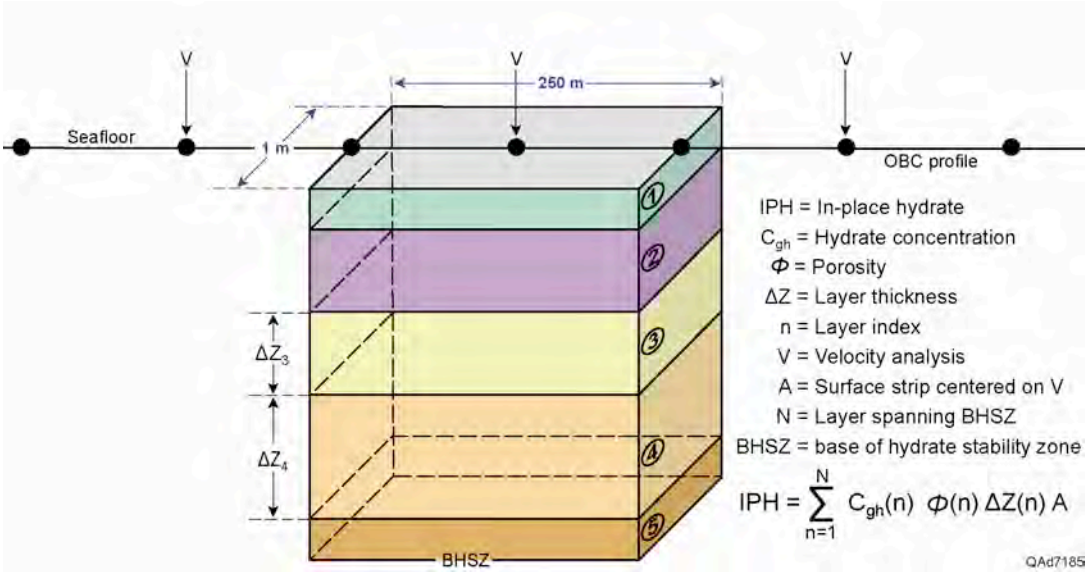

Figure 15. Model used to estimate the amount of in-place hydrate along each OBC profile. Velocity analyses were done at intervals of 250 m along each profile to define the thickness and interval velocity of sub-seafloor strata. After doing joint inversions of velocity and resistivity (Figure12) at calibration wells to optimize the parameters used in velocity inversion, interval velocities were used for the critical inversion to hydrate concentration along each profile as described in Sava and Hardage 2006 (Appendix C).

The resulting maps of in-place hydrate across the study areas are shown as Figure 16 and 17. Our seismic-based quantification of in situ hydrate indicates the largest accumulation of hydrate exists in Green Canyon Block GC116 north of Genesis Field (Figure 17). At some locations across this trend, the amount of in-place hydrate is estimated to be as much as 2000 to 4000 m^3 beneath 1-m × 250-m rectangular strips centered on receiver stations where V_P interval velocities were determined for estimating hydrate concentration. Other significant accumulations of hydrate are shown by the green to red colors that are shown at several locations across the OBC grid.

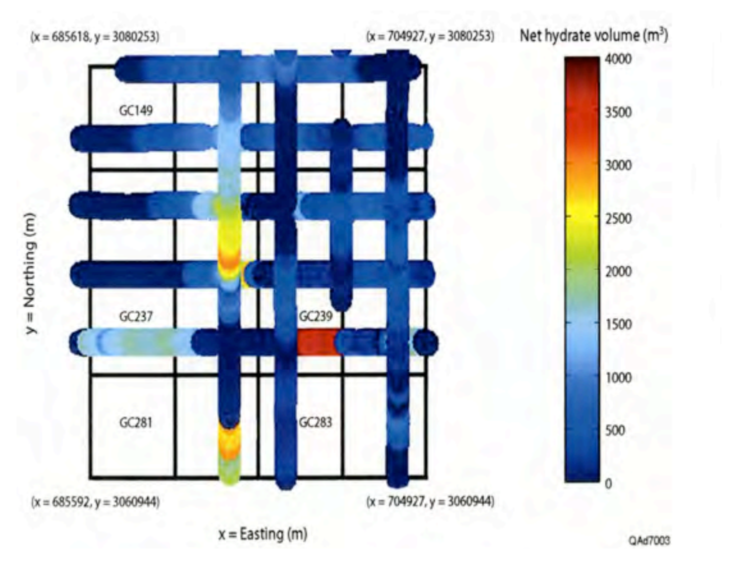

Figure 16. Amount of in situ hydrate across Study Site 1, Typhoon Field area. The values plotted on this map are the product: (hydrate concentration) × (layer porosity) × (layer thickness) × (250 m). The 250-m factor is the distance between adjacent velocity analysis points where V_P velocities are calculated. The color bar defines the amount of in-place hydrate (in units of cubic meters) below a 1-m × 250-m strip centered on the sequence of seafloor receiver stations where velocity analyses were done.

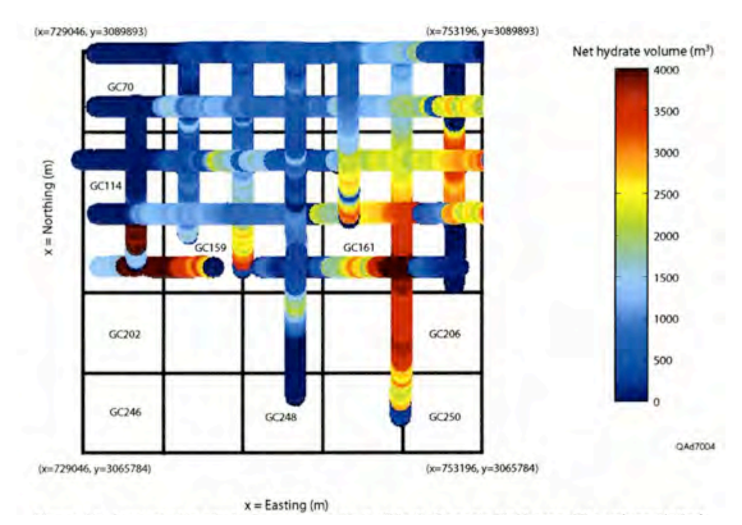

Figure 17. Amount of in situ hydrate across Study Site 2, Genesis Field area. The values plotted on this map are the product: (hydrate concentration) × (layer porosity) × (layer thickness) × (250 m). The 250-m factor is the distance between adjacent velocity analysis points where V_P velocities are calculated. The color bar defines the amount of in-place hydrate (in units of cubic meters) below a 1-m × 250-m strip centered on the sequence of seafloor receiver stations where velocity analyses were done.

10. COMPARING LOAD-BEARING AND FREE-FLOATING HYDRATE ASSUMPTIONS

The hydrate distributions displayed as Figures 16 and 17 were estimated using the assumption that the hydrate granules embedded in the sediment bear a proportionate part of the sediment weight. This assumption leads to the “load-bearing” rock physics theory described as Model A in Appendix C. An alternate assumption that has merit is that unit volumes of hydrate float in the pore spaces of the host sediment and are not part of the load-bearing matrix. This assumption leads to the “free-floating” rock physics theory described as Model B in Appendix D.

For a given value of V_P within a near-seafloor layer, a free-floating assumption for the hydrate-sediment morphology results in greater hydrate saturation than does a load-bearing assumption. A comparison of the hydrate concentrations predicted by these two hydrate-morphology models along OBC profile 557 is displayed as Figure 18. For the range of interval V_P velocities that we found within the hydrate stability zone in the Green Canyon area, our free-floating-hydrate theory causes approximately five more percentage points to be added to the hydrate fraction than what is predicted by our load-bearing-hydrate theory. If our load-bearing-hydrate calculation at location 1 yielded a hydrate fraction of 16% and a fraction of 22% at location 2, our free-floating-hydrate theory predicted approximately 21% and 27% respectively, at these same two locations. The almost-constant difference of approximately five percentage points of hydrate concentration that results when using these two hydrate-morphology assumptions is illustrated by the profiles displayed as Figure 18.

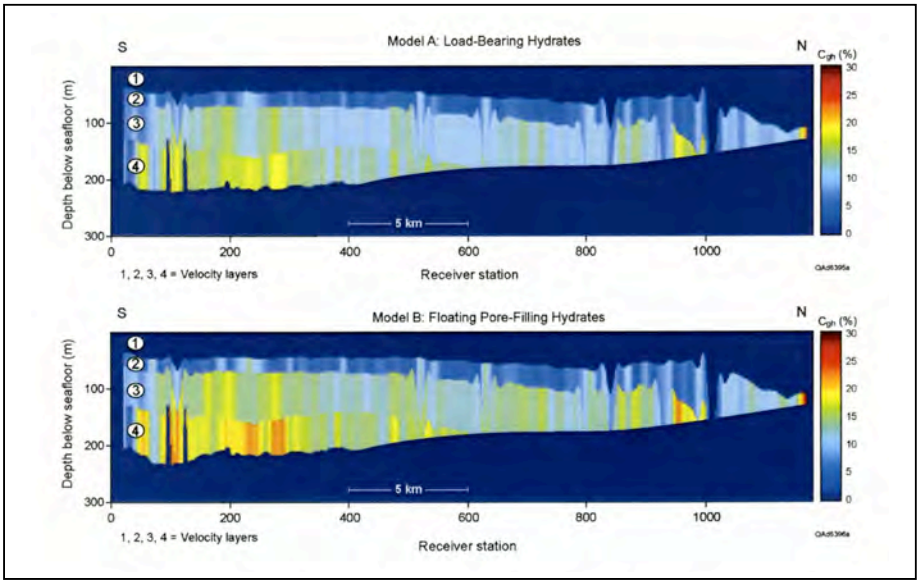

Figure 18. Comparison of hydrate concentrations predicted along OBC profile 557 when hydrate is load-bearing (top) or free-floating (bottom). The same color bar is used in each display. For the range of sub-seafloor V_P interval velocities determined along this profile, an assumption of free-floating hydrate (bottom) results in an almost uniform increase of approximately five percentage points in the hydrate fraction along the entire profile.

It should be emphasized that the difference of approximately five percentage points of hydrate fraction predicted by these two theories applies only when the V_P interval velocity is in the range of 1550 m/s to 1800 m/s, as can be seen by comparing the suite of curves for Model A on Figure 2 of Appendix D with the corresponding suite of curves for Model B on Figure 3 in that same paper. For values of V_P greater than 1800 m/s, a free-floating-hydrate morphology will result in an increase of more than five percentage points in the hydrate fraction, sometimes an increase as large as seven or eight percentage points.

11. WELL LOG DATA

We did not acquire digital log data for this study. The only log data that we could locate that measured properties of the hydrate stability zone were gamma-ray, resistivity, conductivity, temperature, and rate-of-penetration data. We created a consistent petrophysical definition of the hydrate-bearing interval at each well by extracting only two log curves from each log suite: (1) the gamma-ray response and (2) a consistent depth-of-investigation resistivity curve, with this latter curve displayed by a linear scale ranging from 0 to 2 ohm-m.

11.1. WELL LOG DATA: TYPHOON FIELD AREA (STUDY SITE 1)

Green Canyon lease blocks surrounding Typhoon Field (Block GC237) are outlined on Figure 2. Unfortunately, many wells in the Typhoon Field area were drilled without the use of logging while drilling (LWD) technology, with the result that:

a. The acquisition of log data often started at depths below the base of the hydrate stability zone, or
b. The hydrate interval was not logged until several days after the interval was drilled and some hydrate had dissociated near the well, or
c. The resistivity sonde sometimes exhibited unacceptably poor sensitivity across intervals of near-seafloor sediment.

Superimposed on this map as lettered red triangles are the locations of five wells (A, B, C, D, E) where log data were acquired that could be used to estimate hydrate concentration.

Well log cross sections along the profiles of Typhoon-area calibration wells B, C, A and wells B, D, E are displayed as Figures 19 and 20, respectively. Because these log data were acquired using LWD technology within a few minutes of the bit penetrating each logged depth, the data should define in situ resistivity before any significant hydrate dissociation has occurred. The base of the hydrate stability zone labeled (BHSZ(90%)) drawn on each profile was determined using the model that Milkov and Sassen (2001) developed for a natural gas having 90.4% methane (Figure 21). This Milkov/Sassen model is based on the chemistry of gases found in nearby Block GC185 and on geothermal gradients local to our study area. Also noted on the log cross-sections is a second estimate, labeled BHSZ(R), of the depth of the BHSZ. The BHSZ(R) marks a decrease in formation resistivity that: (1) can be interpreted as the BHSZ, and (2) is “close to” the depth BHSZ(90%) predicted by the Milkov and Sassen model.

The Milkov/Sassen estimation of the sub-seafloor thickness of the hydrate stability zone is shown by the three solid-line curves on Figure 21. These curves show that the BHSZ boundary moves deeper as the amount of methane decreases in the local natural gases and is replaced by a greater percentage of higher molecular weight hydrocarbon gases (ethane, butane, propane). We have added a fourth dash-line curve to this Milkov/Sassen model to represent (approximately) a natural gas that has 85% methane, a gas chemistry suggested as appropriate for this area by scientists at the Minerals Management Service (private communication).

On Figures 19 and 20, the upper boundary of the BHSZ labeled BHDZ represents the inferred base of the hydrate depletion zone. Above this horizon, hydrate is absent through chemical interactions with sulfates migrating down from the seawater (sulfate reduction zone) or by thermally induced dissociation caused by spin-off eddies from the warm Loop Current, or because of other biological, chemical, and physical processes.

Zones on the resistivity logs that have resistivities greater than 1 ohm-m are shaded gray on the well log cross-section profiles to define intervals that possibly have increased hydrate concentration. Several intervals where the gamma-ray response implies an increase in grain size are shaded yellow on the gamma-ray curves and indicate quasi-reservoir-quality lithofacies. Blue-shaded layers define units where increased resistivity (shaded red) indicates a possible increase in hydrate concentration internal to these larger-grain facies.

These blue/red zones could be candidates for hydrate production tests because they are not only a preferred reservoir facies but also represent a local increase in the concentration of hydrate. Important observations that can be made upon examining the well log data shown on Figures 19 for the Typhoon Field and associated areas are:

a. The hydrate-bearing interval beneath the Typhoon Field area spans a depth interval of approximately 460 m (~1,500 ft).
b. The resistivity relationships imply the hydrate concentration within the zone of hydrate stability ranges from about 20 to 40% of the available pore space.

11.2. WELL LOG DATA: GENESIS FIELD AREA (STUDY SITE 2)

Lease blocks around Genesis Field (Blocks GC205 and GC161) are outlined in Figure 2. The red triangles define wells where log data exist that are appropriate for determining hydrate concentration. There are more hydrate-calibration wells (13) in the vicinity of Genesis Field than near Typhoon Field (5) because more wells were drilled in the area of Genesis Field after the early 1990's when LWD logging technology was widely used by GOM operators.

These numerous calibration wells allow a variety of well-log cross-section profiles to be made across the Genesis Field area. We show west-to-east profiles traversing wells A, B, C as Figure 22, along wells D, E, F, G as Figure 23, and along wells H, I, L, J as Figure 24. The BHSZ(90%) horizons drawn on these profiles were defined in the same manner as was done at Typhoon Field using the Milkov and Sassen (2001) model defined in Figure 21. Depths BHSZ(R) again indicate decreases in formation resistivity that: (1) may indicate the base of stable hydrate, and (2) are "close to" the BHSZ(90%) prediction of the BHSZ boundary provided by the Milkov and Sassen (2001) model. In interpreting these resistivity profiles, we used the following guidelines:

a. A resistivity value ≤1 ohm-m indicates a hydrate concentration of less than 20%.
b. Resistivities greater than 1 ohm-m indicate hydrate concentrations in excess of 20%, with a resistivity of 2 ohm-m representing a hydrate concentration of almost 60%.
c. Reduced gamma-ray readings indicate larger-grain sediment (shaded yellow), and within some of these larger-grain intervals are units (shaded blue/red) with relatively high hydrate concentration.

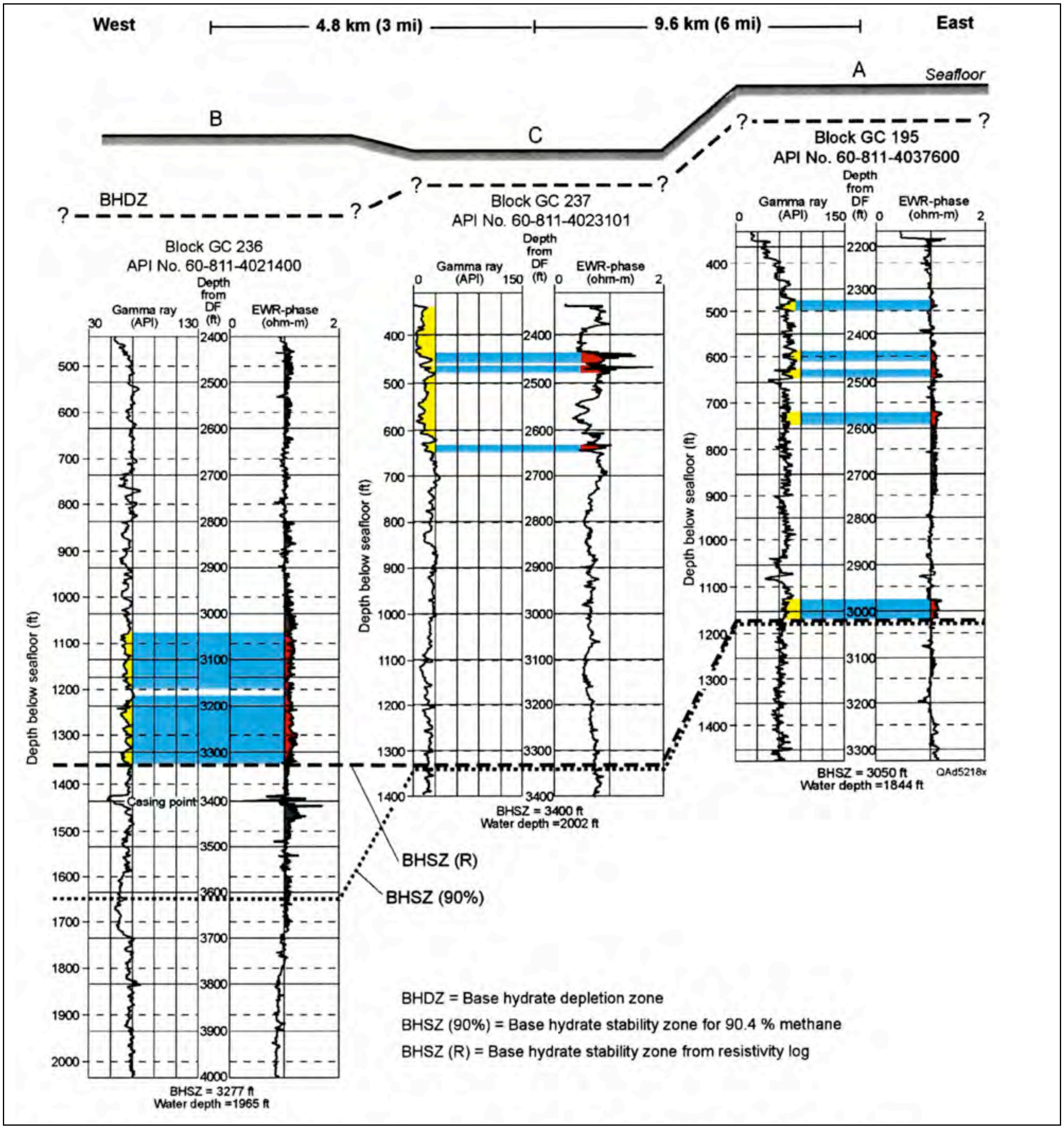

Figure 19. Well log cross section across calibration wells B, C, A, Typhoon Field area. There is a low concentration of hydrate along this profile. Well locations defined on Figure 2. The BHSZ(90%) depth labeled below each log suite is the depth of the base of the hydrate stability zone associated with the 90.4% methane curve from Figure 21. At each well, the BHSZ(R) horizon is drawn at a resistivity anomaly that is “close to” the depth coordinate suggested by the 90.4% methane curve. Gray zones emphasize intervals where resistivity exceeds 1 ohm-m. Yellow zones indicate possible larger-grain facies. Red identifies units that have both increased grain size and increased resistivity.

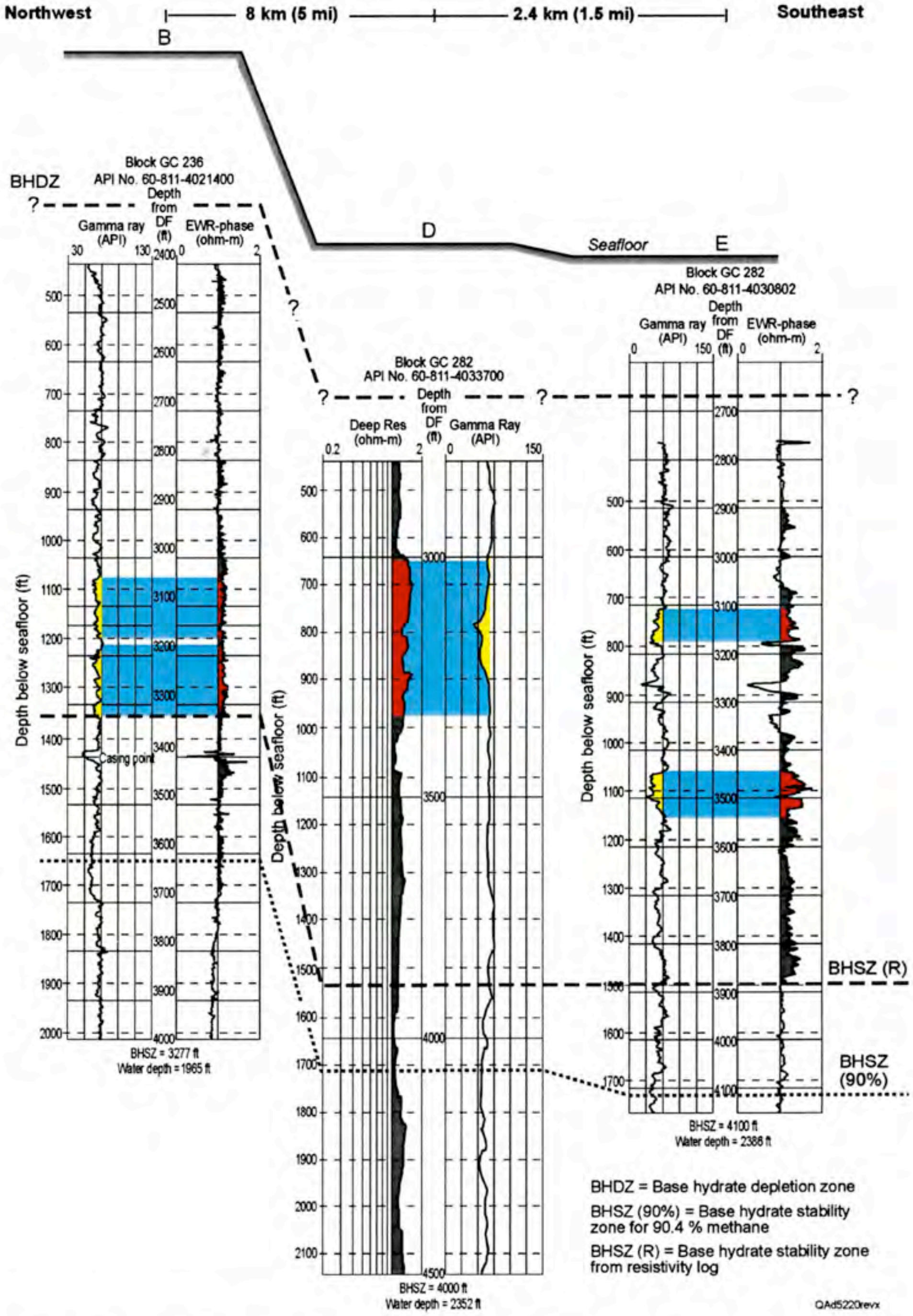

Figure 20. Well log cross section along the profile of calibration wells B, D, E, Typhoon Field area. Well locations defined in Figure 2. Hydrate concentration increases along the southeast part of this profile. At each well, the BHSZ(R) horizon is drawn at a resistivity anomaly that is “close to” the depth coordinate suggested by the 90.4% methane curve. Gray zones emphasize intervals where resistivity exceeds 1 ohm-m. Yellow zones indicate possible larger-grain facies. Red identifies units that have both increased grain size and increased resistivity

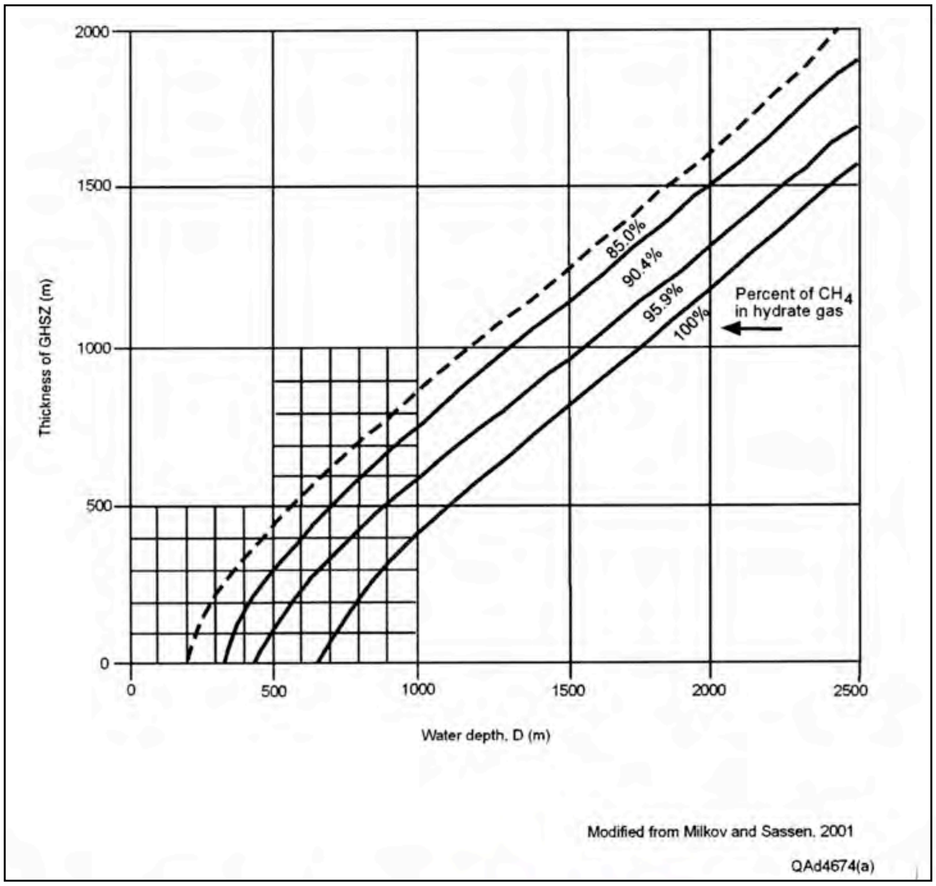

Figure 21. Thicknesses of hydrate stability zones for various water depths and gas chemistries. The three solid-line curves were developed by Milkov and Sassen (2001) and are based on gas chemistry from Block GC185 and on geothermal gradients local to our Green Canyon study area. The dash-line curve is our approximation of the behavior of the thickness of the stability zone for a natural gas that has 85% methane, a gas chemistry favored by some scientists at the Minerals Management Service. We added a detailed coordinate grid that covers the range of water depths encountered across our research area.

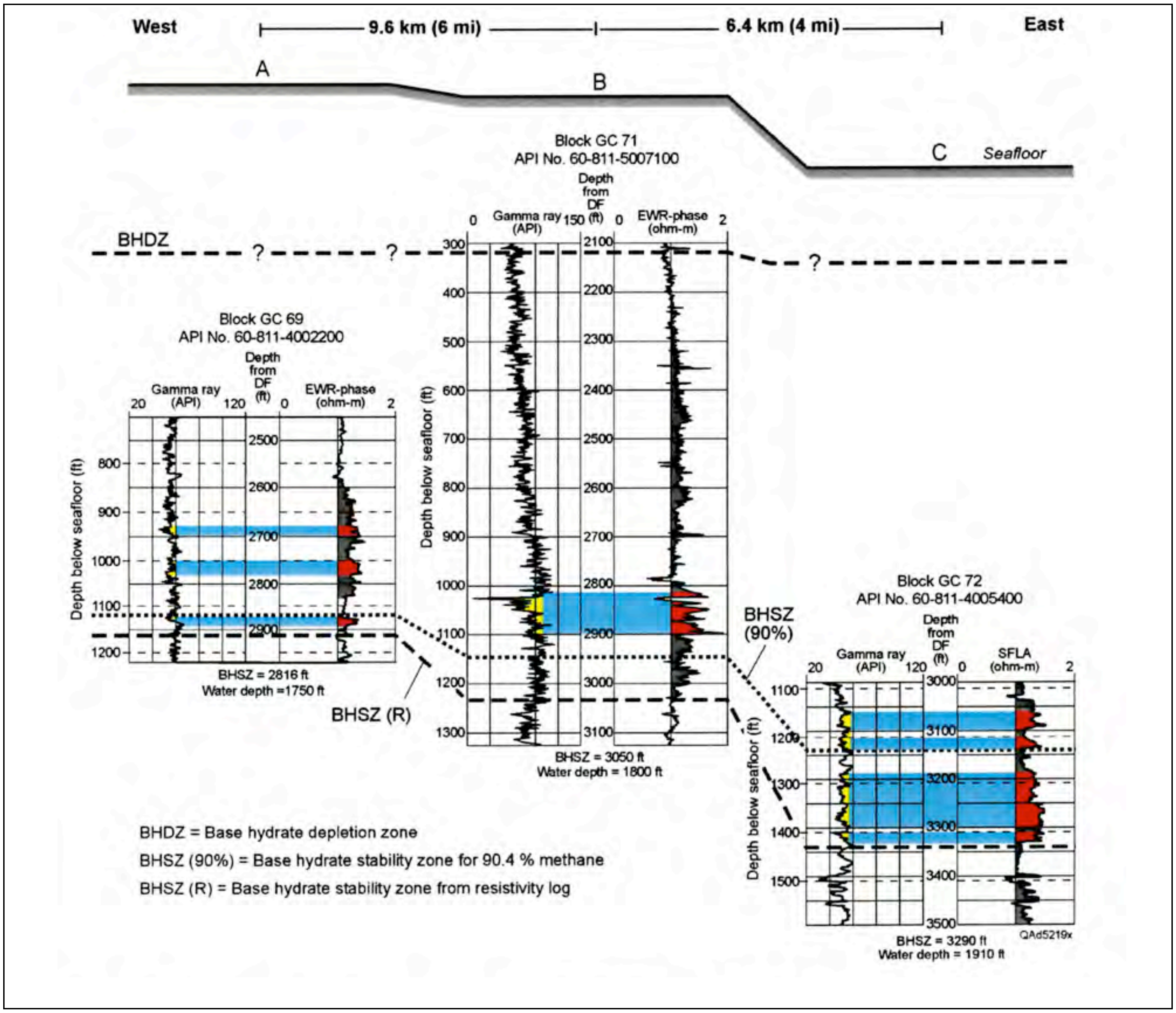

Figure 22. Well log cross section along the profile of calibration wells A, B, C, Genesis Field. There is a robust hydrate system along this profile. Well locations are defined on Figure 2. The BHSZ(90%) depth labeled below each log suite is the depth of the base of the hydrate stability zone associated with the 90.4% methane curve from Figure 21. At each well, the BHSZ(R) horizon is drawn at a resistivity change that is "close to" the depth coordinate suggested by the 90.4% methane curve. Gray zones emphasize intervals where resistivity exceeds 1 ohm-m. Yellow zones indicate possible larger-grain facies. Red identifies units that have both increased grain size and increased resistivity.

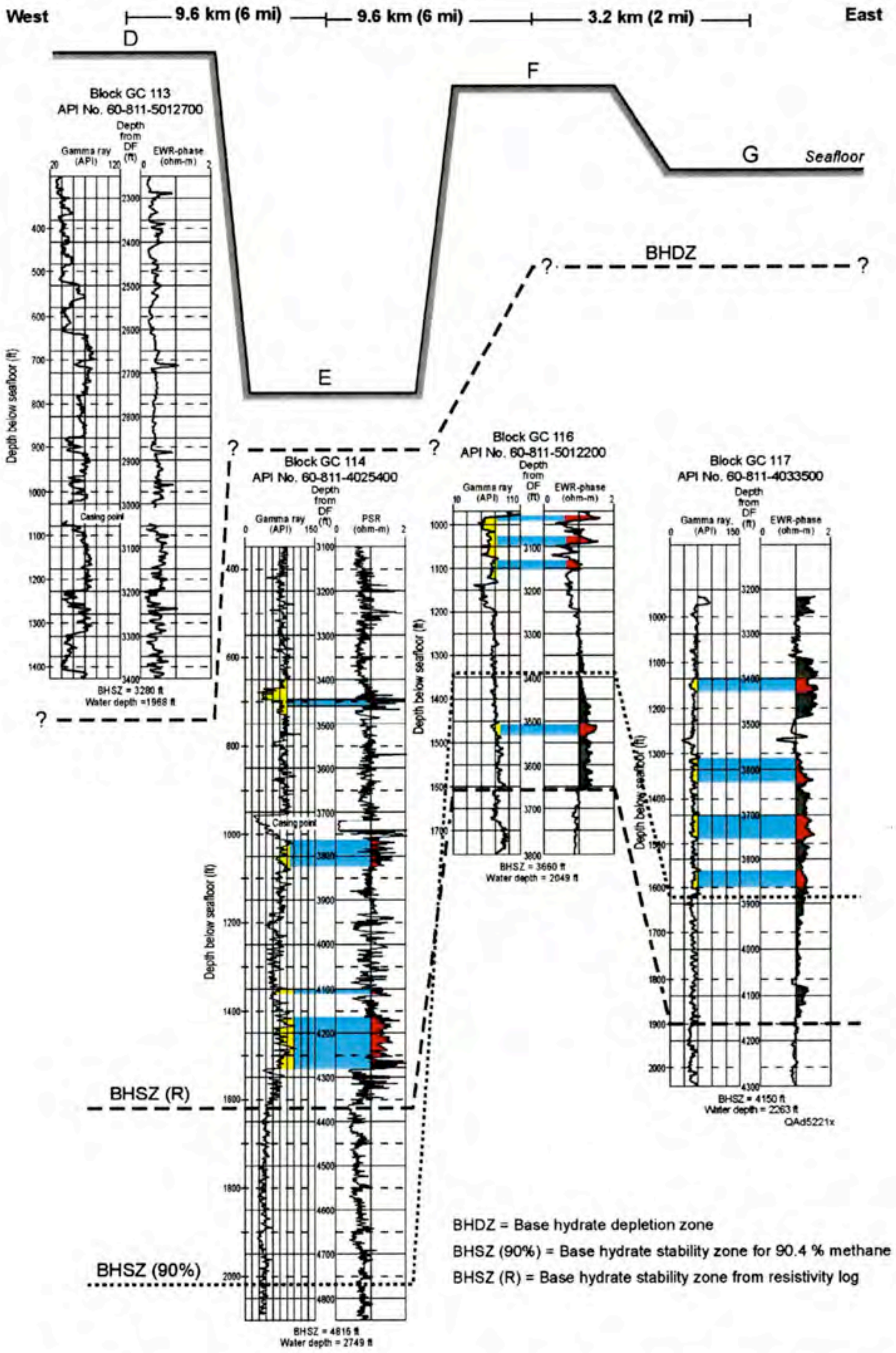

Figure 23. Well log cross section along the profile of calibration wells D, E, F, G, Genesis Field. This profile shows that there is no hydrate at well D but identifies several hydrate intervals that enlarge to the east. Well locations are defined on Figure 2. At each well, the BHSZ(R) horizon is drawn at a resistivity change that is “close to” the depth coordinate suggested by the 90.4% methane curve. Gray zones emphasize intervals where resistivity exceeds 1 ohm-m. Yellow zones indicate possible larger-grain facies. Red identifies units that have both increased grain size and increased resistivity.

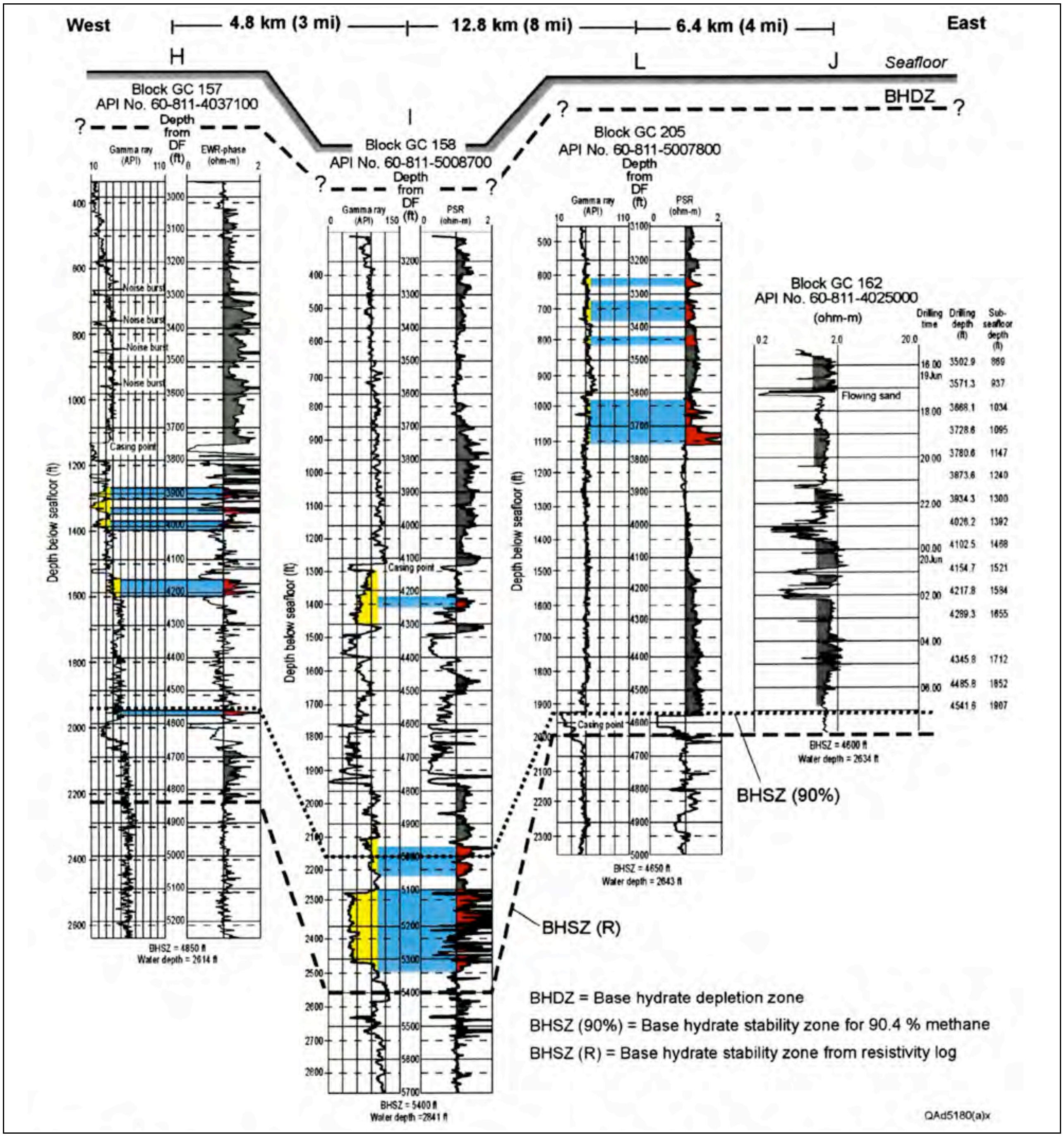

Figure 24. Well log cross section along the profile of calibration wells **H**, **I**, **L**, **J**, Genesis Field. This profile traverses thick hydrate sections. Well locations are defined on Figure 2. At each well, the BHSZ(R) horizon is drawn at a resistivity change that is “close to” the depth coordinate suggested by the 90.4% methane curve. Gray zones emphasize intervals where resistivity exceeds 1 ohm-m. Yellow zones indicate possible larger-grain facies. Red identifies units that have both increased grain size and increased resistivity.

These log data imply that a more robust hydrate system exists in the vicinity of Genesis Field than what was found across the Typhoon area. Important observations that can be made by examining the well log data for the Genesis Field and associated areas are:

1. The hydrate interval varies from a thickness of about 365 m (~1,200 ft) at wells A and B (Figure 22) to about 760 m (~2,500 ft) at well I (Figure 24). Well D (Figure 23) is unusual in that the resistivity response indicates that no hydrate is present.
2. Hydrate occupies 20 to 40% of the pore volume over most of the interval between the boundaries marked BSRZ and BHSZ.

Numerous depositional units, some as thick as approximately 50 ft (~15 m), appear to have hydrate concentrations that exceed 0%.

11.3. AVAILABLE DATA: GC240 (STUDY SITE 3)

No well log data existed local to Study Site 3, GC 240 (Figure 2). Hydrate concentration had to be estimated across this third site from seismic interval velocities only. For this purpose, we determined interval velocities along the two OBC profiles (284 and 288) shown on Figure 2a that traversed Block GC240 from west to east. Our analyses of the P-P and P-SV data acquired along these two profiles are exhibited as Figures 25 and 26. Our velocity inversion procedure led to the conclusion that there was a small area of robust hydrate concentration in Block GC239 local to OBC profile 288; the bright red interval shown for this profile on the map display of Figure 16.

Figures 25a and 26a show the P-P and P-SV images side-by-side for ease of comparison, followed by illustrations of the interpreted depth-equivalent horizons in P-P image space and P-SV image space, and the V_P and V_S interval velocities determined along the profile. Figures 25b and 26b repeat the first page with the exception that the V_S velocity panel (lower right on the bottom row) is replaced with a display of the estimated hydrate concentration along the profile. The boundaries of blocks GC239 and GC240 are indicated on parts a and b of Figure 25 (OBC line 288) to aid in identifying the attributes of the seismic data across these two lease blocks.

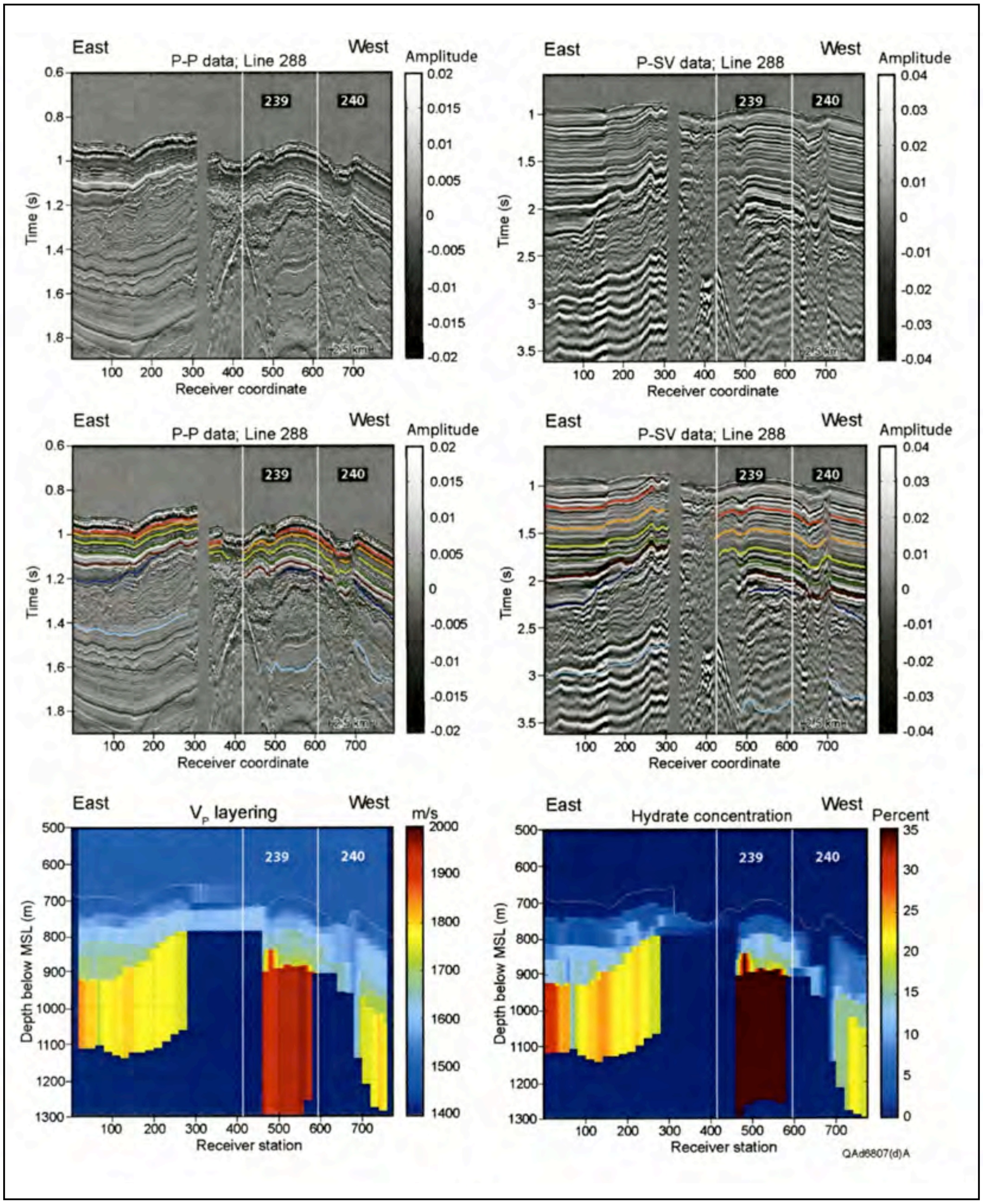

Figure 25a. Critical information developed along profile 288, Study Site 3 (Block GC240). Top row shows uninterpreted P-P and P-SV images. Center row displays interpreted images showing depth-equivalent horizons. Bottom presents V_P layer velocities (left) and V_S layer velocities (right). The boundaries of blocks GC239 and GC240 are marked on each data panel.

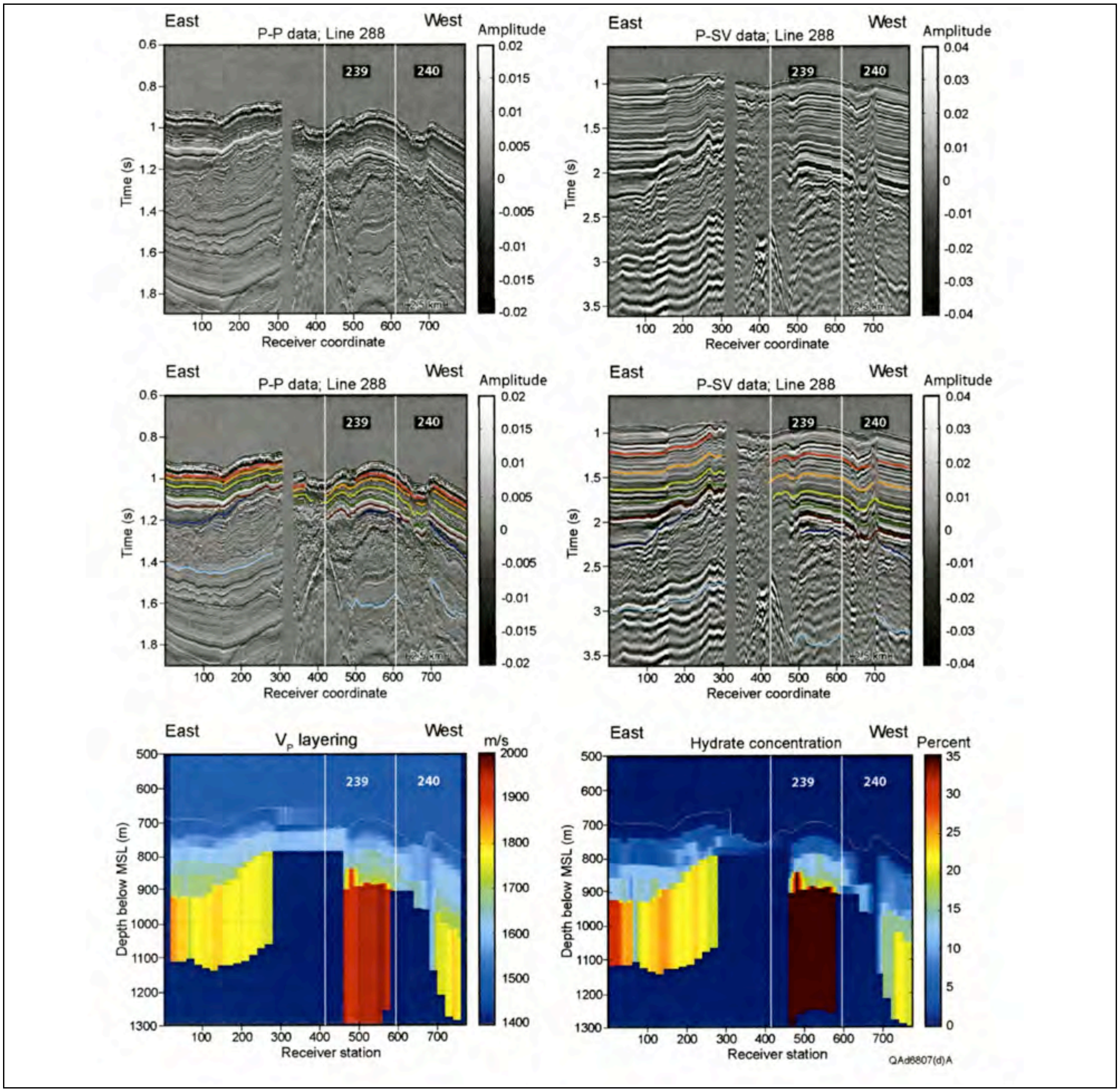

Figure 25b. Critical information developed along profile 288, Study Site 3 (Block GC240). Top row shows uninterpreted P-P and P-SV images. Center row displays interpreted images showing depth-equivalent horizons. Bottom presents V_P layer velocities (left) and estimate of hydrate concentration expressed as "percent of pore space occupied by hydrate" (right). The boundaries of blocks GC239 and GC240 are marked on each data panel.

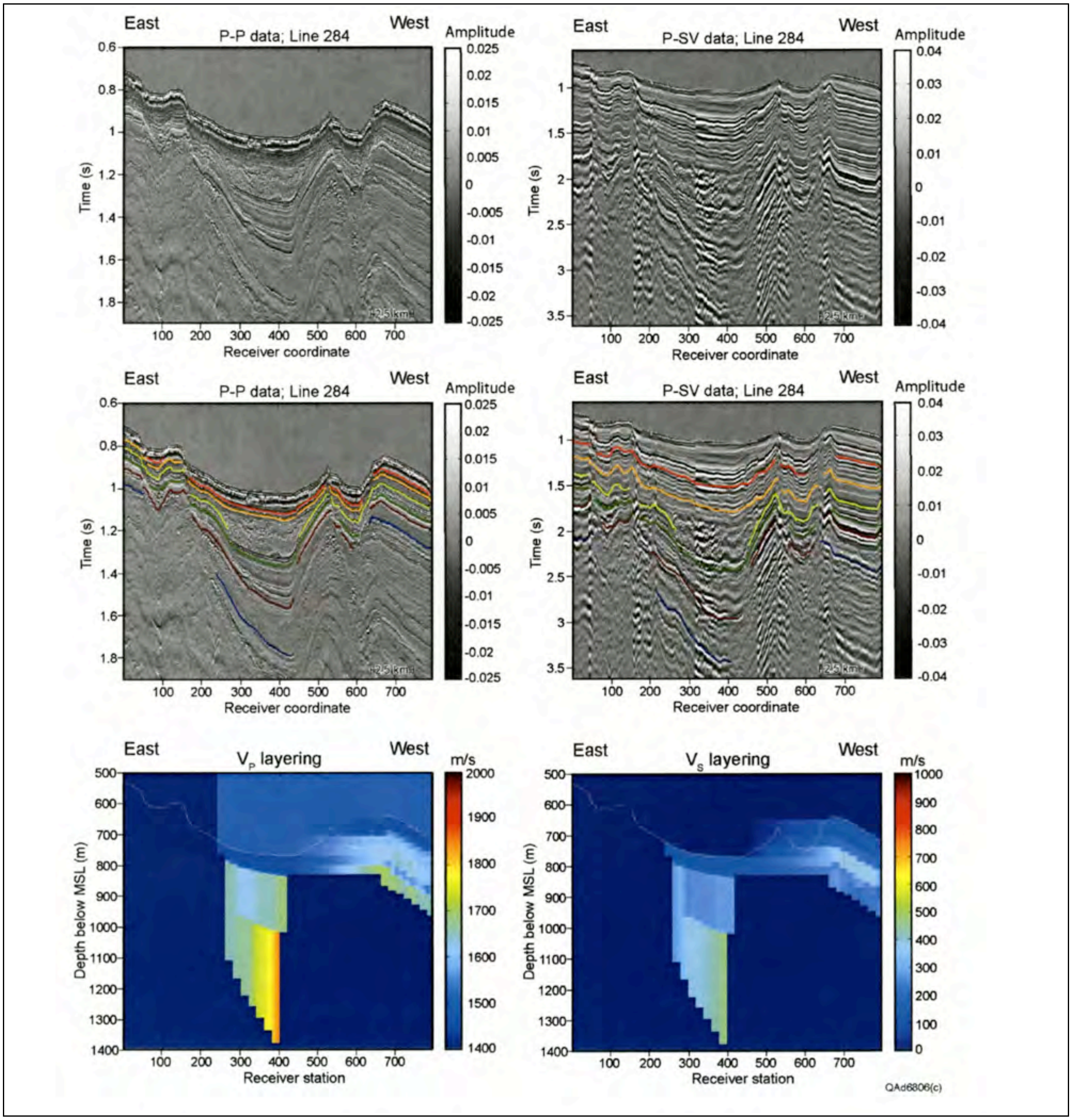

Figure 26a. Critical information developed along profile 284, Study Site 3 (Block GC240). Top row shows uninterpreted P-P and P-SV images. Center row displays interpreted images showing depth-equivalent horizons. Bottom presents VP layer velocities (left) and VS layer velocities (right).

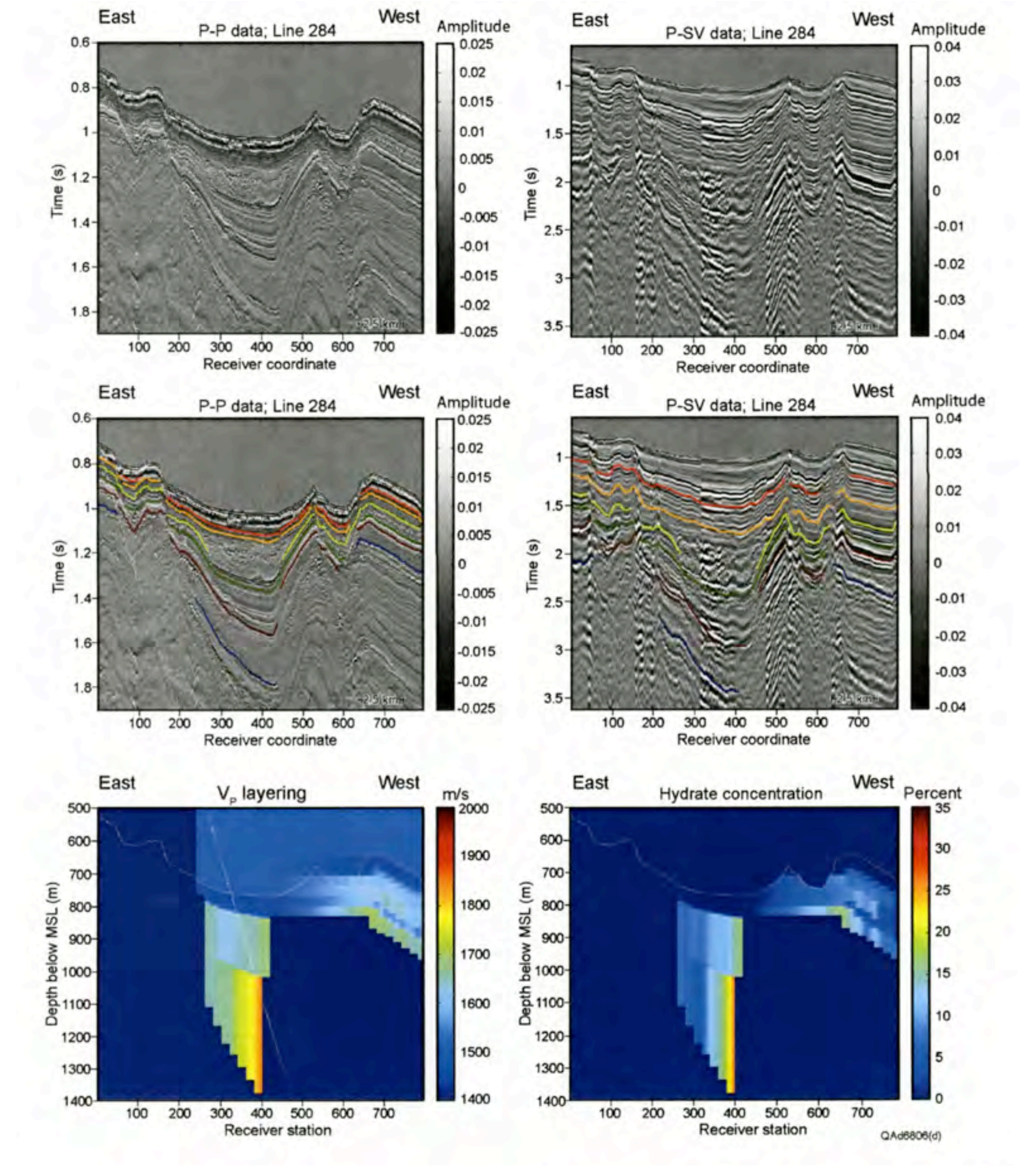

Figure 26b. Critical information developed along profile 284, Study Site 3 (Block GC240). Top row shows uninterpreted P-P and P-SV images. Center row displays interpreted images showing depth-equivalent horizons. Bottom presents V_P layer velocities (left) and estimate of hydrate concentration expressed as “percent of pore space occupied by hydrate” (right).

12. SUMMARY AND CONCLUSIONS

Assessment of gas hydrate within the shallow stratigraphic section of deep water areas has been a problem without having direct evidence provided by drilling and associated core samples. The use of four-component ocean-bottom-cable (4-C OBC) technology offers an alternative to standard surface-towed 3D-seismic technology for indirect and remotely sensed evaluation of the geologic configuration of the subsurface and for investigating the occurrence of gas hydrate that occurs in the shallow stratigraphic section. This technology involves a surface acoustic source (usually an air-gun) and long lines of ocean bottom sensors that are capable of recording three-dimensional vector motion of the seafloor with 3-component geophones, as well as scalar pressure variations with hydrophones. The advantage of the 4-C OBC data-collection is that standard compressional wave data (P-P), as well as converted shear wave data (P-SV), can be acquired simultaneously as backscatter from subsurface reflection horizons. These data are acquired in approximately the 10-200 Hz frequency range. From a regional grid of data acquired by WesternGeco in the northern Gulf of Mexico, outer-shelf to upper slope depth range, this study was given access to 4-C OBC data associated with three sites within the Minerals Management Service’s (MMS) Green Canyon Lease Area: GC 204, GC 237, and GC 240. Direct observations from manned submersible dives confirm gas hydrate deposits as surface exposures at two of these sites, GC 204 and GC 237. Only the GC 240 site has no direct confirmation of gas hydrate at the modern seafloor.

The overall objective of the MMS-sponsored research project described in this report was to investigate the use of 4-C OBC data from our three study sites for identifying properties within the shallow stratigraphic section that relate to the presence and amount of gas hydrate. One of the most significant contributions made by this research project was the development of methodologies of data reduction and analysis to meet this project objective. As an additional dataset, high resolution seismic profiles (chip sonar) were acquired along the 4-C OBC lines at each of the key sites. Collected by an autonomous underwater vehicle (AUV), the chirp data have a frequency of about 1-10 kHz. Comparisons were made of AUV data compressional wave data (P-P) and 4C-OBC converted shear wave data (P-SV) for resolution and imaging of shallow subsurface. Using data processing methodologies described in this report and in the scientific paper by Backus et al. (2006) of Appendix B, our research demonstrated that low frequency converted-shear (P-SV) representations of the subsurface using 4-C OBC seismic data provided spatial resolution of shallow stratigraphy equivalent to, and sometimes better than, the resolution achieved with high frequency chirp sonar data.

The GC 204 site is adjacent to Chevron’s Genesis Field, and BHP-Billiton’s Typhoon Field is adjacent to our GC 237 site. Both of these fields had well logs available for use in our study. Well log data were extremely important to this study for calibrating acoustic properties of the subsurface to rock properties. Most well log data spanned at least part of the gas hydrate stability interval and were therefore important calibration data used to make estimations of gas hydrate concentrations, especially the resistivity log measurements. Only the GC 240 site did not have supporting well log data from an adjacent oil and/or gas field.

A ray tracing method was used to adjust the thicknesses of equivalent stratigraphic intervals derived as separate P-P and P-SV images. Since representations of the subsurface are different using P-P as compared to P-SV data, the ray tracing method was employed to adjust layer thickness and interval velocities (Vp and Vs) so that other datasets such as those from resistivity logs could be compared to converted shear wave data (P-SV) images of the subsurface. The interval from the seafloor to the base of the hydrate stability zone was analyzed at each of our three study sites. Using this methodology, velocity layers or stratigraphic units were defined as a function of depth below the seafloor.

A key to interpreting the presence of gas hydrate and perhaps bubble-phase gas in stratigraphic intervals defined by velocity data was the integration of several primary datasets: (1) resistivity (well log data), (2) interval velocity, and (3) seismic images (P-P and P-SV). However, the relationships between gas hydrate occurrence/concentration with resistivity data, as well as the relationships between seismic propagation velocity and gas hydrate occurrence/concentration, were found to be non-unique. Spatial variations in host sediment properties and the nature of gas hydrate (e.g., small crystals in pore spaces to massive layers) within the hydrate stability zone accounted for much of the uncertainty in interpretations. By combining gas hydrate-dependent geophysical data (e.g., velocity estimates and formation resistivity measurements), predictions of gas hydrate concentrations were constrained. A rock physics model that related seismic velocity to gas hydrate concentration was used (methodology described in Appendix C). This model accounted for the uncertainty of all parameters used in the calculation of gas hydrate concentration.

Estimates of gas hydrate were made for calibration wells using primary data from resistivity logs and seismic velocity estimates (Vp and Vs) for given stratigraphic intervals defined from the ray tracing method. Depth dependent increases in Vp and Vs were incorporated and used in the gas hydrate assessment employing normal sediment compaction theory. Stratigraphic intervals within the gas hydrate stability zone where both interval velocities and resistivity values were greater than those expected with normal compaction were interpreted as zones of hydrate concentration. Using a probability function described in this report, the amount of pore space occupied by gas hydrate was calculated. At intervals of 10 receiver stations (250 m) along each OBC profile, velocity layering and estimated gas hydrate concentrations were calculated. Our results indicate: (1) gas hydrate was pervasive throughout the sites we studied in the Green Canyon lease area; (2) concentrations of gas hydrate ranged from zero to one-third of available pore space, but values of 10-20% of the pore volume were typical of most areas; (3) free-gas was found immediately underlying the base of the gas hydrate stability zone (not easily determined from resistivity logs alone); and, (4) the estimation of gas hydrate stability zone thickness from resistivity logs alone produced an overestimation of gas hydrate zone thickness and amount present.

Applying our analysis methodologies to 4-C OBC data calibrated to well log data in Typhoon Field area (lease blocks surrounding GC 237) the following conclusions can be drawn:

1. Gas hydrate occurs in the shallow subsurface throughout the Typhoon Field area and it manifests itself at the seafloor in GC 237 where flux rates of gas and fluids toward the modern ocean bottom eliminate the sulfate reducing zone where gas hydrate does not form.
2. Depth of the hydrate-bearing stratigraphic interval beneath the Typhoon Field is approximately 460 m.

3. Resistivity relationships indicate that gas hydrate concentrations within the approximately 460 m thick zone of hydrate stability range from approximately 20-40 % of available pore space.

Our results from analyzing 4-C OBC seismic data and well logs from the Genesis Field (lease blocks surrounding GC 204) lead to the following conclusions:

1. Data suggest that the shallow subsurface associated with the Genesis Field supports more gas hydrate than the Typhoon Field area.
2. The gas hydrate stability zone ranges in thickness across the Genesis Field area from approximately 365 m to 760 m.
3. Within the variable zone of gas hydrate stability, we estimate that 20-40 % of the pore space is filled with gas hydrate.

Because no well logs were available for our third study site, GC 240, gas hydrate concentrations were interpreted from seismic interval velocities only. The following conclusions can be stated:

1. The gas hydrate stability zone is highly variable and ranges from less than 800 to nearly 1400 m.
2. Compression of the hydrate stability zone is related to a prominent expulsion center in the study area where fluid/gases and heat are transported toward the modern seafloor. This process moves the base of the hydrate stability zone (BHSZ) stratigraphically upward.
3. Estimates of gas hydrate in the pore space of host sediments based on velocity data alone range from approximately 12 to 30% of the pore space.

13. REFERENCES

Backus, M.M., P.E. Murray, B.A. Hardage, and J. Graebner. 2006. High-resolution multicomponent seismic imaging of deepwater gas-hydrate systems. The Leading Edge 25:578-596.

Diegel, F.A. and R.W. Cook. 1990. Palinspastic reconstruction of salt-withdrawal growth-fault systems, northern Gulf of Mexico. Geological Society of America Abstracts with Programs 22:A48.

Diegel, F.A., J.F. Karlo, D.C. Schuster, R.C. Shoup, and P.R. Tauvers. 1995. Cenozoic structural evolution and tectono-stratigraphic framework of the northern Gulf coast continental margin. In: Jackson, M.P.A., D.G. Roberts, and S. Snelson, eds. Salt tectonics: A global perspective. American Association of Petroleum Geologists Memoir 65:109-151.

Domenico, S.N. 1976. Effect of brine-gas mixture on velocity in an unconsolidated sand reservoir. Geophysics 41:882-894.

Ferrell, R.E., Jr. and P. Aharon. 1994. Mineral assemblages occurring around hydrocarbon vents in the northern Gulf of Mexico. Geo-Marine Letters 14:74-80.

McBride, B.C. 1995. Evaluation of subsalt petroleum potential using structural restorations. AAPG Annual Convention Program 4:62A.

McBride, B.C. 1996. Geometry and evolution of allochthonous salt and its impact on petroleum systems, northern Gulf of Mexico Basin: studies in three- and four-dimensional analysis, Ph.D. Thesis, University of Colorado, Boulder, CO. 276 pp.

McDonald, I.R., N.L. Guinasso, Jr., R. Sassen, J.M. Brooks, L. Lee, and K.T. Scott. 1994. Gas hydrate that breaches the sea floor on the continental slope of the Gulf of Mexico. Geology 22:699-792.

Milkov, A.V. and R. Sassen. 2001. Estimate of gas hydrate resource, northwestern Gulf of Mexico continental slope. Marine Geology 179:71-83.

Peel, F.J., C.J. Travis, and J.R. Hossack. 1995. Genetic structural provinces and salt tectonics of the Cenozoic offshore U.S. Gulf of Mexico: a preliminary analysis. In: Jackson, M.P.A., D.G. Roberts, and S. Snelson, eds. Salt tectonics: A global perspective. American Association of Petroleum Geologists Memoir 65:153-175.

Ratcliff, D.W. 1993. New technologies improve seismic images of salt bodies. Oil and Gas Journal 91:41-49.

Ritger, S., B. Carson, and E. Suess. 1987. Methane-derived authigenic carbonates formed by subduction-induced pore-water expulsion along the Oregon/Washington margin. Geological Society of America Bulletin 98:147-156.

Roberts, H.H. 2001. Fluid and gas expulsion on the northern Gulf of Mexico continental slope: Mud-prone to mineral-prone responses. In: Paull, C.K. and W.P. Dillon, eds. Natural gas hydrates: Occurrence, distribution, and detection. Geophysical Monograph 124:145-161.

Roberts, H.H. and R.C. Carney. 1997. Evidence of episodic fluid, gas, and sediment venting on the northern Gulf of Mexico continental slope. Economic Geology 92:863-879.

Roberts, H.H., D.J. Cook, and M.K. Sheedlo. 1992a. Hydrocarbon seeps of the Louisiana continental slope: Seismic amplitude signature and sea floor response. Transactions 42nd Annual Gulf Coast Association of Geological Societies Convention, p. 349-362.

Roberts, H.H., P. Aharon, and M.M. Walsh. 1992b. Cold-seep carbonates of the Louisiana continental slope-to basin floor. In: Rezak, R. and D. Lavoie, eds. Carbonate microfabrics. Berlin: Springer-Verlag. Pp. 95-104.

Roberts, H.H., B.A. Hardage, W.W. Shedd, and J. Hunt Jr. 2006. Seafloor reflectivity—An important seismic property for interpreting fluid/gas expulsion geology and the presence of gas hydrate. The Leading Edge 25:620-628.

Rowan, M.G. 1995. Structural styles and evolution of allochthonous salt, central Louisiana outer shelf and upper slope. In: Jackson, M.P.A., D.G. Roberts, and S. Snelson, eds. Salt tectonics: A global perspective. American Association of Petroleum Geologists Memoir 65:199-228.

Sava, D. and B.A. Hardage. 2006. Rock physics characterization of hydrate-bearing deepwater sediments. The Leading Edge 25:616-619.

Sava, D. and B. Hardage. 2008. Rock-physics models for gas-hydrate systems associated with marine sediments. In: Collett, T., A. Johnson, C. Knapp, and R. Boswell, eds. Natural Gas Hydrates: Energy Resource Potential and Associated Geologic Hazards. AAPG Special Publication, 2008.

Tarantola, A. 1987. Inverse problem theory. Amsterdam, Netherlands. Elsevier Science B. V.

Vendeville, B.C. and M.P.A. Jackson. 1992. The rise of diapirs during thin-skinned extension. Marine and Petroleum Geology 9:331-352.

Walton, K. 1987. The effective elastic moduli of a random packing of spheres. J. Mech. Phys. Solids 35:213-226.

Worral, D.M. and S. Snelson. 1989. Evolution of the northern Gulf of Mexico, with emphasis on Cenozoic growth faulting and the role of salt. In: Bally, A.W. and A.R. Palmer, eds. The geology of North America: An overview. Geological Society of America Decade of North American Geology A:97-138.

APPENDIX A

SEAFLOOR REFLECTIVITY—AN IMPORTANT SEISMIC PROPERTY FOR INTERPRETING FLUID/GAS EXPULSION GEOLOGY AND THE PRESENCE OF GAS HYDRATE

Seafloor reflectivity—An important seismic property for interpreting fluid/gas expulsion geology and the presence of gas hydrate

Harry H. Roberts, Louisiana State University, Baton Rouge, USA
Bob A. Hardage, Bureau of Economic Geology, Austin, USA
William W. Shedd and Jesse Hunt Jr., Minerals Management Service, New Orleans, USA

A bottom-simulating reflection (BSR) is a seismic reflectivity phenomenon that is widely accepted as indicating the base of the gas-hydrate stability zone. The acoustic impedance difference between sediments invaded with gas hydrate above the BSR and sediments without gas hydrate, but commonly with free gas below, are accepted as the conditions that create this reflection. The relationship between BSRs and marine gas hydrate has become so well known since the 1970s that investigators, when asked to define the most important seismic attribute of marine gas-hydrate systems, usually reply, "a BSR event." Research conducted over the last decade has focused on calibrating seafloor seismic reflectivity across the geology of the northern Gulf of Mexico (GoM) continental slope surface to the seafloor. This research indicates that the presence and character of seafloor bright spots (SBS) can be indicators of gas hydrates in surface and near-surface sediments (Figure 1). It has become apparent that SBSs on the continental slope generally are responses to fluid and gas expulsion processes. Gas-hydrate formation is, in turn, related to these processes. As gas-hydrate research expands around the world, it will be interesting to find if SBS behavior in other deepwater settings is as useful for identifying gas-hydrate sites as in the GoM.

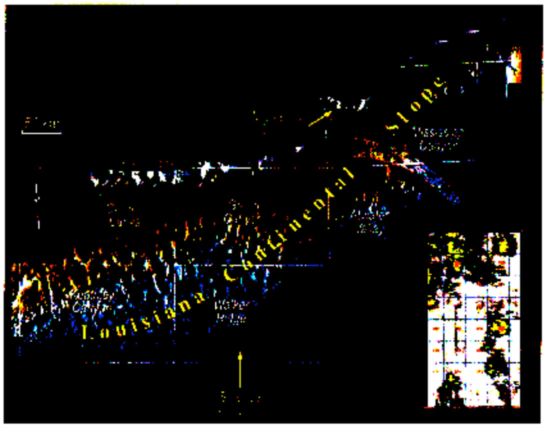

Figure 1. Computer-enhanced multibeam bathymetry image of the northern Gulf of Mexico continental slope showing a small sector of the Mississippi Canyon lease area and its seafloor bright spots (SBS) or local areas of high seismic seafloor reflectivity across the continental slope surface.

Research background. Joint research with the Minerals Management Service (MMS), through a cooperative agreement with the Coastal Marine Institute at Louisiana State University, has resulted in a study using the university's GoM-wide 3D seismic data coverage. Seafloor reflectivity across the northern GoM's continental slope has been mapped, and numerous SBS areas like those illustrated in Figure 1 have been identified. Through research projects funded primarily by MMS and NOAA, manned submersible dives on many SBS sites have provided direct observations and samplings to calibrate the actual geologic character of the seafloor to seismic reflectivity. These investigations have led to the model illustrated in Figure 2 which defines three qualitative ranges in the rates of fluid and gas expulsion coupled to geologic-biologic response at the seafloor. These reflector-anomaly sites also indicate three gas-hydrate domains that can be associated with these seafloor reflectivity behaviors.

The block diagram shown in Figure 2 illustrates that fluids and gases have various migration pathways to the modern seafloor and that delivery rates, as well as fluid-gas composition, impact geologic response on the continental slope surface. Deep-cutting faults that intersect the overpressured zone frequently form the migration routes for hydrocarbons, formation fluids, and sometimes fluidized sediments. In addition, considerable heat can accompany these products, which eliminates the gas-hydrate stability

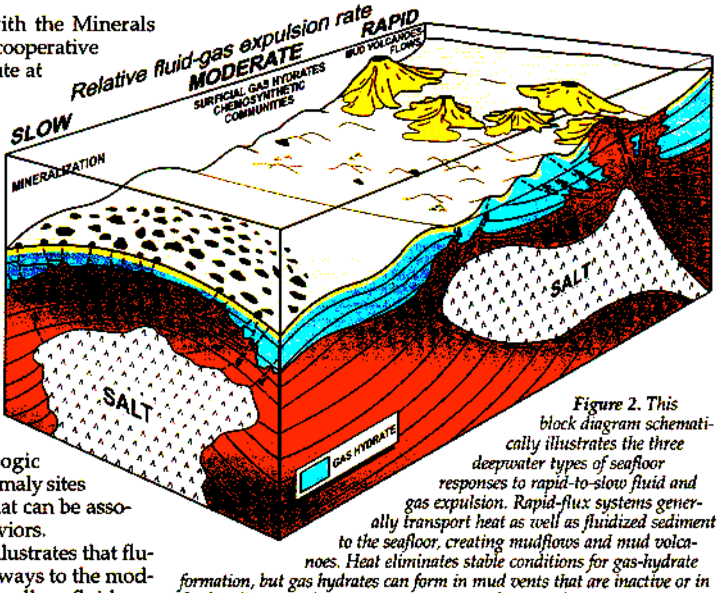

Figure 2. This block diagram schematically illustrates the three deepwater types of seafloor responses to rapid-to-slow fluid and gas expulsion. Rapid-flux systems generally transport heat as well as fluidized sediment to the seafloor, creating mudflows and mud volcanoes. Heat eliminates stable conditions for gas-hydrate formation, but gas hydrates can form in mud vents that are inactive or in flank sediments. Slow seepage promotes seafloor lithification processes mediated by microbial utilization of hydrocarbons. Authigenic carbonates are the most common lithification products. Gas hydrate may occur in the subsurface, but never at the seafloor. Between rapid venting and slow seepage, conditions are compatible with creating and sustaining gas hydrate at the modern seafloor. These areas exhibit highly variable seafloor features, from productive chemosynthetic communities to localized areas of lithification (Modified from Roberts, 2001).

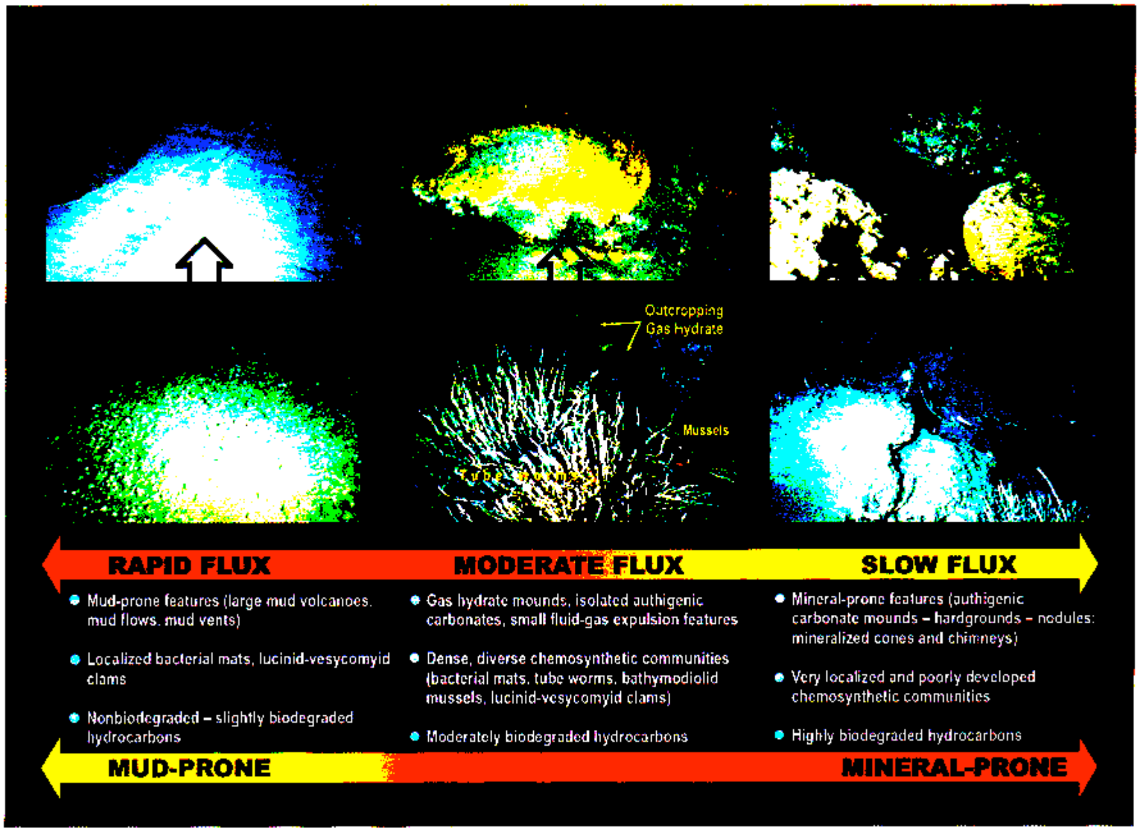

Figure 3. *This figure summarizes the response at the seafloor of venting-to-seepage rates of hydrocarbons, formation fluids, and fluidized sediment (modified from Roberts, 2001). Rapid-flux systems are generally accompanied by fluidized sediment resulting in mudflows and mud volcanoes of various dimensions. Sedimentation rates are typically too high to support complex communities of benthic organisms. Bacterial mats (Beggiatoa) and lucinid-vesycomyid clams occur on the surfaces of recently deposited sediments laced with hydrocarbons. Slow-flux systems are characterized by hardgrounds and mound-like buildups of authigenic carbonates. Intermediate-flux areas support large and densely populated communities of chemosynthetic mussels and tube worms. Localized authigenic carbonate hardgrounds and bacterial mats are also common to this setting. Each picture has a field of view of 2–4 m across.*

zone or dramatically shifts it toward the seafloor in the migration pathways. Rapid flux or venting of these products in sufficient volumes can create mud flows or mud volcanoes. Because venting of hydrocarbon-laced mud is a sporadic process, mud flows and the flanks of mud volcanoes may partially cement if the interval between expulsion events is long.

In contrast, short migration routes are common to slow-flux, or seepage, of hydrocarbon to the continental slope surface, and cementation of surficial sediments is widespread across these systems. The process of cementation is associated with microbial communities that utilize the hydrocarbons and then produce authigenic carbonates as by-products. The most common carbonate mineral is magnesium-calcite even though aragonite and dolomite also occur. These carbonate minerals share a common characteristic. They all are ^{13}C-depleted, indicating that ^{12}C, microbially separated from the hydrocarbons, is incorporated into the calcium-magnesium carbonate molecules. For the slow-seepage case illustrated in Figure 2, migration pathways are associated with a shallow salt mass.

Between the extremes of rapid-flux and slow-flux settings, conditions are optimal for creating gas hydrates in the very shallow subsurface, with some hydrate being exposed as localized outcrops. At these sites, gas is supplied at such a rate that seafloor exposures of gas hydrate are maintained and rebuilt after hydrate instability and dissociation related to thermal loading by the water column, e.g., the Loop Current. These intermediate flux areas generally display a highly variable seafloor character, including exposed gas hydrates, localized outcrops of authigenic carbonate, and diverse and densely populated communities of chemosynthetic organisms. It has been suggested that exposed and shallow-subsurface gas-hydrate deposits in these settings provide the trophic resources to sustain chemosynthetic communities that live primarily on microbially mediated hydrocarbon gas and hydrogen sulfide. Slow-flux and rapid-flux environments do not support well-populated and diverse chemosynthetic communities.

Before illustrating seismic examples of seafloor reflectivity across these three fluid gas expulsion rate categories, we first show photographs in Figure 3 of seafloor sites representing each type of expulsion rate and gas-hydrate setting. These direct observations illustrate actual seafloor conditions associated with each of the three major types of fluid-gas expulsion environments, rapid-to-slow flux, and the associated settings for three different occurrences of gas hydrate at the surface or in near-surface sediments.

Gas-hydrate domain 1—rapid fluid-gas expulsion. It has long been recognized that during rapid venting of fluids and

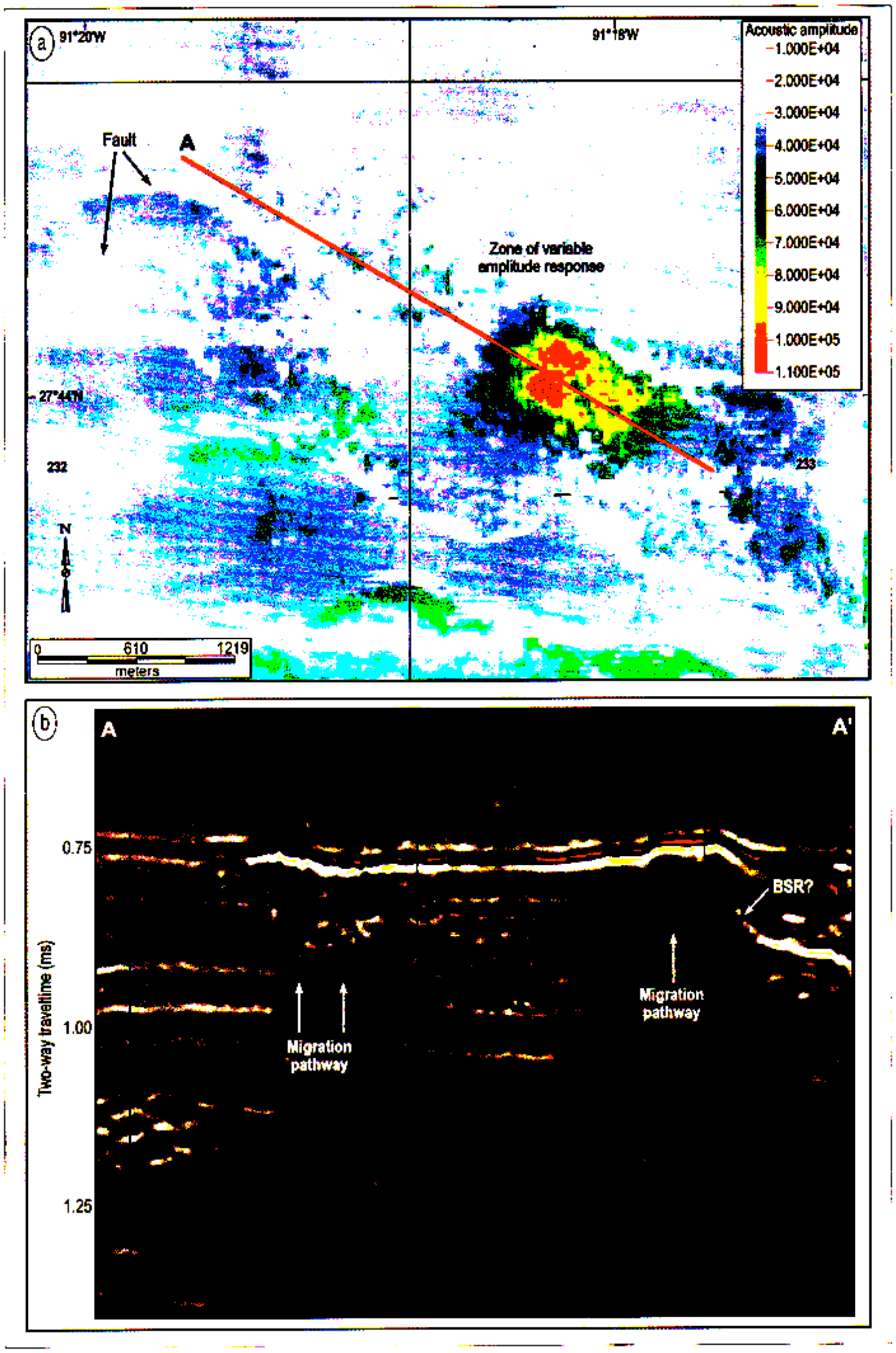

Figure 5. (a) A 3D seismic seafloor reflectivity map across Block GC232 illustrating the variable seafloor reflectivity patterns typical of sites where seafloor exposures of gas hydrate are frequently found. This site is highly faulted and was the first site where a surface exposure of gas hydrate was recognized. The highly reflective area in GC233 represents carbonate hardgrounds, while gas hydrates are found in the extremely variable, but generally low-amplitude zones that display wavelet interference effects across low-impedance gas expulsion sites. (b) Seismic profile across the gas-hydrate site identified by the red line on the reflectivity map. A strong wavelet interference occurs in the seafloor reflection at the left side of the seismic profile. This area is invaded with massive vein-filling and nodular gas hydrates.

Both the diagenetic products and shell beds indicate that the flows are not new. As discussed above, the carbonates arise as by-products from microbial oxidation of hydrocarbons in the extruded muds. The lucinid-vesycomyid clams exploit hydrogen sulfide produced as microbes metabolize hydrocarbons incorporated in the mudflows. Once this trophic resource is depleted, the clams die, leaving a surface "pavement" of clam shells like those illustrated in Figure 3 (lower-left panel). So, the high surface reflectivity is related to both the clam shells and diagenetic carbonate products.

The seismic profile of Figure 4 cuts through the two prominent expulsion centers shown in the accompanying seafloor reflectivity map. Note the high-amplitude events near the seafloor. Beneath these events is the acoustically transparent migration pathway that is the vertical transport route for fluids, gases, and heat. These shallow, high-amplitude events

Table 1. *Seafloor reflectivity and gas-hydrate domain.*

Gas-hydrate domain	Seafloor reflectivity	Reflectivity pattern	Seafloor features	Gas-hydrate occurrence
Rapid fluid-gas delivery	Expulsion centers have low, positive reflectivity with common phase reversals	Circular expulsion centers	Gas-charged and/or gas-emitting expulsion centers	None in active expulsion centers
	Linear flows can be highly reflective	Linear flows radiating from expulsion centers	Clam beds and nodular carbonates on flow deposits	Subsurface flanks of expulsion centers
Moderate fluid-gas delivery	High spatial variability Phase reversals	Highly variable, frequently fault-aligned	Dense chemosynthetic communities, localized authigenic carbonates	Surface exposures, shallow subsurface
Slow fluid-gas delivery	Highly reflective surface No phase reversals	Broad areas of high reflectivity	Authigenic carbonate mounds and hardgrounds	Subsurface

in the subsurface of the once highly active venting sites are connected to reflections that slope away into the subsurface cutting across stratigraphic horizons. These reflections are interpreted as BSRs, and the high-amplitude event near the seafloor is interpreted as gas hydrate. Increased heat flow and perhaps high-salinity fluids are responsible for elevating the base of the hydrate stability zone (BHSZ) to near the modern seafloor. During active venting, gas hydrate would probably not be present in the migration pathways. Because this site is now inactive, gas hydrate has formed at the vent site, if our interpretations of the seismic data are correct. If these vents remain inactive for long periods of time or they are abandoned entirely, gas hydrate will likely form along the vertical migration pathway. Gas hydrate will not generally be found in the flanking surfacial flow deposits, but the BSR identified in the seismic profile of Figure 4 suggests hydrates should be found in the subsurface.

Gas-hydrate domain 2—moderate fluid–gas expulsion. The intermediate-flux case, as illustrated in Figures 2 and 3, represents a set of conditions that promote gas-hydrate formation at or very close to the modern seafloor. In contrast to the rapid-flux case, where venting of fluidized sediment and heat is not conducive to gas-hydrate formation or to the growth and development of complex chemosynthetic communities, slope-depth intermediate-flux settings promote both. Gas is continually supplied to these sites, as demonstrated by bubble plumes detected in the water column on echo sounder records and other high-resolution acoustic data sets. Mounds and outcrops of gas hydrate are generally observed at these sites. The association between shallow-subsurface or exposed gas hydrates and the presence of diverse and densely populated chemosynthetic communities is not a chance happening. For such communities to develop and persist, they must have a constant supply of hydrocarbon gas and hydrogen sulfide.

Gas hydrate, which is stable at temperatures and pressures below water depths of 400–500 m in the GoM, functions as a reservoir that can produce and store the necessary products to sustain these communities. If gas supply from the subsurface varies with time, gas hydrate probably functions as a low-pass process filter to stabilize trophic resources to maintain chemosynthetic life. Anaerobic microbial utilization of hydrocarbons in these environments produces bicarbonate, which is responsible for triggering the precipitation of authigenic carbonates in the form of nodular masses in the sediment, crusts, and mound-like buildups. It is also common that in areas where gas hydrates are exposed at the surface that small mud vents extruding fluidized mud and hypersaline fluids are present. Expulsion of salt in the hydrate-forming process is involved in the creation of these features. So, intermediate-flux settings are highly complex in terms of their seafloor geology and biology. This complexity is reflected in both the patterns and strengths of seafloor reflectivity values derived from 3D seismic data.

Figure 5 illustrates the seafloor reflectivity response in an area of Green Canyon Block 232 (GC232) where the first exposure of gas hydrate on the seafloor was recognized while conducting manned submersible research in 1991. Gas hydrate has been discovered in cores from many sites across the upper slope since the early 1980s. After the discovery of outcropping gas hydrate in GC232, many similar outcrops have been observed at SBS sites across the northern Gulf of Mexico's continental slope. These exposures of gas hydrate usually occur in localized mounds a few meters in diameter and in some settings they align themselves with well defined faults. Figure 3 (center panel) illustrates one of these mounds that is covered with an orange bacterial mat (*Beggiatoa*). The gas hydrate in this mound occurred as white layers exposed at the edge of the mound. *Beggiatoa* mats act as semipermeable membranes that collect migrating hydrocarbons beneath. Anaerobic microbial utilization of hydrocarbon depletes oxygen and encourages sulfate reduction to produce hydrogen sulfide needed for *Beggiatoa* growth. Therefore, because of this and other microbial interactions, hydrocarbons in moderate flux settings, like GC232, demonstrate the characteristics associated with biodegradation.

The wide range of seafloor reflectivities and their complex plan-view patterns observed in Figure 5a are typical of SBS sites that support gas hydrate at or very near the modern seafloor. Phase reversals of the surface reflection (Figure 5b) frequently occur where gas hydrates and associated vent sites are found at the surface. Highly populated communities of chemosynthetic mussels and tube worms accompanied by authigenic carbonate hardgrounds are scattered throughout these areas.

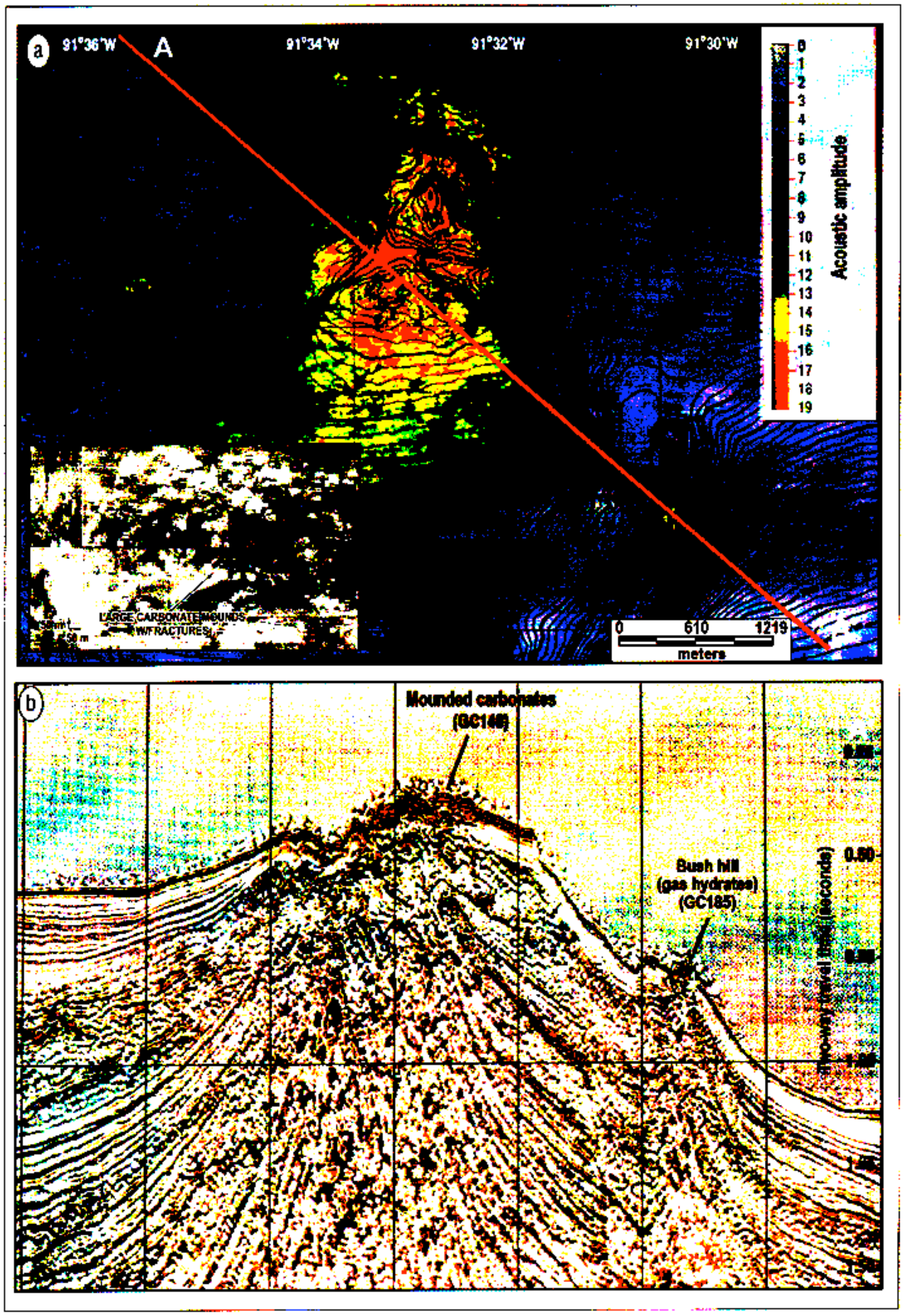

Figure 6. (a) A 3D seismic seafloor reflectivity map of the dome top in GC140. The extremely high reflectivity is related to the presence of authigenic carbonate mounds and hardgrounds scattered over the top of this feature. The inset is a side-scan sonar image from the dome top illustrating the spatial arrangement and shapes of the carbonate mounds. (b) This NW-SE seismic profile across the GC140 dome illustrates the highly reflective surface of the dome, subsurface structure, and "Bush Hill," a mound invaded with gas hydrate on the flank of the GC140 dome.

Gas-hydrate domain 3—slow fluid–gas expulsion. At the slow-seepage end of the fluid-gas expulsion spectrum, hydrocarbons and other fluids do not arrive at the seafloor in sufficient quantities to support chemosynthetic communities of macroorganisms or to build topography through expulsion of large volumes of fluidized sediment. However, microbial communities in both reduced and oxidized, surface to shallow-subsurface environments utilize seep-delivered hydrocarbons and produce conditions conducive to authigenic carbonate precipitation. Hydrocarbon oxidation in aerobic environments produce CO_2 and decrease pH, which in sufficient quantities can favor dissolution of carbonates rather than precipitation. However, anaerobic microbial sulfate reduction involving hydrocarbon substrates results in sulfide depletion and both bicarbonate and hydrogen sulfide enrichments. The increase in carbonate alkalinity of pore fluids resulting from these microbial reactions produces calcium-magnesium carbonate by-products. These carbonates can take the forms of small nodular masses in sediments, hardground slabs or pavements, and mound-like buildups (Figure 3, right panel). Areas of seafloor where these processes are prevalent and widespread display high reflectivity on seismic records.

Figure 6 illustrates the 3D seismic seafloor reflectivity response and profile character of a site, Green Canyon Block 140 (GC140), that is characterized by slow hydrocarbon seepage and an abundance of resulting authigenic carbonate mounds, plus seafloor hardgrounds. Analysis of both 3D and higher-frequency seismic data as well as numerous manned submersible dives at this site revealed no obvious gas plumes in the water column or sites of fluid-gas expulsion on the seafloor. Only one localized site of a few macrochemosynthetic organisms was observed in a fissure through one of the authigenic carbonate mounds. However, bacterial mats on the seafloor and in fissures and around pores in the authigenic carbonate mounds were frequently observed. This pattern of bacterial mat occurrence with the near total absence of macrochemosynthetic organisms and an abundance of authigenic carbonates suggests long-term, slow seepage of hydrocarbons. The carbonates are primarily magnesium-calcite and dolomite. Both mineral phases are ^{13}C-depleted with δ^{13}C values as negative as -55 per mille with respect to the PDB standard belemnite.

The 3D seismic data reveal a high reflectivity of the GC140 mound surface. The positive polarity and strength of the surface reflection suggests a hard bottom which certainly is the case. The absence of areas of negative polarity in the surface reflection, lack of obvious gas plumes in the water column, and the lack of macrochemosynthetic organisms collectively suggest that gas-hydrate deposits are probably not present in the very shallow subsurface as is the case in intermediate-delivery systems. In slow-seepage systems, the sulfate reducing zone which limits gas-hydrate occurrence can be quite thick compared to that of moderate-to-rapid-flux settings.

Conclusions. Nearly two decades of research have been conducted across the northern Gulf of Mexico's continental slope using seismic data, coring, and manned submersible dives to study the impacts of fluid-gas expulsion on the geology and biology of the modern seafloor. These investigations have been made primarily in water depths of 1000 m or shallower. They clearly establish that areas of seafloor reflectivity (seafloor bright spots, or SBS), easily identified on 3D seismic data, are generally areas impacted by hydrocarbon venting-to-seepage. A few exceptions, such as recently deposited sand-rich slope fans, do occur. At the shelf edge, biogenic carbonate veneers on shelf edge knolls are highly reflective, but by far the greatest number of SBS sites in the zone of gas-hydrate stability across the middle-to-upper slope are related to the fluid-gas expulsion process. Seafloor response to the expulsion process is qualitatively related to delivery rate of hydrocarbons, formation fluids, and sometimes fluidized sediment. Patterns of seafloor reflectivity are clues to the delivery rate, seafloor responses, and ways gas hydrates may be associated with various sites representing different fluid-gas expulsion rates. Table 1 summarizes the general relationships between gas-hydrate occurrence and fluid-gas expulsion domain. The authors acknowledge the high degree of variability in seafloor reflectivity associated with seep and vent sites. Relationships between reflectivity and gas hydrate are offered as general cases based on both seismic data and direct seafloor observations.

Rapid-delivery expulsion systems generally build seafloor topography such as mud volcanoes and display mud flows that transport fluidized sediment down slope from an expulsion site or vent. Seafloor reflectivity patterns clearly distinguish these features as shown in Figure 4. High seafloor reflectivity can be caused by precipitation of authigenic carbonates in the hydrocarbon-laced sediment flows and clam shells (lucinid-vesycomyid clams) left after exploiting the limited supply of hydrogen sulfide microbially generated in these deposits. Where a BSR can confidently be identified in association with a rapid-delivery system, this reflector rises to the seafloor, or near it, in the fluid-gas migration pathway, as shown in Figure 4. Heat and perhaps high-salinity fluids transported during expulsion events change the boundary conditions for gas-hydrate stability and force the boundary toward the seafloor as illustrated in this GC204 example. Therefore, if gas hydrate occurs in the migration pathway of a recently waning system like GC204, it is likely to be a very thin shallow deposit. In active venting situations, it is probable that no gas hydrate will occur in association with the vent. As the interpreted BSR of Figure 4 suggests, if gas-hydrate deposits are to be found in rapid-delivery settings, they occur lateral to the vent sites and their subsurface migration pathways.

Moderate delivery rates of hydrocarbons to the modern seafloor provide the optimal set of conditions for gas-hydrate formation at or near the seafloor. Under these conditions the sulfate reducing zone is very thin or essentially at the seabed. Therefore shallow-to-exposed gas-hydrate deposits can be expected under these conditions. Seafloor reflectivity, as determined from 3D seismic data, is highly variable for most moderate-delivery settings (Figure 5). These sites support diverse and densely populated communities of chemosynthetic organisms and display scattered areas of seafloor lithification and may even display small areas of fluidized mud venting.

Because pervasive seafloor lithification is a product of microbial oxidation of hydrocarbon in slow-delivery settings, seafloor reflectivity is very high, as displayed on 3D seismic seafloor reflectivity maps like the one illustrated in Figure 6. These areas can have relatively thick sulfate reducing zones, limiting gas-hydrate formation near the seafloor. Heat flow from the deep subsurface is low in comparison to rapid and moderate flux settings. However, if low-delivery-rate settings occur above a shallow salt body, the efficient heat transfer from the deep subsurface through the salt may limit the thickness of the hydrate stability zone, as schematically illustrated in Figure 2.

Suggested reading. Several summaries of gas hydrate and hydrocarbon seep research have been published recently. "Natural Gas Hydrates: Occurrence, Distribution, and Detection" by Paull and Dillon (American Geophysical Union, *Geophysical Monograph 124*, 2001). *Methane Hydrate in Quaternary Climate Change* by Kennett et al. (American Geophysical Union, 2003). *Submarine Gas Hydrates* by Ginsburg and Soloviev (Norma Publishers, 1998). *Clathrate Hydrate of Natural Gases* by Sloan (Marcel Dekker, 1998). "Hydrocarbon Migration and Its Near-Surface Expression" by Schumacher and Abrams (AAPG *Memoir 66*, 1996). *Seabed Pockmarks and Seepages: Impacts on Geology, Biology, and the Marine Environment* by Hovland and Judd (Graham & Trotman, 1989). TLE

Acknowledgment: The authors thank the Minerals Management Service for support of several research projects related to the use of 3D seismic data for studying impacts of fluid and gas expulsion on the northern Gulf of Mexico continental slope. Manned submersible time has been supported by NOAA-NURP, MMS, Louisiana Education Quality Support funds, and the Gulf of Mexico Hydrates Research Consortium at the University of Mississippi.

Corresponding author: hrober3@lsu.edu

APPENDIX B

HIGH-RESOLUTION MULTICOMPONENT SEISMIC IMAGING OF DEEPWATER GAS-HYDRATE SYSTEMS

Seafloor reflectivity—An important seismic property for interpreting fluid/gas expulsion geology and the presence of gas hydrate

Harry H. Roberts, Louisiana State University, Baton Rouge, USA
Bob A. Hardage, Bureau of Economic Geology, Austin, USA
William W. Shedd and Jesse Hunt Jr., Minerals Management Service, New Orleans, USA

A bottom-simulating reflection (BSR) is a seismic reflectivity phenomenon that is widely accepted as indicating the base of the gas-hydrate stability zone. The acoustic impedance difference between sediments invaded with gas hydrate above the BSR and sediments without gas hydrate, but commonly with free gas below, are accepted as the conditions that create this reflection. The relationship between BSRs and marine gas hydrate has become so well known since the 1970s that investigators, when asked to define the most important seismic attribute of marine gas-hydrate systems, usually reply, "a BSR event." Research conducted over the last decade has focused on calibrating seafloor seismic reflectivity across the geology of the northern Gulf of Mexico (GoM) continental slope surface to the seafloor. This research indicates that the presence and character of seafloor bright spots (SBS) can be indicators of gas hydrates in surface and near-surface sediments (Figure 1). It has become apparent that SBSs on the continental slope generally are responses to fluid and gas expulsion processes. Gas-hydrate formation is, in turn, related to these processes. As gas-hydrate research expands around the world, it will be interesting to find if SBS behavior in other deepwater settings is as useful for identifying gas-hydrate sites as in the GoM.

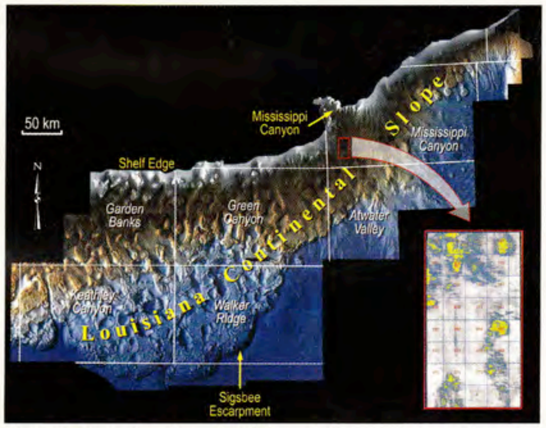

Figure 1. *Computer-enhanced multibeam bathymetry image of the northern Gulf of Mexico continental slope showing a small sector of the Mississippi Canyon lease area and its seafloor bright spots (SBS) or local areas of high seismic seafloor reflectivity across the continental slope surface.*

Research background. Joint research with the Minerals Management Service (MMS), through a cooperative agreement with the Coastal Marine Institute at Louisiana State University, has resulted in a study using the university's GoM-wide 3D seismic data coverage. Seafloor reflectivity across the northern GoM's continental slope has been mapped, and numerous SBS areas like those illustrated in Figure 1 have been identified. Through research projects funded primarily by MMS and NOAA, manned submersible dives on many SBS sites have provided direct observations and samplings to calibrate the actual geologic character of the seafloor to seismic reflectivity. These investigations have led to the model illustrated in Figure 2 which defines three qualitative ranges in the rates of fluid and gas expulsion coupled to geologic-biologic response at the seafloor. These reflector-anomaly sites also indicate three gas-hydrate domains that can be associated with these seafloor reflectivity behaviors.

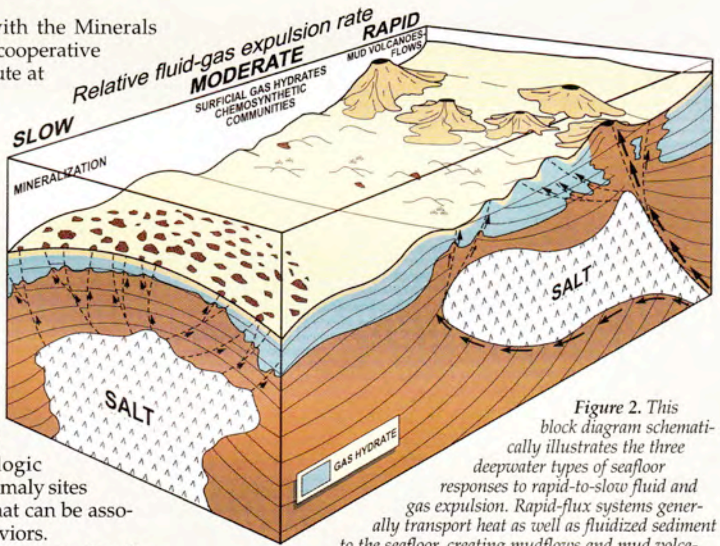

Figure 2. *This block diagram schematically illustrates the three deepwater types of seafloor responses to rapid-to-slow fluid and gas expulsion. Rapid-flux systems generally transport heat as well as fluidized sediment to the seafloor, creating mudflows and mud volcanoes. Heat eliminates stable conditions for gas-hydrate formation, but gas hydrates can form in mud vents that are inactive or in flank sediments. Slow seepage promotes seafloor lithification processes mediated by microbial utilization of hydrocarbons. Authigenic carbonates are the most common lithification products. Gas hydrate may occur in the subsurface, but never at the seafloor. Between rapid venting and slow seepage, conditions are compatible with creating and sustaining gas hydrate at the modern seafloor. These areas exhibit highly variable seafloor features, from productive chemosynthetic communities to localized areas of lithification (Modified from Roberts, 2001).*

The block diagram shown in Figure 2 illustrates that fluids and gases have various migration pathways to the modern seafloor and that delivery rates, as well as fluid-gas composition, impact geologic response on the continental slope surface. Deep-cutting faults that intersect the overpressured zone frequently form the migration routes for hydrocarbons, formation fluids, and sometimes fluidized sediments. In addition, considerable heat can accompany these products, which eliminates the gas-hydrate stability

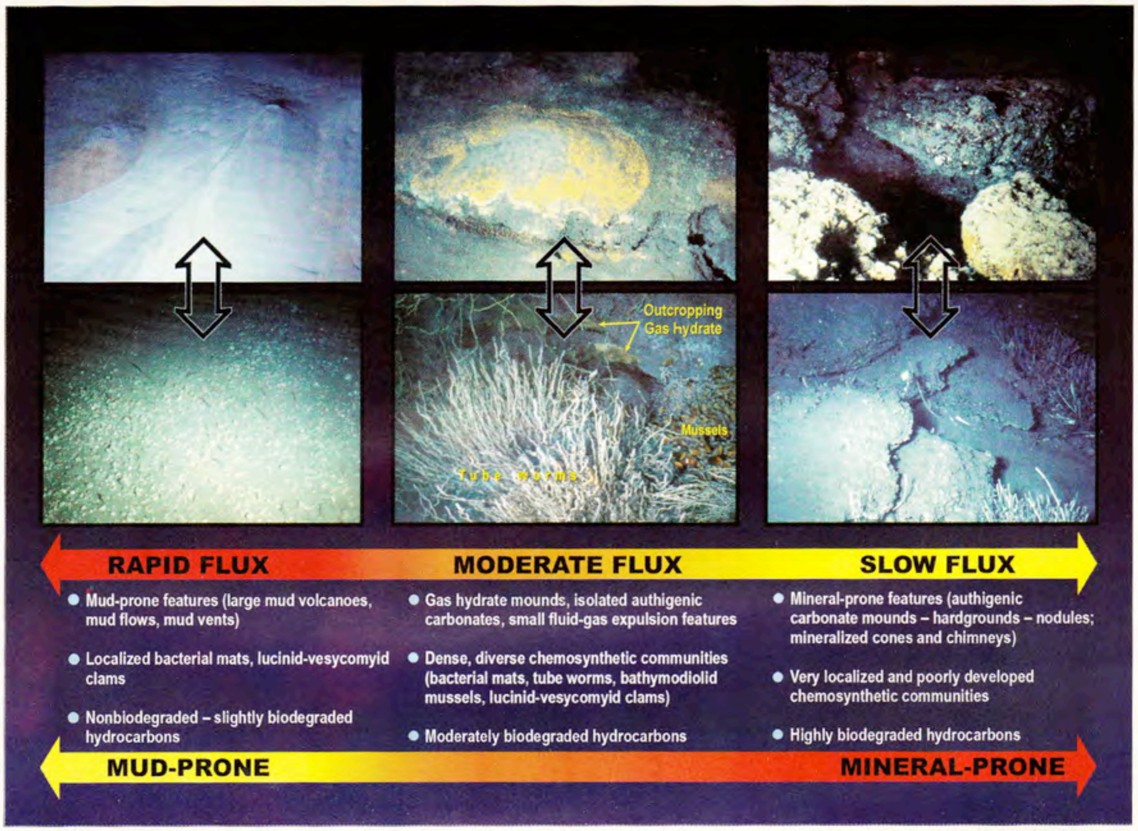

Figure 3. *This figure summarizes the response at the seafloor of venting-to-seepage rates of hydrocarbons, formation fluids, and fluidized sediment (modified from Roberts, 2001). Rapid-flux systems are generally accompanied by fluidized sediment resulting in mudflows and mud volcanoes of various dimensions. Sedimentation rates are typically too high to support complex communities of benthic organisms. Bacterial mats (*Beggiatoa*) and lucinid-vesycomyid clams occur on the surfaces of recently deposited sediments laced with hydrocarbons. Slow-flux systems are characterized by hardgrounds and mound-like buildups of authigenic carbonates. Intermediate-flux areas support large and densely populated communities of chemosynthetic mussels and tube worms. Localized authigenic carbonate hardgrounds and bacterial mats are also common to this setting. Each picture has a field of view of 2–4 m across.*

zone or dramatically shifts it toward the seafloor in the migration pathways. Rapid flux or venting of these products in sufficient volumes can create mud flows or mud volcanoes. Because venting of hydrocarbon-laced mud is a sporadic process, mud flows and the flanks of mud volcanoes may partially cement if the interval between expulsion events is long.

In contrast, short migration routes are common to slow-flux, or seepage, of hydrocarbon to the continental slope surface, and cementation of surficial sediments is widespread across these systems. The process of cementation is associated with microbial communities that utilize the hydrocarbons and then produce authigenic carbonates as by-products. The most common carbonate mineral is magnesium-calcite even though aragonite and dolomite also occur. These carbonate minerals share a common characteristic. They all are ^{13}C-depleted, indicating that ^{12}C, microbially separated from the hydrocarbons, is incorporated into the calcium-magnesium carbonate molecules. For the slow-seepage case illustrated in Figure 2, migration pathways are associated with a shallow salt mass.

Between the extremes of rapid-flux and slow-flux settings, conditions are optimal for creating gas hydrates in the very shallow subsurface, with some hydrate being exposed as localized outcrops. At these sites, gas is supplied at such a rate that seafloor exposures of gas hydrate are maintained and rebuilt after hydrate instability and dissociation related to thermal loading by the water column, e.g., the Loop Current. These intermediate flux areas generally display a highly variable seafloor character, including exposed gas hydrates, localized outcrops of authigenic carbonate, and diverse and densely populated communities of chemosynthetic organisms. It has been suggested that exposed and shallow-subsurface gas-hydrate deposits in these settings provide the trophic resources to sustain chemosynthetic communities that live primarily on microbially mediated hydrocarbon gas and hydrogen sulfide. Slow-flux and rapid-flux environments do not support well-populated and diverse chemosynthetic communities.

Before illustrating seismic examples of seafloor reflectivity across these three fluid gas expulsion rate categories, we first show photographs in Figure 3 of seafloor sites representing each type of expulsion rate and gas-hydrate setting. These direct observations illustrate actual seafloor conditions associated with each of the three major types of fluid-gas expulsion environments, rapid-to-slow flux, and the associated settings for three different occurrences of gas hydrate at the surface or in near-surface sediments.

Gas-hydrate domain 1—rapid fluid-gas expulsion. It has long been recognized that during rapid venting of fluids and

Figure 5. *(a) A 3D seismic seafloor reflectivity map across Block GC232 illustrating the variable seafloor reflectivity patterns typical of sites where seafloor exposures of gas hydrate are frequently found. This site is highly faulted and was the first site where a surface exposure of gas hydrate was recognized. The highly reflective area in GC233 represents carbonate hardgrounds, while gas hydrates are found in the extremely variable, but generally low-amplitude zones that display wavelet interference effects across low-impedance gas expulsion sites. (b) Seismic profile across the gas-hydrate site identified by the red line on the reflectivity map. A strong wavelet interference occurs in the seafloor reflection at the left side of the seismic profile. This area is invaded with massive vein-filling and nodular gas hydrates.*

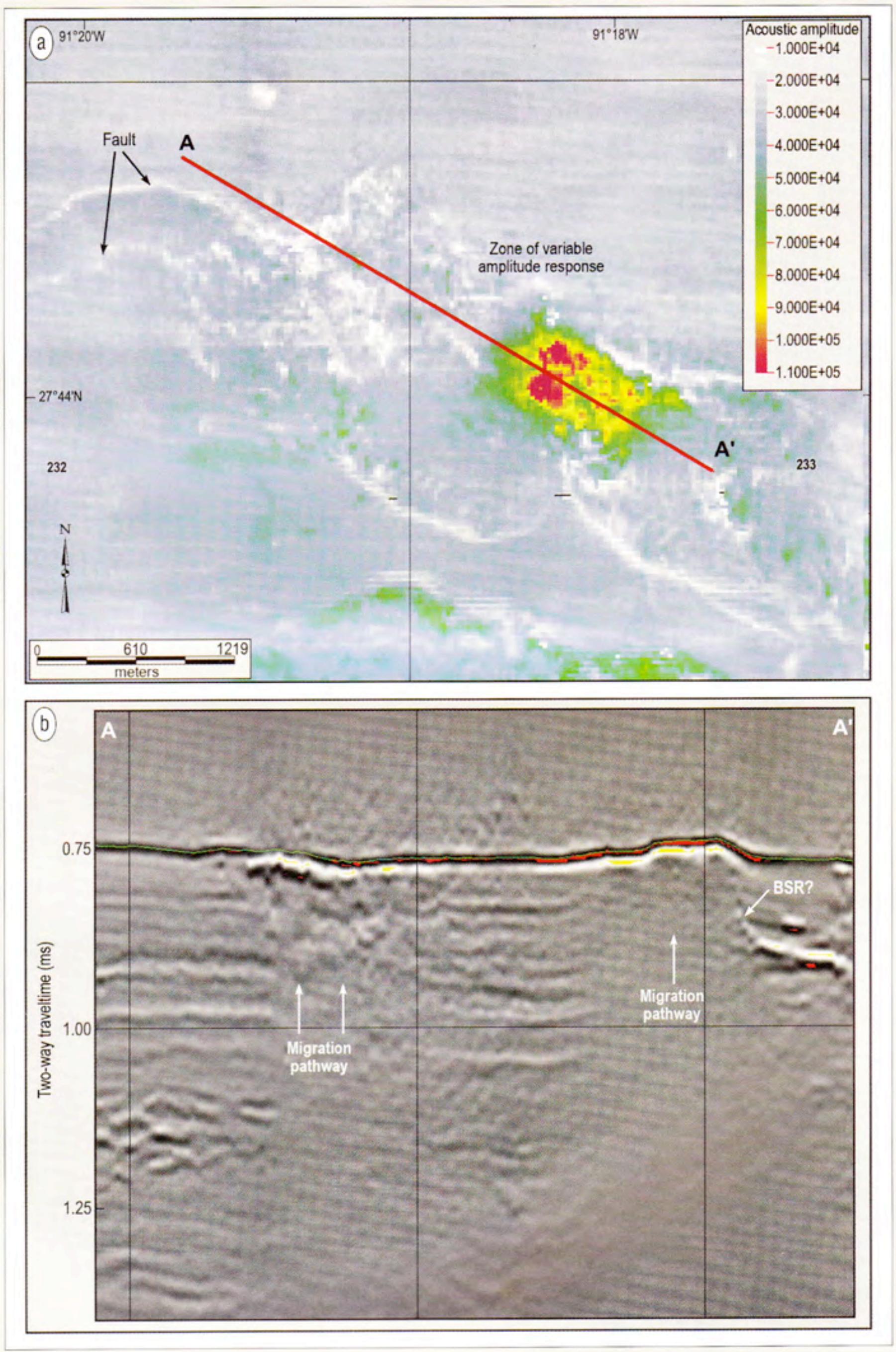

Both the diagenetic products and shell beds indicate that the flows are not new. As discussed above, the carbonates arise as by-products from microbial oxidation of hydrocarbons in the extruded muds. The lucinid-vesycomyid clams exploit hydrogen sulfide produced as microbes metabolize hydrocarbons incorporated in the mudflows. Once this trophic resource is depleted, the clams die, leaving a surface "pavement" of clam shells like those illustrated in Figure 3 (lower-left panel). So, the high surface reflectivity is related to both the clam shells and diagenetic carbonate products.

The seismic profile of Figure 4 cuts through the two prominent expulsion centers shown in the accompanying seafloor reflectivity map. Note the high-amplitude events near the seafloor. Beneath these events is the acoustically transparent migration pathway that is the vertical transport route for fluids, gases, and heat. These shallow, high-amplitude events

Table 1. *Seafloor reflectivity and gas-hydrate domain.*

Gas-hydrate domain	Seafloor reflectivity	Reflectivity pattern	Seafloor features	Gas-hydrate occurrence
Rapid fluid-gas delivery	Expulsion centers have low, positive reflectivity with common phase reversals Linear flows can be highly reflective	Circular expulsion centers Linear flows radiating from expulsion centers	Gas-charged and/or gas-emitting expulsion centers Clam beds and nodular carbonates on flow deposits	None in active expulsion centers Subsurface flanks of expulsion centers
Moderate fluid-gas delivery	High spatial variability Phase reversals	Highly variable, frequently fault-aligned	Dense chemosynthetic communities, localized authigenic carbonates	Surface exposures, shallow subsurface
Slow fluid-gas delivery	Highly reflective surface No phase reversals	Broad areas of high reflectivity	Authigenic carbonate mounds and hardgrounds	Subsurface

in the subsurface of the once highly active venting sites are connected to reflections that slope away into the subsurface cutting across stratigraphic horizons. These reflections are interpreted as BSRs, and the high-amplitude event near the seafloor is interpreted as gas hydrate. Increased heat flow and perhaps high-salinity fluids are responsible for elevating the base of the hydrate stability zone (BHSZ) to near the modern seafloor. During active venting, gas hydrate would probably not be present in the migration pathways. Because this site is now inactive, gas hydrate has formed at the vent site, if our interpretations of the seismic data are correct. If these vents remain inactive for long periods of time or they are abandoned entirely, gas hydrate will likely form along the vertical migration pathway. Gas hydrate will not generally be found in the flanking surfacial flow deposits, but the BSR identified in the seismic profile of Figure 4 suggests hydrates should be found in the subsurface.

Gas-hydrate domain 2—moderate fluid–gas expulsion. The intermediate-flux case, as illustrated in Figures 2 and 3, represents a set of conditions that promote gas-hydrate formation at or very close to the modern seafloor. In contrast to the rapid-flux case, where venting of fluidized sediment and heat is not conducive to gas-hydrate formation or to the growth and development of complex chemosynthetic communities, slope-depth intermediate-flux settings promote both. Gas is continually supplied to these sites, as demonstrated by bubble plumes detected in the water column on echo sounder records and other high-resolution acoustic data sets. Mounds and outcrops of gas hydrate are generally observed at these sites. The association between shallow-subsurface or exposed gas hydrates and the presence of diverse and densely populated chemosynthetic communities is not a chance happening. For such communities to develop and persist, they must have a constant supply of hydrocarbon gas and hydrogen sulfide.

Gas hydrate, which is stable at temperatures and pressures below water depths of 400–500 m in the GoM, functions as a reservoir that can produce and store the necessary products to sustain these communities. If gas supply from the subsurface varies with time, gas hydrate probably functions as a low-pass process filter to stabilize trophic resources to maintain chemosynthetic life. Anaerobic microbial utilization of hydrocarbons in these environments produces bicarbonate, which is responsible for triggering the precipitation of authigenic carbonates in the form of nodular masses in the sediment, crusts, and mound-like buildups. It is also common that in areas where gas hydrates are exposed at the surface that small mud vents extruding fluidized mud and hypersaline fluids are present. Expulsion of salt in the hydrate-forming process is involved in the creation of these features. So, intermediate-flux settings are highly complex in terms of their seafloor geology and biology. This complexity is reflected in both the patterns and strengths of seafloor reflectivity values derived from 3D seismic data.

Figure 5 illustrates the seafloor reflectivity response in an area of Green Canyon Block 232 (GC232) where the first exposure of gas hydrate on the seafloor was recognized while conducting manned submersible research in 1991. Gas hydrate has been discovered in cores from many sites across the upper slope since the early 1980s. After the discovery of outcropping gas hydrate in GC232, many similar outcrops have been observed at SBS sites across the northern Gulf of Mexico's continental slope. These exposures of gas hydrate usually occur in localized mounds a few meters in diameter and in some settings they align themselves with well defined faults. Figure 3 (center panel) illustrates one of these mounds that is covered with an orange bacterial mat (*Beggiatoa*). The gas hydrate in this mound occurred as white layers exposed at the edge of the mound. *Beggiatoa* mats act as semipermeable membranes that collect migrating hydrocarbons beneath. Anaerobic microbial utilization of hydrocarbon depletes oxygen and encourages sulfate reduction to produce hydrogen sulfide needed for *Beggiatoa* growth. Therefore, because of this and other microbial interactions, hydrocarbons in moderate flux settings, like GC232, demonstrate the characteristics associated with biodegradation.

The wide range of seafloor reflectivities and their complex plan-view patterns observed in Figure 5a are typical of SBS sites that support gas hydrate at or very near the modern seafloor. Phase reversals of the surface reflection (Figure 5b) frequently occur where gas hydrates and associated vent sites are found at the surface. Highly populated communities of chemosynthetic mussels and tube worms accompanied by authigenic carbonate hardgrounds are scattered throughout these areas.

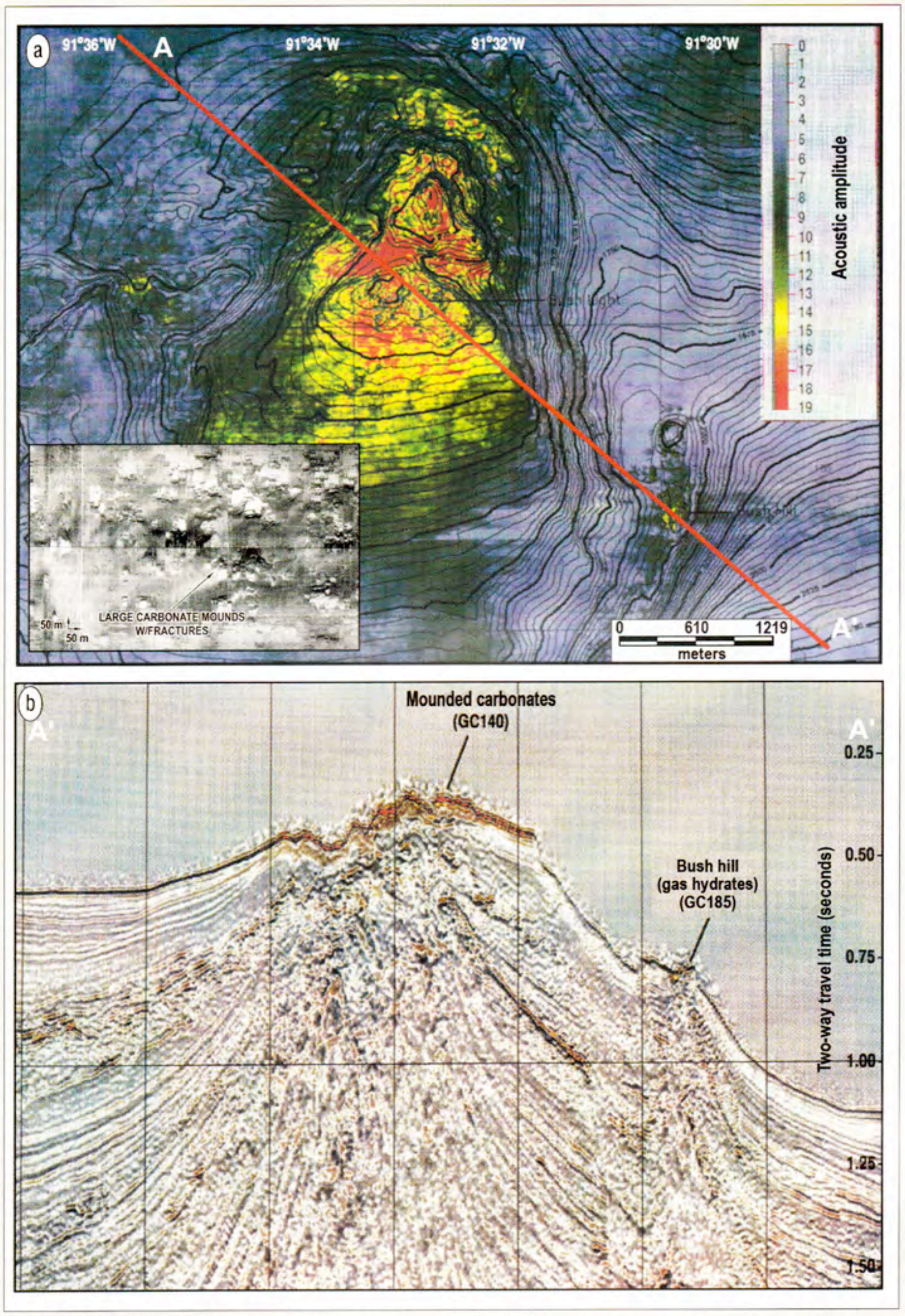

Figure 6. (a) A 3D seismic seafloor reflectivity map of the dome top in GC140. The extremely high reflectivity is related to the presence of authigenic carbonate mounds and hardgrounds scattered over the top of this feature. The inset is a side-scan sonar image from the dome top illustrating the spatial arrangement and shapes of the carbonate mounds. (b) This NW-SE seismic profile across the GC140 dome illustrates the highly reflective surface of the dome, subsurface structure, and "Bush Hill," a mound invaded with gas hydrate on the flank of the GC140 dome.

Gas-hydrate domain 3—slow fluid–gas expulsion. At the slow-seepage end of the fluid-gas expulsion spectrum, hydrocarbons and other fluids do not arrive at the seafloor in sufficient quantities to support chemosynthetic communities of macroorganisms or to build topography through expulsion of large volumes of fluidized sediment. However, microbial communities in both reduced and oxidized, surface to shallow-subsurface environments utilize seep-delivered hydrocarbons and produce conditions conducive to authigenic carbonate precipitation. Hydrocarbon oxidation in aerobic environments produce CO_2 and decrease pH, which in sufficient quantities can favor dissolution of carbonates rather than precipitation. However, anaerobic microbial sulfate reduction involving hydrocarbon substrates results in sulfide depletion and both bicarbonate and hydrogen sulfide enrichments. The increase in carbonate alkalinity of pore fluids resulting from these microbial reactions produces calcium-magnesium carbonate by-products. These carbonates can take the forms of small nodular masses in sediments, hardground slabs or pavements, and mound-like buildups (Figure 3, right panel). Areas of seafloor where these processes are prevalent and widespread display high reflectivity on seismic records.

Figure 6 illustrates the 3D seismic seafloor reflectivity response and profile character of a site, Green Canyon Block 140 (GC140), that is characterized by slow hydrocarbon seepage and an abundance of resulting authigenic carbonate mounds, plus seafloor hardgrounds. Analysis of both 3D and higher-frequency seismic data as well as numerous manned submersible dives at this site revealed no obvious gas plumes in the water column or sites of fluid-gas expulsion on the seafloor. Only one localized site of a few macrochemosynthetic organisms was observed in a fissure through one of the authigenic carbonate mounds. However, bacterial mats on the seafloor and in fissures and around pores in the authigenic carbonate mounds were frequently observed. This pattern of bacterial mat occurrence with the near total absence of macrochemosynthetic organisms and an abundance of authigenic carbonates suggests long-term, slow seepage of hydrocarbons. The carbonates are primarily magnesium-calcite and dolomite. Both mineral phases are ^{13}C-depleted with δ^{13}C values as negative as -55 per mille with respect to the PDB standard belemnite.

The 3D seismic data reveal a high reflectivity of the GC140 mound surface. The positive polarity and strength of the surface reflection suggests a hard bottom which certainly is the case. The absence of areas of negative polarity in the surface reflection, lack of obvious gas plumes in the water column, and the lack of macrochemosynthetic organisms collectively suggest that gas-hydrate deposits are probably not present in the very shallow subsurface as is the case in intermediate-delivery systems. In slow-seepage systems, the sulfate reducing zone which limits gas-hydrate occurrence can be quite thick compared to that of moderate-to-rapid-flux settings.

Conclusions. Nearly two decades of research have been conducted across the northern Gulf of Mexico's continental slope using seismic data, coring, and manned submersible dives to study the impacts of fluid-gas expulsion on the geology and biology of the modern seafloor. These investigations have been made primarily in water depths of 1000 m or shallower. They clearly establish that areas of seafloor reflectivity (seafloor bright spots, or SBS), easily identified on 3D seismic data, are generally areas impacted by hydrocarbon venting-to-seepage. A few exceptions, such as recently deposited sand-rich slope fans, do occur. At the shelf edge, biogenic carbonate veneers on shelf edge knolls are highly reflective, but by far the greatest number of SBS sites in the zone of gas-hydrate stability across the middle-to-upper slope are related to the fluid-gas expulsion process. Seafloor response to the expulsion process is qualitatively related to delivery rate of hydrocarbons, formation fluids, and sometimes fluidized sediment. Patterns of seafloor reflectivity are clues to the delivery rate, seafloor responses, and ways gas hydrates may be associated with various sites representing different fluid-gas expulsion rates. Table 1 summarizes the general relationships between gas-hydrate occurrence and fluid-gas expulsion domain. The authors acknowledge the high degree of variability in seafloor reflectivity associated with seep and vent sites. Relationships between reflectivity and gas hydrate are offered as general cases based on both seismic data and direct seafloor observations.

Rapid-delivery expulsion systems generally build seafloor topography such as mud volcanoes and display mud flows that transport fluidized sediment down slope from an expulsion site or vent. Seafloor reflectivity patterns clearly distinguish these features as shown in Figure 4. High seafloor reflectivity can be caused by precipitation of authigenic carbonates in the hydrocarbon-laced sediment flows and clam shells (lucinid-vesycomyid clams) left after exploiting the limited supply of hydrogen sulfide microbially generated in these deposits. Where a BSR can confidently be identified in association with a rapid-delivery system, this reflector rises to the seafloor, or near it, in the fluid-gas migration pathway, as shown in Figure 4. Heat and perhaps high-salinity fluids transported during expulsion events change the boundary conditions for gas-hydrate stability and force the boundary toward the seafloor as illustrated in this GC204 example. Therefore, if gas hydrate occurs in the migration pathway of a recently waning system like GC204, it is likely to be a very thin shallow deposit. In active venting situations, it is probable that no gas hydrate will occur in association with the vent. As the interpreted BSR of Figure 4 suggests, if gas-hydrate deposits are to be found in rapid-delivery settings, they occur lateral to the vent sites and their subsurface migration pathways.

Moderate delivery rates of hydrocarbons to the modern seafloor provide the optimal set of conditions for gas-hydrate formation at or near the seafloor. Under these conditions the sulfate reducing zone is very thin or essentially at the seabed. Therefore shallow-to-exposed gas-hydrate deposits can be expected under these conditions. Seafloor reflectivity, as determined from 3D seismic data, is highly variable for most moderate-delivery settings (Figure 5). These sites support diverse and densely populated communities of chemosynthetic organisms and display scattered areas of seafloor lithification and may even display small areas of fluidized mud venting.

Because pervasive seafloor lithification is a product of microbial oxidation of hydrocarbon in slow-delivery settings, seafloor reflectivity is very high, as displayed on 3D seismic seafloor reflectivity maps like the one illustrated in Figure 6. These areas can have relatively thick sulfate reducing zones, limiting gas-hydrate formation near the seafloor. Heat flow from the deep subsurface is low in comparison to rapid and moderate flux settings. However, if low-delivery-rate settings occur above a shallow salt body, the efficient heat transfer from the deep subsurface through the salt may limit the thickness of the hydrate stability zone, as schematically illustrated in Figure 2.

Suggested reading. Several summaries of gas hydrate and hydrocarbon seep research have been published recently. "Natural Gas Hydrates: Occurrence, Distribution, and Detection" by Paull and Dillon (American Geophysical Union, *Geophysical Monograph 124*, 2001). *Methane Hydrate in Quaternary Climate Change* by Kennett et al. (American Geophysical Union, 2003). *Submarine Gas Hydrates* by Ginsburg and Soloviev (Norma Publishers, 1998). *Clathrate Hydrate of Natural Gases* by Sloan (Marcel Dekker, 1998). "Hydrocarbon Migration and Its Near-Surface Expression" by Schumacher and Abrams (AAPG *Memoir 66*, 1996). *Seabed Pockmarks and Seepages: Impacts on Geology, Biology, and the Marine Environment* by Hovland and Judd (Graham & Trotman, 1989).

Acknowledgment: The authors thank the Minerals Management Service for support of several research projects related to the use of 3D seismic data for studying impacts of fluid and gas expulsion on the northern Gulf of Mexico continental slope. Manned submersible time has been supported by NOAA-NURP, MMS, Louisiana Education Quality Support funds, and the Gulf of Mexico Hydrates Research Consortium at the University of Mississippi.

Corresponding author: hrober3@lsu.edu

APPENDIX C

ROCK PHYSICS CHARACTERIZATION OF HYDRATE-BEARING DEEPWATER SEDIMENTS

Rock physics characterization of hydrate-bearing deepwater sediments

DIANA SAVA and BOB A. HARDAGE, Bureau of Economic Geology, Austin, USA

Estimates of worldwide hydrate resources are large, but they are also uncertain because of inherent difficulties in determining the amount of gas hydrate present in ocean sediments. Estimates of gas-hydrate concentrations across a deepwater site can vary widely. For example, estimates of the volume of gas existing in gas hydrates and as free gas on Blake Ridge offshore South Carolina (USA) range from about 70 trillion m^3 over an area of 26 000 km^2 (Dickens et al., 1997) to about 80 trillion m^3 for a larger area of 100 000 km^2 (Holbrook et al., 1996). Discrepancies between some estimates of hydrate concentrations can partly be attributed to poor understanding of how gas hydrates are distributed in their host sediments. In particular, estimates based on seismic measurements, if not supported by reliable rock physics models and by in-situ observations, can be inaccurate.

The need for rock physics. The goal of our rock physics modeling of deepwater gas-hydrate systems is to develop a methodology by which gas-hydrate concentration can be inferred from seismic measurements. To achieve this goal, we define the elastic properties of deepwater gas-hydrate systems in terms of (1) elastic properties of the unconsolidated sediments that host the hydrates, (2) elastic properties of the embedded gas hydrates, (3) concentration of hydrates in the sediments, and (4) geometrical details of the distribution of hydrates within their host sediments.

Theoretical models for unconsolidated deepwater sediments. Most rock physics models for unconsolidated sediments are based on contact models, such as Hertz and Mindlin's theory (see Mavko et al.) for describing the elastic properties of granular materials. The model we propose for unconsolidated sediments is based on an approach by Dvorkin and colleagues, with the distinction that the elastic properties of newly deposited deepwater sediments are described by Walton's smooth model (see Mavko et al.), as opposed to the Hertz-Mindlin model. Walton's theory is particularly appropriate for highly unconsolidated sediments at low effective pressure where grain rotation and slip along grain boundaries are likely to occur. Walton's smooth model better explains the low shear strengths and high V_P/V_S ratios observed in deepwater multicomponent seismic data and in lab measurements made on unconsolidated sediments.

We consider four rock physics models for deepwater gas-hydrate systems (Figure 1):

- Model A assumes gas hydrates are uniformly disseminated throughout the whole volume of sediment and act as a part of the load-bearing frame of the host sediments.
- Model B assumes gas hydrates are also disseminated throughout the whole volume of sediment, but they only fill the porous space and do not affect the dry mineral frame of their host sediments.
- Model C assumes an anisotropic, thin-layered medium having layers of pure gas hydrate intercalated with layers of unconsolidated sediments saturated with brine.
- Model D is also an anisotropic, thin-layered medium. However, in this model, gas hydrates are disseminated in thin layers of sediments, occupying 99% of the porous space of these layers, and act as part of the load-bearing frame. These hydrate-bearing beds are intercalated with layers of unconsolidated sediments saturated with brine.

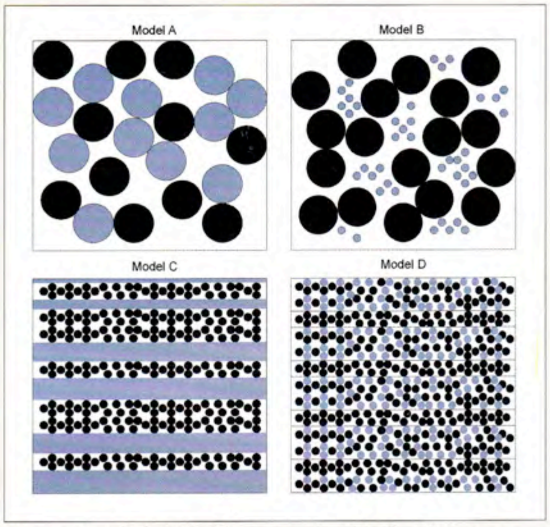

Figure 1. Graphical sketch of four proposed models of gas-hydrate systems: load-bearing gas hydrates (model A); pore-filling gas hydrates (model B); thin layers of pure gas hydrate intercalated with unconsolidated sediments (model C); and thin layers of disseminated, load-bearing gas hydrates intercalated with unconsolidated sediments (model D). Hydrates are represented in light blue and sediment in black.

The key input parameter in all of these models is gas-hydrate concentration. Our goal is to quantitatively relate gas-hydrate concentration to seismic observables such as P- and S-wave velocities and amplitude variation with angle of incidence (AVA). Detailed descriptions of the mathematics used to create each theoretical model have been submitted for publication and will not be presented here. We also will compare our theoretical predictions of velocity attributes in deepwater sediments with laboratory measurements made on synthetic hydrate-bearing sediments to illustrate the validity of the physics and mathematics used in constructing the models.

Relations between P- and S-wave velocities and gas-hydrate concentration. Figures 2, 3, and 4 present modeling results for P-wave velocity (V_P), S-wave velocity (V_S), and V_P/V_S ratio, respectively, as a function of gas-hydrate concentration (C_{gh}) for the four rock physics models considered. In each model, the porosity of the host sediment is assumed to be 0.37, and the effective pressure is 0.01 MPa. For the two anisotropic layered models (C and D), we display two curves corresponding to waves polarized parallel to the layering (solid line) and waves polarized orthogonal to the layers (dotted line). From these figures we observe that relations between seismic velocities and gas-hydrate concentration depend on the geometrical details of how gas hydrates are distributed in their host sediments.

The results presented in Figure 2 show that for all four

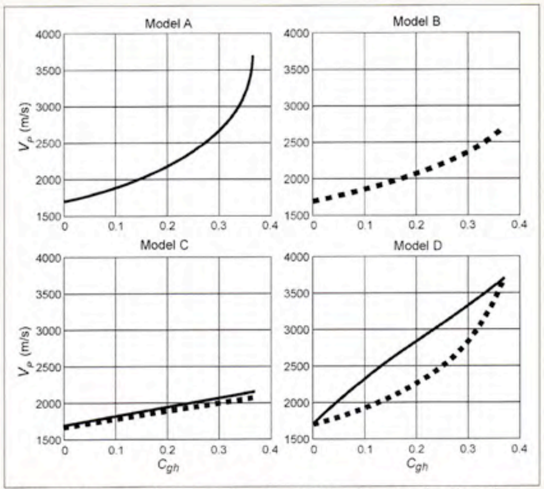

Figure 2. *P-wave velocity as a function of the volumetric fraction of gas hydrate in the sediment (C_{gh}) for four rock-physics models. Model A = load-bearing gas hydrates disseminated in the whole volume of sediments; model B = pore-filling gas hydrates disseminated in the whole volume of sediment; model C = layers of pure gas hydrates producing slow polarization (dotted line) and fast polarization (solid line); and model D = layers of disseminated, load-bearing gas hydrates producing slow polarization (dotted line) and fast polarization (solid line). Sediment porosity is assumed to be 0.37, and effective pressure is 0.01MPa.*

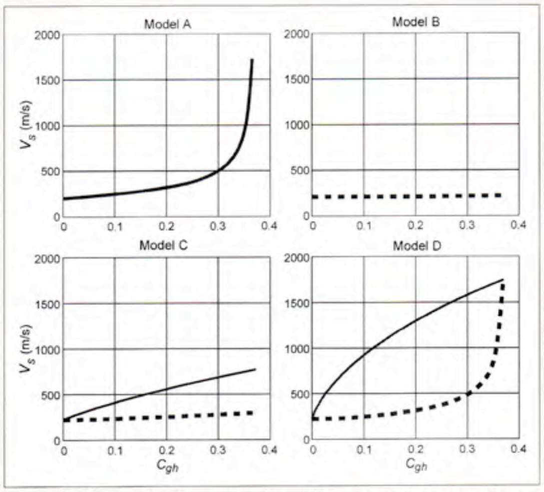

Figure 3. *S-wave velocity as a function of the volumetric fraction of gas hydrate in the sediment (C_{gh}) for four rock-physics models. Model A = load-bearing gas hydrates disseminated in the whole volume of sediments; model B = pore-filling gas hydrates disseminated in the whole volume of sediment; model C = layers of pure gas hydrates producing slow polarization (dotted line) and fast polarization (solid line); and model D = layers of disseminated, load-bearing gas hydrates producing slow polarization (dotted line) and fast polarization (solid line). Sediment porosity is assumed to be 0.37, and effective pressure is 0.01MPa.*

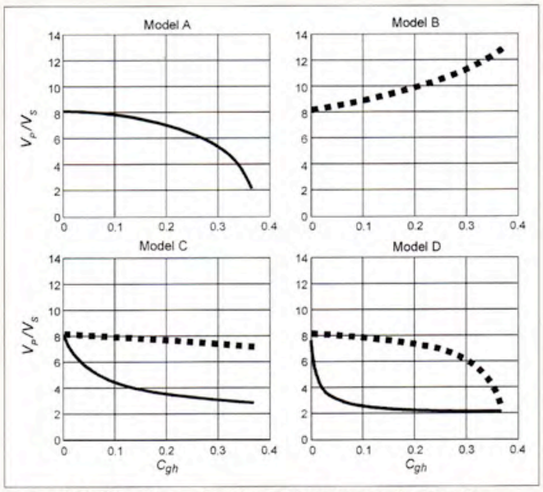

Figure 4. V_P/V_S *ratio as a function of the volumetric fraction of gas hydrate in the sediment (C_{gh}) for four rock-physics models. Model A= load-bearing gas hydrates disseminated in the whole volume of sediments; model B = pore-filling gas hydrates disseminated in the whole volume of sediment; model C = layers of pure gas hydrates producing slow polarization (dotted line) and fast polarization (solid line); and model D = layers of disseminated, load-bearing gas hydrates producing slow polarization (dotted line) and fast polarization (solid line). Sediment porosity is assumed to be 0.37, and effective pressure is 0.01MPa.*

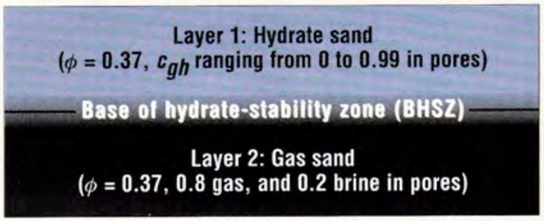

Figure 5. *Model assumed for base of hydrate-stability zone (BHSZ).*

rock physics models considered, an increase in gas-hydrate concentration increases the P-wave velocity in the sediments. The smallest increase in P-wave velocity occurs for the thin-bedded model (C) having layers of pure gas hydrates, whereas the largest increase in P-wave velocity is obtained for the models having disseminated, load-bearing gas hydrates (A and D). The key point is that any value of V_P measured across a hydrate-bearing interval can be related to hydrate concentration only if a specific hydrate-to-sediment morphology is assigned to that interval.

From Figure 3 we observe, as expected, that S-wave velocity does not vary with gas-hydrate concentration for model B in which hydrates fill the porous space of the sediments. However, a large, almost linear increase in S-wave velocity occurs when S-waves are polarized parallel to the layers of a medium having thin beds of disseminated, load-bearing gas hydrates (model D, solid line). The S-wave anisotropy in this model is large, as shown by the difference between S-wave velocities polarized parallel (solid line) and orthogonal (model D, dotted line) to layers of disseminated, load-bearing gas hydrates. S-wave anisotropy for a system of thin layers of pure gas hydrates (model C) is also large. If gas hydrates occur in thin layers within near-seafloor strata, we should thus expect significant S-wave anisotropy. This anisotropy can be used with other seismic information to aid in estimating gas-hydrate concentrations in layered seafloor strata. The concept emphasized by these calculations is that we must first define the correct geometrical distribution of hydrate within the host sediment before a measured value of V_S can be interpreted in terms of hydrate concentration.

Figure 4 presents the V_P/V_S ratio for the four rock physics models. This velocity ratio decreases with gas-hydrate con-

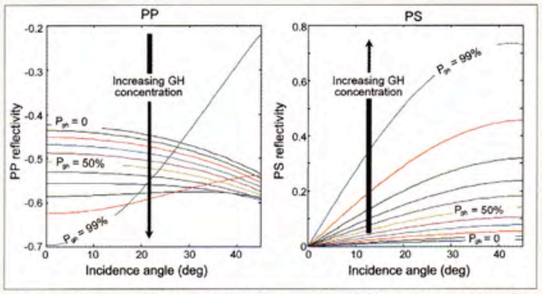

Figure 6. *Results of AVA model A showing PP (left) and PS (right) reflectivity as a function of incidence angle at the interface between the base of gas-hydrate stability zone and the sediments below containing free gas. Each curve corresponds to a different gas-hydrate concentration in layer 1 of Figure 5. In this model, gas hydrates are disseminated and act as part of the load-bearing frame of the host sediments.*

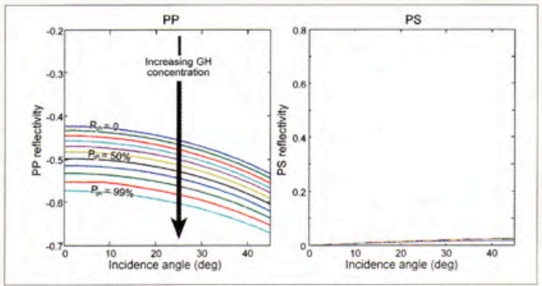

Figure 7. *Results of AVA model B showing PP (left) and PS (right) reflectivity as a function of incidence angle at the interface between the base of gas-hydrate stability zone and the sediments below containing free gas. Each curve corresponds to a different gas-hydrate concentration in layer 1 of Figure 5. In this model, gas hydrates fill the porous space without changing the dry mineral frame of the host sediments.*

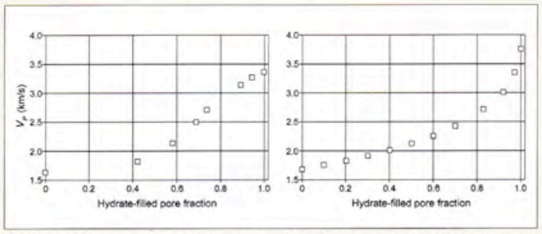

Figure 8. *Comparison of laboratory and model A results for P-wave velocities as a function of gas-hydrate concentration in the pores. (Left) Work by Yun and colleagues at Georgia Institute of Technology (USA). (Right) Rock-physics modeling results when gas hydrates are assumed to be part of the dry frame of the sediments.*

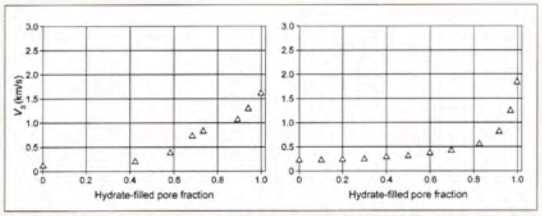

Figure 9. *Comparison of laboratory and model A results for S-wave velocities as a function of gas-hydrate concentration in the pores. (Left) Work by Yun and colleagues at Georgia Institute of Technology (USA). (Right) Rock-physics modeling results when gas hydrates are assumed to be part of the dry frame of the sediments.*

centration for all models except model B, which assumes pore-filling gas hydrates. This anomalous behavior occurs for model B because P-wave velocity increases with gas-hydrate concentration in that type of media (Figure 2), whereas S-wave velocity remains practically constant (Figure 3). For anisotropic models C and D, there is a significant decrease in V_P/V_S ratio at low gas-hydrate concentrations for waves polarized parallel to the layers (fast direction). This modeling result suggests that for thin-layered gas-hydrate morphologies, we may be able to detect small gas-hydrate concentrations in sediments using V_P/V_S ratios and anisotropy information. Again, we find there is a wide range in the functional dependence of V_P/V_S on hydrate concentration, depending on how the hydrate is distributed throughout the host sediment.

PP and PS AVA modeling—base of hydrate-stability zone. To evaluate the potential value of amplitude-versus-angle (AVA) technology for studying gas-hydrate systems, we simulate the AVA response for PP and PS reflections from an interface between the base of the gas-hydrate stability zone and sediments immediately below that interface that contain free gas (Figure 5).

The gas-hydrate systems considered in this AVA modeling are represented by isotropic rock physics models A and B (Figure 1), which have gas hydrates disseminated in the host sediments.

Figure 6 presents the results for AVA modeling of PP (left panel) and PS (right panel) reflectivity as a function of incidence angle for the model of load-bearing gas hydrates (model A). Each curve corresponds to a different gas-hydrate concentration in the sediments. The arrow indicates increasing gas-hydrate concentration in the pores, which ranges from 0% to 99% of available pore space. For this model we observe that PP reflectivity at small incidence angles (near offsets) can better differentiate gas-hydrate concentrations than can PP reflectivity at larger angles of incidence (far offsets).

As hydrate concentration increases beyond 0.7, the PP AVA behavior shifts from a class 3 to a class 4 reservoir response. This change occurs because at large hydrate concentration there is a significant increase in V_S in the layer above the gas reservoir (layer 1, Figure 5). This V_S behavior is required for a class 4 PP AVA response (Castagna et al., 1998). PS AVA response for angles of incidence greater than 20° is more sensitive to gas hydrate concentration than is the PP AVA response. By using AVA information from converted PS waves we should be able to better predict hydrate concentration for media represented by model A.

Figure 7 shows the results for AVA modeling of PP (left panel) and PS (right panel) reflectivity as a function of incidence angle for the model of pore-filling gas hydrates (model B). In this case only PP reflectivity exhibits any sensitivity to gas-hydrate concentration. All PP AVA reflectivity curves in Figure 7 are class 3 responses. For this model, the shear strengths of the sediments containing gas hydrates do not change with gas-hydrate concentration. Moreover, shear velocities in sediments containing pore-filling gas hydrates and in sediments containing free gas are similar. Therefore, all PS reflections are weak and vary little as gas-hydrate concentration increases.

The modeling results presented in Figures 6 and 7 show that PP reflectivity cannot differentiate between the two hypotheses of gas-hydrate occurrence (models A and B). However, PS reflectivity is different for load-bearing gas hydrates (model A) and for pore-filling gas hydrates (model B). Therefore, multicomponent seismic technology—in particular, the use of PS-mode AVA behavior—can be a powerful tool to understand the way gas hydrates are distributed in relation to their host sediments (Figures 6 and 7). Using combinations of V_P/V_S ratios and AVA analyses of P-waves and converted PS-waves should improve estimates of deepwater gas-hydrate concentrations.

Comparing rock physics modeling results with laboratory measurements. In Figures 8 and 9 we compare laboratory measurements made by Yun and colleagues from Georgia Institute of Technology (USA) of P- and S-wave velocities as a function of gas-hydrate concentration with our results for rock physics model A (load-bearing gas hydrates). The left panels in these figures show the lab measurements, and the right panels show our rock physics modeling results. The unconsolidated sediments in the rock physics model are represented by quartz grains at critical porosity, assumed to be 0.37, the same porosity as that of the sand samples used in the laboratory measurements. The effective pressure used in the model is 0.01 MPa, and the mean effective pressure in the lab is also approximately 0.01 MPa.

Figure 8 shows that P-wave velocity increases with gas-hydrate concentration for both lab measurements and the rock physics model of load-bearing gas hydrates. The increase in P-wave velocity is nonlinear and is larger when gas-hydrate concentrations in pores exceed 50%. For gas-hydrate concentration smaller than 50%, the increase in the P-wave velocity due to the presence of gas hydrates is small. We observe a rather good agreement between the laboratory measurements of P-wave velocity as a function of gas-hydrate concentration and our rock physics modeling results, which implies the mathematical structure and physical concepts used in the numerical modeling are sound.

Figure 9 shows that S-wave velocity increases with gas-hydrate concentration for both lab measurements and the rock physics model of load-bearing gas hydrates. The increase in S-wave velocity is again larger when gas-hydrate concentration in pores exceeds 50%. For gas-hydrate concentration smaller than 50%, the increase in S-wave velocity due to the presence of gas hydrates is very small. The agreement between these laboratory measurements of V_S and our calculations indicates Walton's model is a good physical model for deepwater, unconsolidated, near-seafloor media.

Conclusions. Rock physics modeling results show that the elastic properties of gas-hydrate units depend on the geometrical details of gas-hydrate distribution within the sediments. If hydrates occur in thin beds, the effective elastic properties of stratified near-seafloor sediments containing gas hydrates are highly anisotropic, and the acquisition of fast and slow components of multicomponent seismic data has great value.

AVA modeling is a second indication that multicomponent seismic technology can be important for understanding the way gas hydrates are distributed in relation to their host sediments and for estimating gas-hydrate concentrations. Using combinations of PP and PS AVA reflectivity, P- and S-wave interval velocities, and V_P/V_S ratios should improve our understanding of deepwater hydrate systems.

Comparing our rock physics models and laboratory measurements made at the Georgia Institute of Technology on synthetic gas hydrates in unconsolidated sands suggests that gas hydrates are disseminated throughout deepwater media as a part of the load-bearing frame of near-seafloor sediments. We find satisfactory agreement between our theoretical predictions for P- and S-wave velocities corresponding to this rock physics model (our model A) and laboratory measurements of V_P and V_S velocities.

We conclude that rock physics modeling is a critical tool for understanding gas-hydrate distributions in deepwater environments and for quantifying the amount of gas hydrate present in deepwater, near-seafloor sediments under different geologic scenarios.

Suggested reading. "Direct measurement of in-situ methane quantities in a large gas-hydrate reservoir" by Dickens et al. (*Nature*, 1997). "Methane hydrate and free gas on the Blake Ridge from vertical seismic profiling" by Holbrook et al. (*Science*, 1996). "Rock-physics of a gas hydrate reservoir" by Dvorkin et al. (*TLE*, 2003). "Compressional and shear wave velocities in uncemented sediment containing gas hydrate" by Yun et al. (*Geophysical Research Letters*, 2005). *The Rock Physics Handbook* by Mavko et al. (Cambridge, 1998). "Framework for AVO gradient and intercept interpretation" by Castagna et al. (GEOPHYSICS, 1998). "Elastic-wave velocity in marine sediments with gas hydrates: Effective medium modeling" by Helgerud et al. (*Geophysical Research Letters*, 1999). TLE

Acknowledgments: Research support for this study is provided by the U.S. Department of Energy (Contract DE-PS26-05NT42405) and by the Minerals Management Service (MMS Contract 0105CT39388).

Corresponding author: sava@beg.utexas.edu

APPENDIX D

EVALUATION OF DEEPWATER GAS-HYDRATE SYSTEMS

Evaluation of deepwater gas-hydrate systems

Bob A. Hardage, Paul Murray, Diana Sava, Milo M. Backus, Randy Remington, and Robert Graebner, Bureau of Economic Geology, University of Texas at Austin, USA
Harry H. Roberts, Louisiana State University, Baton Rouge, USA

The world's offshore continental margins contain vast reserves of gas hydrate, a frozen form of natural gas that is embedded in cold, near-seafloor strata. Published estimates suggest that the energy represented by gas hydrate may exceed the energy available from conventional fossil fuel by a factor of 2 or more. Understanding marine hydrate systems has become critical for long-term worldwide energy planning. Groups in several nations are attempting to evaluate the resource and to define seafloor stability problems across hydrate accumulations.

Affordable, reliable, remotely based methodologies for evaluating deepwater gas-hydrate systems have been slow to develop. Four-component ocean-bottom-cable (4-C OBC) technology offers an option for remote, detailed evaluation of deepwater, near-seafloor geology. Increasing use of marine multicomponent seismic technology by oil and gas companies now allows marine gas-hydrate systems to be studied over areas of many square kilometers and the geomechanical properties of the strata that confine these hydrates to be analyzed.

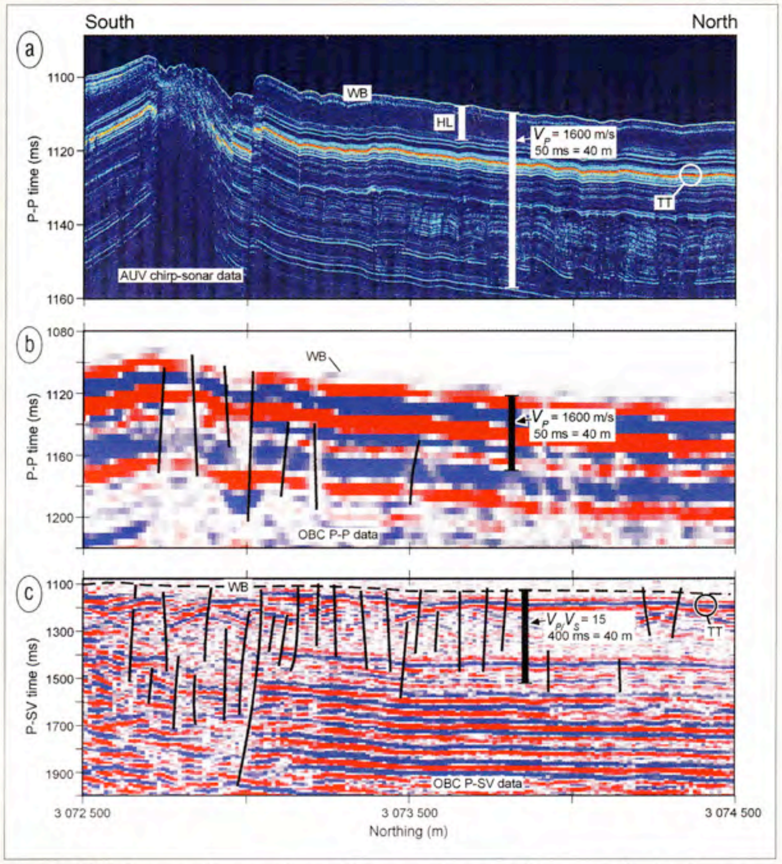

Figure 1. *High-frequency chirp-sonar image of (a) near-seafloor strata, (b) corresponding low-frequency OBC P-P image, and (c) P-SV image along profile 549, Green Canyon Block 204, about 300 km south of New Orleans, USA. The seafloor feature at the south end of the profiles is a fluid/gas expulsion chimney that serves as a methane source for gas-hydrate formation. WB = water bottom, which is not imaged by the backscattered SV data (c) because of the P-SV data-processing techniques that were used. HL = regional hemipelagic layer. TT = interval of thin regional turbidites. Numerous faults with vertical throws of 1 m or less can be seen on chirp-sonar images (a). Some of these faults are interpreted on the P-P and P-SV images (b and c) and shown as thin vertical lines. Water depth averages about 840 m along the profile.*

Data acquisition and calibration. Marine multicomponent seismic data acquisition requires a surface-based air-gun source and long lines of ocean-bottom sensors that record three-dimensional vector motion of the seafloor. Using this combination of surface source and seafloor receivers, standard-frequency (roughly 10–100 Hz) compressional (P-P) and converted shear (P-SV) wavefields can be acquired that backscatter from near-seafloor strata. We used these wavefields to image seafloor strata over distances of several kilometers across the Green Canyon area of the Gulf of Mexico. For calibration purposes, high-frequency, chirp-sonar data were acquired along the same seafloor profiles using an autonomous underwater vehicle (AUV). This AUV system traveled at a height of 40 m above the seafloor and illuminated near-seafloor strata with a 2–8 kHz chirp-sonar signal. The backscattered, high-frequency, P-P data acquired with this system imaged geology to a depth of a few tens of meters below the seafloor.

Data examples and interpretations. A high-frequency chirp-sonar image along one OBC line that traverses Green Canyon Block 204 about 300 km south of New Orleans is illustrated in Figure 1, together with low-frequency (10–100 Hz) P-P and P-SV images constructed from the OBC data acquired along the same profile. The water bottom is not imaged by this particular P-SV image (Figure 1c) because of the manner in which initial parts of the P-SV wavefield were muted during data processing. In the data-processing technique used here, the P-SV image starts 3–4 m below the seafloor. We currently use data-processing techniques that start the P-SV image at the seafloor, and describe that procedure in another paper in this section by Backus et al.

The high-frequency AUV chirp-sonar data provide impressive definitions of near-seafloor strata. Units as thin as 1

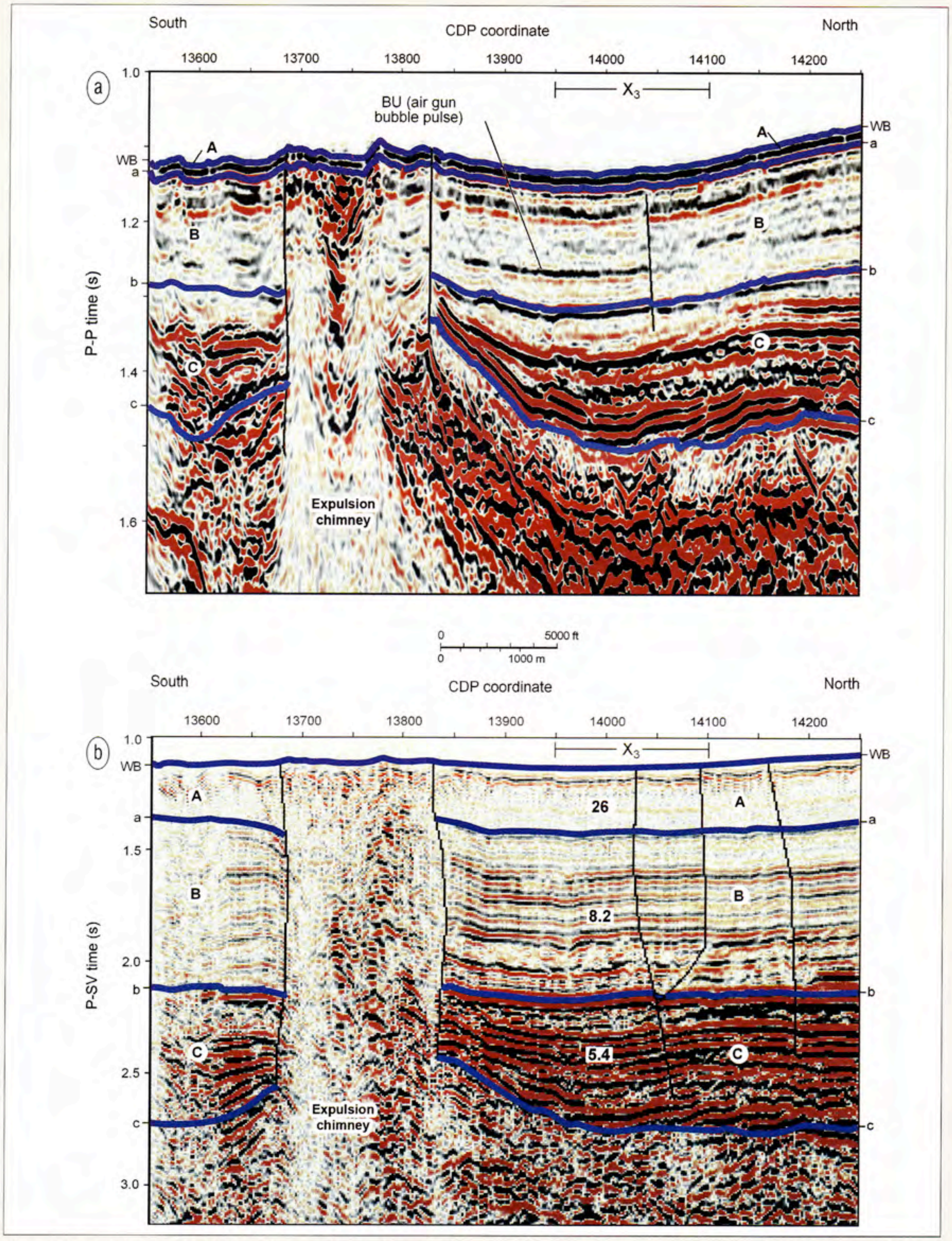

Figure 2. *Expanded views of (a) OBC P-P image and (b) P-SV image along profile 549, where the seismic line traverses a seafloor expulsion site in Green Canyon Block 204. Vertical lines on the images are interpreted faults. The deep expulsion chimney shown in Figure 1 is more obvious in these views. BU = air-gun bubble pulse, not a geologic interface. WB is the water bottom. A, B, and C are depth-equivalent units; a, b, and c are depth-equivalent horizons. The numbers labeled on the P-SV image (b) are representative* V_P/V_S *velocity ratios across interval* X_3.

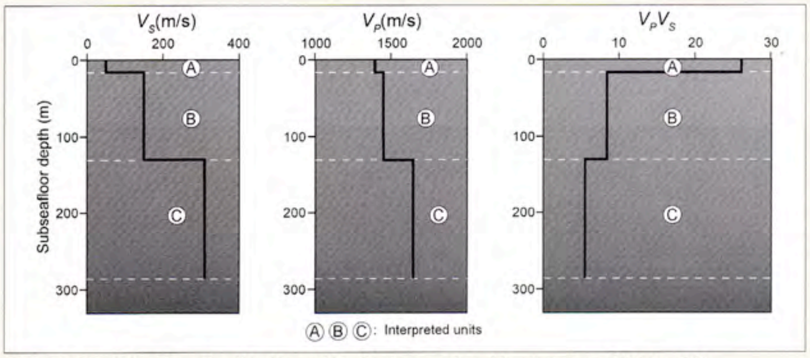

Figure 3. *Depth-based profile of* V_S, V_P, *and* V_P/V_S *from a selected location along OBC line 549.*

m are resolved; units thinner than 1 m are detected. In the data illustrated in this paper, we defined near-seafloor imaging depths by assuming compressional-wave propagation velocity (V_P) in these near-seafloor strata was a constant value of 1600 m/s. We find V_P is as low as 1350 m/s in some unconsolidated near-seafloor sediments along various OBC lines we are studying, but an assumed value of 1600 m/s will be used in this data comparison. Using this velocity assumption at the line coordinate where the 50-ms vertical scale bar is positioned on the AUV chirp image (Figure 1a), the base of the scale bar is 40 m below the seafloor. The 40-m vertical scale bars then placed on the OBC images indicate the intervals in low-frequency P-P image space (Figure 1b) and P-SV image space (Figure 1c) that correspond to the interval imaged by the high-frequency chirp-sonar data. The V_P/V_S velocity ratio measured from AUV and OBC data across the top 5–8 m of seafloor sediment ranged from 20 to 30 (and sometimes higher) along this profile, suggesting that shear-wave velocity V_S is less than 100 m/s immediately below the seafloor in several locations. The 40-m scale bar drawn on the P-SV image in Figure 1c is based on an assumed V_P/V_S ratio of 15 for the total interval. A hemipelagic layer 6–8 m thick has been defined by regional seafloor coring and is the first seafloor unit that drapes across this area. This hemipelagic layer is labeled HL on the chirp-sonar image (Figure 1a). In the AUV data, regional heterolithic turbidites that underlie this hemipelagic drape (again defined by seafloor coring) appear as the 10-ms-thick band of bolder reflections labeled TT that start about 10 ms below the seafloor. This thin turbidite interval cannot be seen in the OBC P-P image (Figure 1b) but appears as the first bold reflection below boundary WB in the P-SV image (Figure 1c).

These data examples show that in deepwater seafloor strata where the V_P/V_S velocity ratio is high (15 to 20), P-SV data acquired with OBC seismic technology using surface-positioned, low-frequency (10–100 Hz) air guns can image small-throw seafloor faults, meter-scale layering, and subtle near-seafloor stratigraphy almost as well as do high-frequency, kilohertz-range, chirp-sonar data collected using deep-running AUV systems.

Identifying gas-hydrate strata. Laboratory measurements have shown that V_P, V_S, and the V_P/V_S velocity ratio are petrophysical properties that help to discriminate lithofacies and rock types. In our work, these velocity attributes are applied to gas-hydrate systems. We analyzed P-P and P-SV data along OBC line 549 where the profile crossed a seafloor fluid/sediment expulsion chimney to determine seismic-based estimates of V_P, V_S, and V_P/V_S in units that form gas-hydrate systems associated with such expulsion features. Our interpretation of depth-equivalent geology on the P-P and P-SV images along this profile is illustrated in Figure 2.

Lowercase letters a, b, and c define depth-equivalent horizons in P-P and P-SV image space. WB is the water bottom, which is not imaged by these particular P-SV data. Uppercase letters A, B, and C define lithostratigraphic units that are depth-equivalent in P-P and P-SV image spaces. Defining depth-equivalent units in P-P and P-SV seismic images is challenging because, as a result of the differences in V_P/V_S velocity ratios from unit to unit, there are (x, y, z)-dependent disparities between P-P and P-SV traveltimes to specified depth coordinates. An illustration of a traveltime disparity to a common depth coordinate is the difference in P-P and P-SV image times spanned by the 40-m scale bar in Figure 1.

To define depth-equivalent geology in P-P and P-SV images, we searched for reflection patterns confirming that P-P and P-SV wavefields were imaging identical geologic conditions. An example of P-P and P-SV data imaging depth-equivalent geology is the series of low-frequency P-P and P-SV reflections that downlap onto and prograde across horizon c interpreted at the base of unit C (Figure 2). Once a depth registration such as this is defined, additional depth registrations above and below that point (such as the boundaries of units A and B) are made by considering vertical transitions in P-P and P-SV reflection patterns (P-P and P-SV seismic facies), using interval velocities to estimate unit thicknesses and, perhaps most importantly, using iterative ray tracing to adjust thicknesses of layered models of V_P and V_S velocities until ray trace arrival times of P-P and P-SV events match arrival times of real P-P and P-SV events in local common-receiver gathers. Numbers labeled on the P-SV image are the average V_P/V_S velocity ratio for each unit across interval X_3 (marked in Figure 2).

Typical depth-based profiles of interval values of V_S, V_P, and V_P/V_S observed along this OBC profile are illustrated in Figure 3. Subseafloor depths in this graph were estimated using seismic velocities and are accurate to probably ±20%. The shallowest unit (A) is about 15 m thick and has a high V_P/V_S ratio (24 and higher). By comparison, massive nodular gas hydrate has a V_P/V_S ratio of 1.9 to 2.0. We conclude unit A contains no gas hydrate. Although unit A is within the pressure-temperature regime for gas-hydrate stability, several reasons are plausible for a disparity between the top of the gas-hydrate stability zone in the sediment (i.e., the seafloor) and the top of the actual zone of gas-hydrate occurrence. First, methane hydrate can form only if the concentration of methane dissolved in pore fluid exceeds methane solubility in seawater and the methane flux exceeds a critical value representing the rate of methane transport by diffusion. These conditions may not exist in unit A. Second, it is possible that vertical advection of gas into unit A may be prevented by capillary sealing. Third, excess pore-water salinities and intrusions of warm loop currents and eddies across the seafloor of the Gulf of Mexico may dissociate gas hydrate in the shallowest seafloor sediments. Fourth, sulphate migrating downward from seawater reacts with upward-migrating methane to create hydrogen sulphide,

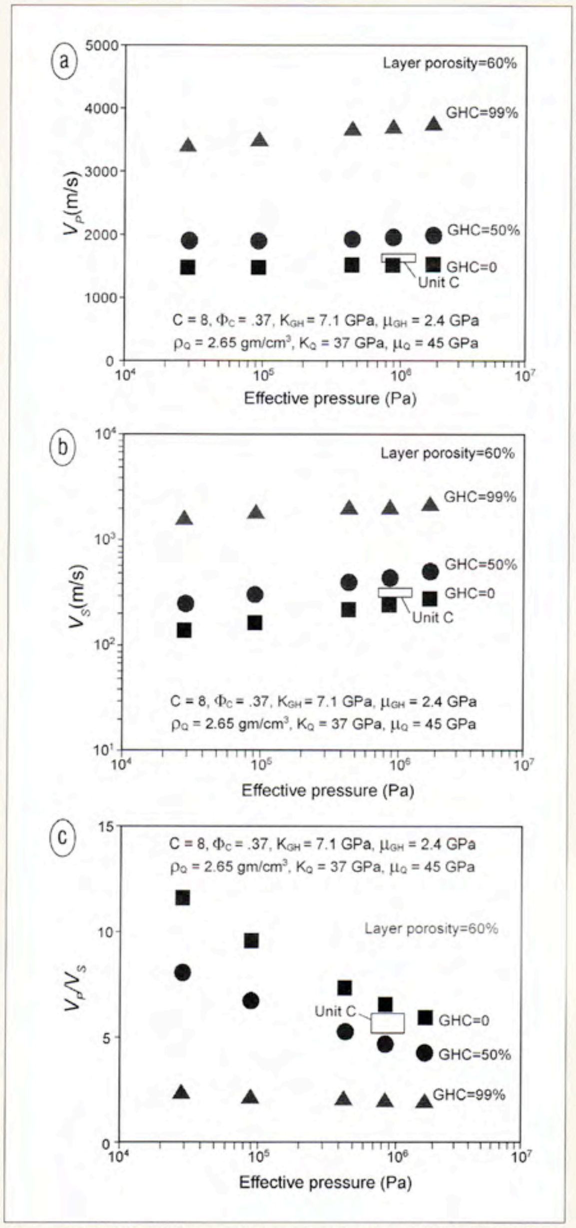

Figure 4. *Model calculations relating seismic estimates of* V_P, V_S, *and* V_P/V_S *to effective pressure and gas-hydrate concentration GHC for a sand-dominated facies. Model parameters are coordination number C, critical porosity* Φ_C, *bulk modulus K, shear modulus* μ, *and grain density* ρ. *Subscripts Q and GH indicate quartz and gas hydrate, respectively. Rectangular outline shows ranges of calculated effective pressure and seismic-measured* V_P, V_S, *and* V_P/V_S *across unit C defined in Figure 2.*

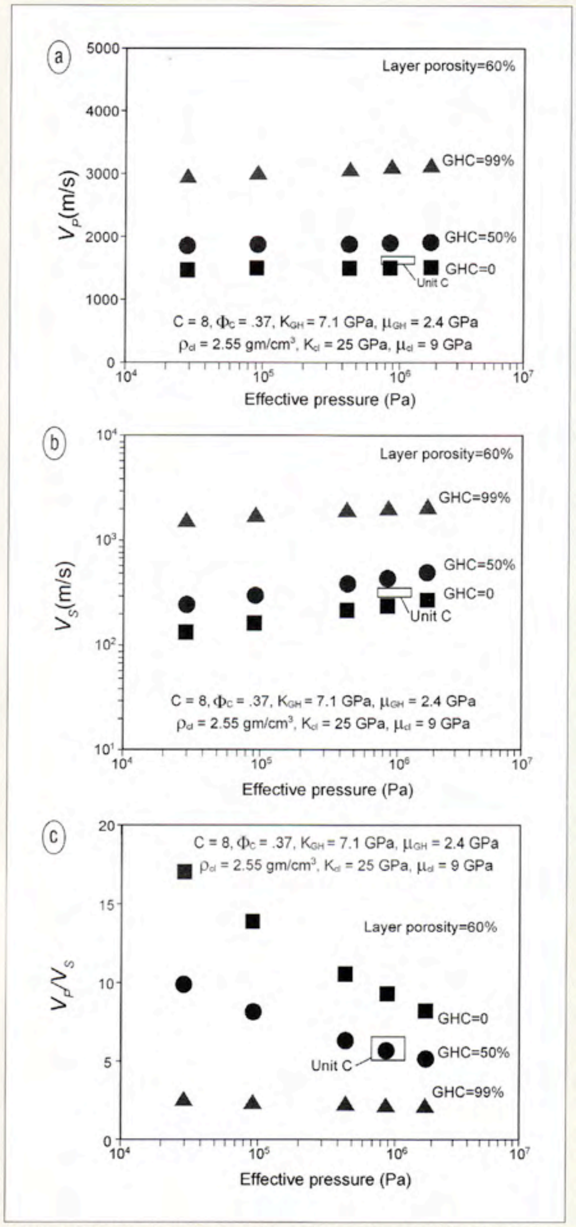

Figure 5. *Model calculations relating seismic estimates of* V_P, V_S, *and* V_P/V_S *to effective pressure and gas-hydrate concentration GHC for a clay-dominated facies. Model parameters and meaning of the rectangular outline are defined in the caption for Figure 4, with the exception that subscript Q (quartz) is now replaced with subscript cl (clay).*

water, and HCO_3. This chemical reaction prevents the formation of gas hydrate to a depth below the seafloor that is determined by the volume flux of the upward-migrating methane. The volume flux of methane at this study location is not known, thus the depth to which gas-hydrate formation is prohibited is unknown.

Below unit A, V_P and V_S increase and the V_P/V_S ratio decreases successively in units B and C, indicating increasing sediment rigidity with depth (Figure 3). We believe the increased rigidity in unit C is caused partially by concentrations of gas hydrate that are distributed throughout the unit as disseminated clathrates that partly fill pore spaces and either bear a part of the overburden weight or float freely in the pore space, or as alternating thin layers of hydrate-free sediment and hydrate-bearing sediment. Rock physics models for each of these morphological possibilities are summarized in the paper by Sava and Hardage in this issue. Core samples are needed to define how gas hydrate is distributed throughout its host sediment at this study site.

Estimating gas-hydrate concentrations. Our study of deepwater gas-hydrate systems has required us to develop effective-medium models of near-seafloor sediments that allow gas-hydrate concentrations to be estimated using seismic-based determinations of V_P, V_S, and V_P/V_S. Key rock-physics model parameters that affect the prediction of these velocity attributes for near-seafloor strata are gas-hydrate concentration (GHC) within available pore space, grain type (quartz or clay) of the host medium, coordination number C (average number of neighboring grains contacted by each grain of the medium at critical porosity), porosity of the medium, and effective pressure.

One effective-medium model used in this study assumes that gas hydrate is uniformly distributed throughout the pore space of a targeted seafloor unit and acts as a part of the load-bearing mechanism of the sedimentary column. Relationships between gas-hydrate concentration, effective pressure, V_P, V_S, and V_P/V_S predicted by this model are illustrated in Figures 4 and 5. The curves in Figure 4 assume that the seismic propagation medium is sand-dominated and has a porosity of 60%. The curves in Figure 5 assume that the medium is clay-dominated and has a porosity of 60%. The curves labeled GHC = 0, 50%, and 99% define velocity conditions that occur when 0, 50%, and 99% of the available pore volume is occupied by gas hydrate. When GHC is less than 100%, the remaining pore space is occupied by water.

The rectangular outlines define the range of effective pressure across unit C (Figure 2) and the ranges of seismic-based estimates of V_P, V_S, and V_P/V_S measured across that unit. Effective pressure was calculated by assuming a depth-dependent porosity behavior from the seafloor to the base of unit C and then assigning a grain density of 2.55 gm/cm^3 to the clay-dominated sediment deposited in this interval. The seismic-based velocity parameters (V_P, V_S, and V_P/V_S) measured across unit C implied the concentration of gas hydrate within the unit was commonly 10–20% if the interval was assumed to be sand-dominated (Figure 4). Occasionally the V_P/V_S ratio implied the hydrate concentration increased to about 40%. The same velocity attributes led to the conclusion hydrate concentration was slightly higher if the interval was clay-dominated (Figure 5).

Several assumptions are embedded in the seismic-based predictions of gas-hydrate concentration that are illustrated here. For example, if the porosity of unit C is less than the assumed value of 60% used in Figures 4 and 5, then the calculated curves of gas-hydrate concentration are displaced in each crossplot space in a direction that reduces the percentage of concentration in the seafloor sediments. The combination of lower porosity and lower gas-hydrate saturation within that porosity significantly affects estimates of gas-hydrate reserves.

Our purpose is not to claim we have made accurate predictions of gas-hydrate concentrations across this particular study area. Rather, our purposes are to describe a new seismic-based, 4-C OBC approach to evaluating deepwater gas-hydrate systems, to illustrate the tremendous resolution of near-seafloor geology that is provided by the P-SV mode of deepwater 4-C OBC seismic data, and to demonstrate how the combination of a calibrated effective-medium model and multicomponent seismic data allows gas-hydrate concentrations to be estimated over large deepwater areas. We believe that with appropriate calibration data, this methodology can produce estimates of hydrate resources that are reasonably accurate.

Technological impact. The investigative approach we illustrate here needs to be refined and applied at other deepwater gas-hydrate sites. Marine multicomponent seismic technology seems to be invaluable as a robust and remotely sensed source of data that can provide great detail about the internal architecture of deepwater gas-hydrate systems, geomechanical properties of deepwater seafloors, and deepwater, near-seafloor geology. Also, gas-hydrate-sensitive parameters, such as V_P, V_S, and V_P/V_S, can be extracted from P-P and P-SV data derived from 4-C seismic data, integrated into calibrated effective-medium models, and used to estimate gas-hydrate concentrations over large deepwater areas. These estimates should lead to better assessments of hydrate volumes in critical energy-dependent regions of the world.

Suggested reading. "Global estimates of hydrate-bound gas in marine sediments: How much is really out there?" by Milkov (*Marine Geology*, 2001). *Clathrate Hydrates of Natural Gases* by Dendy Sloan (Dekker Press, 1998). "Seismic evidence for gas hydrates in the North Makassar Basin, Indonesia" by Jackson (*Petroleum Geoscience*, 2004). "Acoustic imaging of gas hydrates and free gas at the Storegga slide" by Bunz and Mienert (*Journal of Geophysical Research*, 2004).

Acknowledgments: Seismic data were provided by WesternGeco. Background data on the study site, including direct observations and sampling using a manned submersible, were provided by the Minerals Management Service (Contract No. 1435-01-99-CA-30951) and the Hydrates Research Consortium at the University of Mississippi (DOE NETL Contract DE-FC26-02NT41628). Research funding has been partially provided by DOE NETL Contract DE-PS26-05NT42405.

Corresponding author: bob.hardage@beg.utexas.edu

APPENDIX E

GAS HYDRATE IN THE GULF OF MEXICO: WHAT AND WHERE IS THE SEISMIC TARGET?

Gas hydrate in the Gulf of Mexico: What and where is the seismic target?

Bob A. Hardage, Bureau of Economic Geology, Austin, USA
Harry H. Roberts, Louisiana State University, Baton Rouge, USA

Seismic technology will be of key importance for evaluating gas-hydrate resources, particularly across the Gulf of Mexico (GoM) where many seismic surveys have been acquired and will continue to be acquired. To apply seismic technology to gas-hydrate studies in the gulf in an optimal manner, it is essential to understand the seismic target that has to be analyzed.

What is gas hydrate? Gas hydrate is an ice-like crystalline material consisting of structured water molecules linked to form an assembly of cages (or clathrates). Each cage (clathrate) can enclose and trap a gas molecule. The terms *clathrate hydrate* and *gas clathrate* are accurate for describing this ice-like substance, but the term *gas hydrate* is more widely used across the oil and gas industry. Clathrates are observed to grow with water molecules arranged in one of three lattice-forming geometries known as structure I, structure II, and structure H (Figure 1). The arrangement of water molecules forming each structure creates specific cavity geometries, or individual cages. These cage geometries are identified beside each lattice configuration in Figure 1. Each hydrate structure shown in this figure is described as a unit structure (Sloan, 2003), which is the smallest repeating structural element involved in hydrate growth. Each unit structure consists of a specific number of cavity types that are defined in the diagrams.

Clathrate cavities have radii that range from a little less than 4 angstroms to almost 6 angstroms (1 angstrom = 10^{-8} cm). A variety of gas molecules can be trapped inside these cages, with possibilities being methane (CH_4), ethane (C_2H_6), propane (C_3H_8), butane (C_4H_{10}), nitrogen (N_2), carbon dioxide (CO_2), and hydrogen sulfide (H_2S). In Gulf of Mexico gas-hydrate systems, the most common entrapped gas appears to be methane. Models of a methane molecule and a configuration of structure I clathrate lattices are shown side by side in Figure 2 at correct relative scales to show a methane molecule is slightly larger than the openings in structure I lattice faces. Once a methane molecule is encaged in one of the clathrates, it is trapped until the lattice structure is destroyed. Figure 3 shows a structure I assembly of clathrates entrapping several methane molecules.

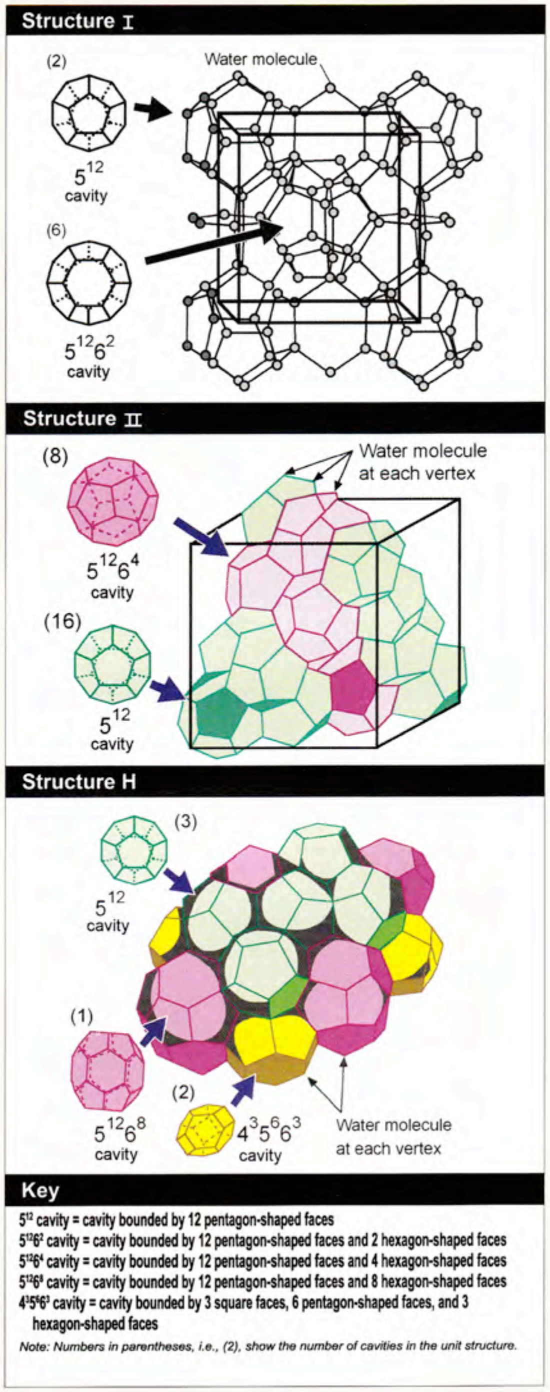

5^{12} cavity = cavity bounded by 12 pentagon-shaped faces
$5^{12}6^2$ cavity = cavity bounded by 12 pentagon-shaped faces and 2 hexagon-shaped faces
$5^{12}6^4$ cavity = cavity bounded by 12 pentagon-shaped faces and 4 hexagon-shaped faces
$5^{12}6^8$ cavity = cavity bounded by 12 pentagon-shaped faces and 8 hexagon-shaped faces
$4^3 5^6 6^3$ cavity = cavity bounded by 3 square faces, 6 pentagon-shaped faces, and 3 hexagon-shaped faces

Note: Numbers in parentheses, i.e., (2), show the number of cavities in the unit structure.

Figure 1. *Clathrate structures of gas hydrate. Structure I (top): Body-centered cubic structure of 5^{12} cavities linked at their vertices. This unit volume has eight cavities (eight possible gas molecules) and 46 water molecules. The host molecule is smaller than propane. Structure II (center): Diamond lattice within a cubic framework with 5^{12} cavities linked at their faces. This unit volume has 24 cavities (24 possible gas molecules) and 136 water molecules. The host molecule is larger than ethane but smaller than pentane. Structure H (bottom): Hexagonal structure with layers of 5^{12} cavities connecting layers of $5^{12}6^8$ and $4^3 5^6 6^3$ cavities. This unit volume has six cavities (six possible gas molecules) and 34 water molecules. The host molecule is a wide range of sizes. The cavity diagrams are views looking down on a cavity with solid lines showing face edges on the top half of the cavity and dotted lines showing face edges on the bottom half. These hydrate diagrams depict unit volumes, the smallest repeating structural elements of hydrate growth. The cluster of cavities in the structure II diagram shows only 12 of the 24 cavities needed for a structure II unit volume. The cluster in the structure H diagram is larger than a six-cavity structure H unit volume. The distributions of the colored cavities are suggestive, not precise (after Sloan, 1998).*

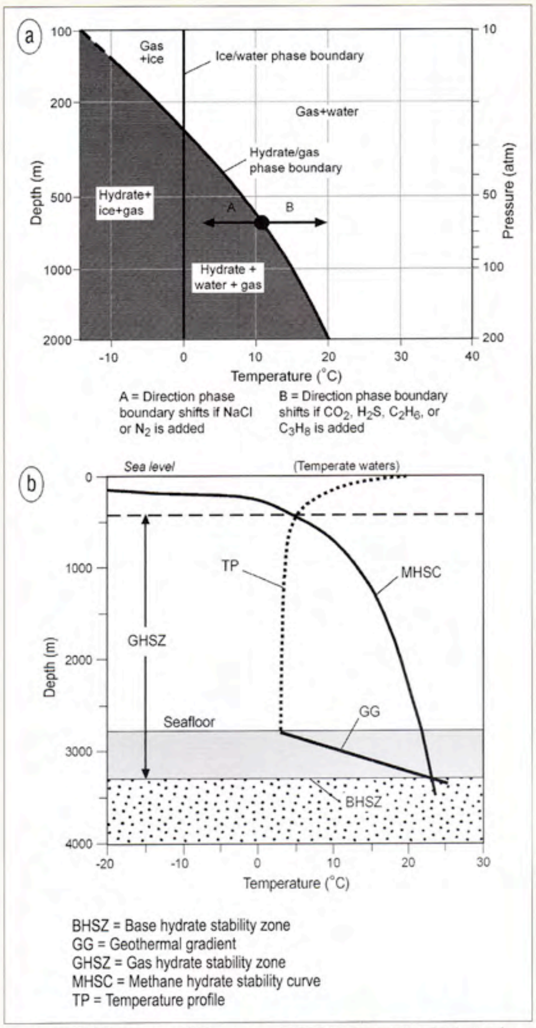

Figure 4. *(a) Pressure and temperature domains separating hydrate phase from gas phase and separating ice phase from water phase. (b) Depth (pressure) and temperature domains defining methane hydrate stability in temperate waters (after Kvenvolden, 1998).*

is bounded by the seafloor and the base hydrate stability zone. Usually a gas-hydrate target is restricted to an even thinner subseafloor layer because, in many locations, gas hydrate is absent across an interval extending from the seafloor to a subseafloor depth of a few tens of meters. Several processes combine to eliminate gas hydrate from this near-seafloor region. The solubility of methane in seawater just described is one factor. A second factor is water salinity. As water salinity increases, geochemistry studies show the hydrate stability curves in Figure 4 move to the left in their pressure-temperature crossplot domain (arrow A in Figure 4a). This movement to lower temperature stability means some seafloor temperatures that once sustained gas hydrate at lower salinity can no longer do so at higher salinity. Hydrate exposed to equivalent temperatures in higher-salinity media will dissociate. Any local increase in salinity, such as proximity to a salt structure or to a fluid-expulsion chimney that brings deep, high-salinity water to the seafloor, can cause some amount of gas hydrate to dissociate near the seafloor.

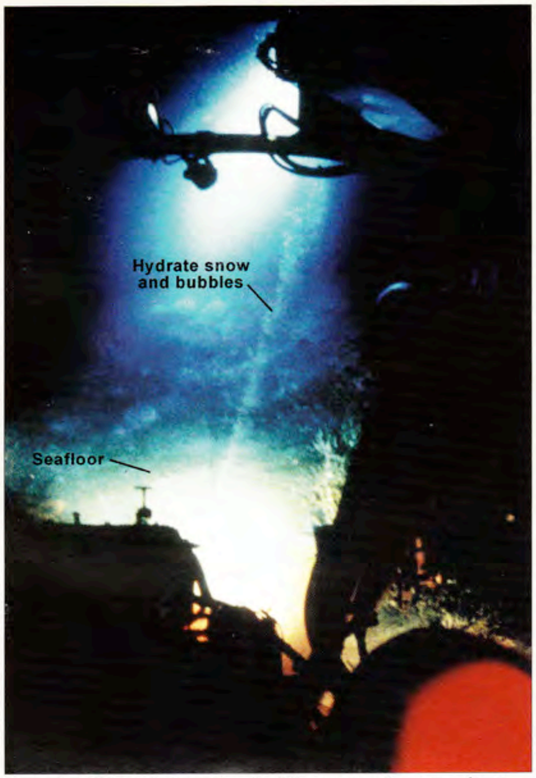

Figure 5. *Gas-hydrate "snow" and bubbles entering the water column from a small seafloor vent in Green Canyon Block 232. This photograph was taken by an LSU/MMS researcher riding in the forward sphere of a* Johnson-Sea-Link *submersible.*

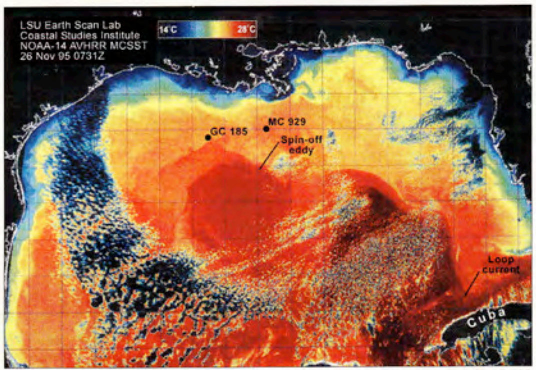

Figure 6. *Satellite image showing sea surface temperature across the Gulf of Mexico in late November 1995. The warm Loop Current and one of its spin-off eddies are labeled. Sites GC 185 and MC 929 were equipped with seafloor instrumentation to record the effects of thermal impacts on gas hydrates exposed on the seafloor (image courtesy of Coastal Studies Institute's Earth Scan Laboratory, Louisiana State University).*

A third factor unique to the GoM is that warm eddies can spin off the Loop Current that passes between Cuba and Florida and circulate across a large part of the gulf (Figure 6). These eddies affect water temperature to depths of about

1000 m. Depending on water depth, some eddies can raise seafloor temperature across a gas-hydrate system as much as 4° C for a period of time. This temperature change is sufficient to dissociate gas hydrate for several meters below the seafloor. Warm eddies are known to dwell as long as a month at any given location across the northern shelf of the GoM. Long residence times of these eddies atop hydrate systems have unknown effects on the volume of hydrate that is dissociated and on the subseafloor depth to which that dissociation occurs.

A fourth factor, perhaps the most important, is sulfate reduction of gas hydrate. Sulfate in seawater migrates down through seafloor sediment and interacts with upward-migrating methane to create hydrogen sulfide, water, and HCO_3. The chemical reaction

$$CH_4 + SO_4 \rightarrow HCO_3 + HS + H_2O \qquad (1)$$

prevents the formation of gas hydrate to a subseafloor depth that depends on the volume flux of upward moving methane (Figure 7). If methane flux is large, sulfate reduction eliminates gas hydrate to only a shallow depth. If methane flux is small, the depth to which sulfate reduction can prevent gas-hydrate formation can be significant (arrow A of Figure 7).

The end result of this is that the likely position of a Gulf of Mexico gas-hydrate seismic target is limited to an interval that starts several tens of meters below the seafloor.

Hydrate/sediment grain-to-grain morphology. The next challenge is to decide how gas hydrate is distributed throughout its seismic target space. Efforts to understand how hydrate clathrates and host-sediment grains mix and interact are the subject of ongoing research. Likely numerous grain-to-grain morphologies, such as the following, occur in some gas-hydrate systems:

- uniform hydrate dissemination throughout available pore space
- alternating layers of hydrate-rich and hydrate-free sediments
- load-bearing clathrates
- thin sheets of hydrate filling laminae and fracture voids

Each of these grain-to-grain morphologies requires a different rock physics model to relate volume concentration of gas hydrate in deepwater sediment to seismic attributes. The best (and only?) way to determine how hydrate is distributed throughout its host sediment is to acquire seafloor cores across gas-hydrate accumulations at numerous sites and measure the spatial configurations and percentages of hydrate, mineral grains, porosity, and pore fluid with accurate laboratory techniques. The need to use core to develop appropriate rock physics models for deepwater gas-hydrate systems is no different from using core to calibrate seismic and wireline-log responses with rock/fluid properties of oil and gas reservoirs. A current barrier to rapid progress in rock physics modeling of gas-hydrate targets is lack of appropriate seafloor core data and core analyses. Until such calibration data are available, hydrate/sediment grain-to-grain morphologies within these gas-hydrate systems will be speculative.

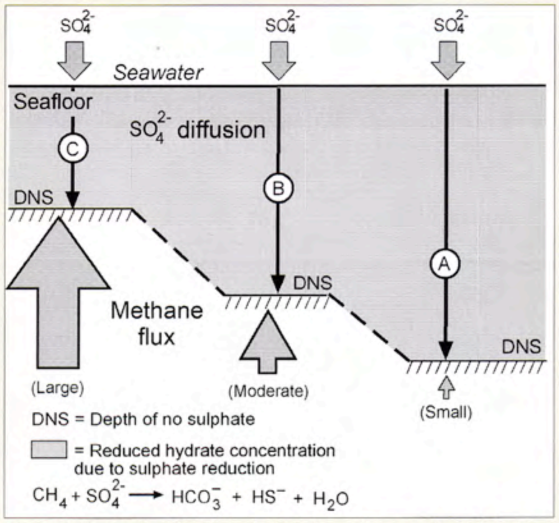

Figure 7. Prevention of methane hydrate formation near the seafloor by sulfate reduction. The depth to which hydrate formation is constrained by downward moving sulfate depends on the magnitude of methane flux moving upward toward the seafloor (after Borowski et al., 1996).

Subseafloor structure and seafloor reflectivity. Particular subseafloor structural features and unique P-wave seafloor reflectivity behaviors seem to be genetically related to gas-hydrate accumulations across the northern shelf of the GoM. Recognizing these hydrate-target indicators helps identify where potential gas hydrate should be positioned in seismic image space. Each target indicator (subseafloor structure and seafloor reflectivity) has a genetic relationship to the type of methane source that created the methane entrapped by hydrate clathrates.

In terms of methane origin, methane that migrates into a gas-hydrate stability zone (Figure 4) can be produced by (1) deep thermal alteration of hydrocarbon source rock, or (2) biogenic action of carbon-consuming microbes. Both thermogenic and biogenic sources of methane occur across the GoM and probably in all deepwater and cold-water areas that overlay commercial deposits of hydrocarbons. Along continental margins that do not have commercial accumulations of hydrocarbons, methane entrapped as gas hydrate is produced dominantly by biogenic processes.

Target indicator 1: Subseafloor structure. Numerous vertical fluid-flow paths extend from considerable depths and reach the seafloor across the northern Gulf of Mexico. Some

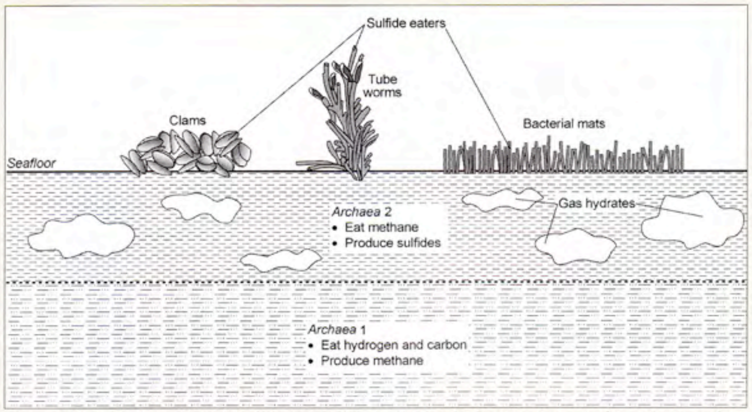

Figure 8. *Symbionic communities associated with marine gas-hydrate systems.* Archaea *1 eats carbon and produces methane. Some of this methane forms gas hydrate; some serves as the food source for* Archaea 2. Archaea 2 *eats methane and produces sulfide. Methane and sulfide support large chemosynthetic seafloor communities. Microbe-generated carbonate hardgrounds and thick layers of mussel shells create local seafloor seismic bright spots, leading to the conclusion that bright seafloor reflectivity is indirect evidence of gas hydrate (after Kunzig, 2004).*

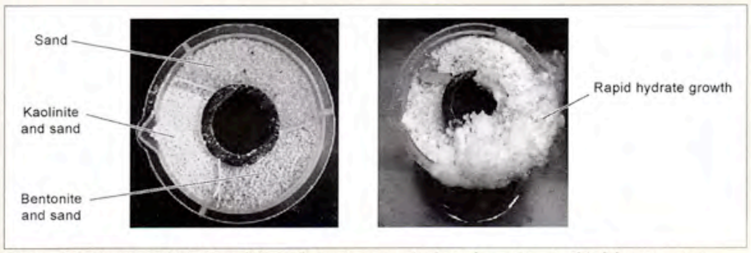

Figure 9. *Influence of GoM-based biosurfactants on gas-hydrate formation. In this laboratory test, surfactant produced by* Bacillus subtilis, *a microbe found in many of the area gas-hydrate systems, causes gas hydrate to preferentially form on bentonite grains rather than on sand or kaolinite grains (courtesy of Rudy Rogers, Swalm School of Chemical Engineering, Mississippi State University).*

of these vertical conduits are fault planes; some are fluid/gas expulsion chimneys. Each type of fluid-flow feature allows deep thermogenic methane to migrate upward and enter the gas-hydrate stability zone where it becomes entrapped in hydrate cages. Many of these vertically oriented faults and gas chimneys are detectable with conventional towed-cable marine seismic data. If such subseafloor structural features are observed in water depths that sustain gas hydrate, there is a good possibility a gas-hydrate accumulation is genetically related to the fault and/or chimney.

Target indicator 2: Seafloor reflectivity. Two types of *Archaea* microbes are abundant in seafloor sediment. One, identified as *Archaea* 1 in Figure 8, consumes carbon from the abundant carbon compounds existing in seafloor sediment and produces methane. These microbes are the source of most of the methane entrapped in gas hydrate along continental margins where there is minimal thermal generation of deep gas. They are also responsible for a portion of the methane confined in gas hydrate across prolific gas-producing areas of the GoM. The second family of microbes, labeled *Archaea* 2, eats methane and produces sulfides. The methane needed by *Archaea* 2 can be provided by deep thermogenic methane sources or by methane produced by *Archaea* 1.

Numerous seafloor organisms thrive on methane and sulfide produced by *Archaea* 1 and 2, such as mussels, clams, tube worms, and bacterial mats (Figure 8). Mussels consume methane; clams consume hydrogen sulfide. Another byproduct of microbial activity is Ca/Mg carbonate precipitated in surficial sediments. These carbonates form "hardgrounds" on the seafloor which cause large increases in the seafloor reflection coefficient. Thick layers of mussel shells stacked on methane-rich sediment also produce large increases in seafloor reflectivity; thus, robust increases in seafloor reflection amplitudes, when observed at water depths appropriate for gas-hydrate stability, are valuable indicators of upwelling sulfide-producing methane, which in turn, implies the presence of subseafloor gas hydrate. The Minerals Management Service and Louisiana State University have a long-running program of mapping areas of high-amplitude seafloor reflections and conducting deep dives in each location. These dives define seafloor conditions that create each high-amplitude seismic response and confirm the presence or absence of gas hydrate across the reflection anomalies. Their work is showing a high correlation between bright, deepwater seafloor reflectivity and presence of gas hydrate.

What is the host medium for gas hydrate? To produce methane from gas hydrate as a commercial venture, gas hydrate needs to be embedded in a host medium that has high porosity for volumetric storage of methane and high permeability for deliverability requirements. A high-porosity, unconsolidated sand would be an ideal host medium. So then, what type of sediment does gas hydrate prefer as a host? This is a question that is not yet satisfactorily answered; however, Rudy Rogers at Mississippi State University has done some interesting experiments with Gulf sediments and microbial communities that warrant consideration. One of his experimental tests is shown in Figure 9.

In this experiment, three typical Gulf of Mexico seafloor sediments, sand, kaolinite/sand mix, and bentonite/sand mix, were placed in segregated compartments of a test cell. These sediments were then saturated with surfactin produced by *Bacillus subtilis*, a microbe common to gas-hydrate systems across the GoM. A blend of 90% methane, 6% ethane, and 4% propane was introduced into the sediment, and the test cell was subjected to pressure and temperature typical of gas-hydrate stability zones in the GoM. The photo in Figure 9 shows prolific and rapid growth of gas hydrate on bentonite surfaces and minor growth on sand and kaolinite surfaces. The implication is surfactin produced by *Bacillus subtilis* encourages methane and structured water to preferentially congregate and nucleate at common sites on the surfaces of bentonite grains, not on sand grains or kaolinite grains. Gas hydrate in the GoM may thus be more prone to accumulate in fine-grained sediment than in coarse-grained sediment. Determining what type of sediment is the preferred host medium for gas hydrate in this area requires more research.

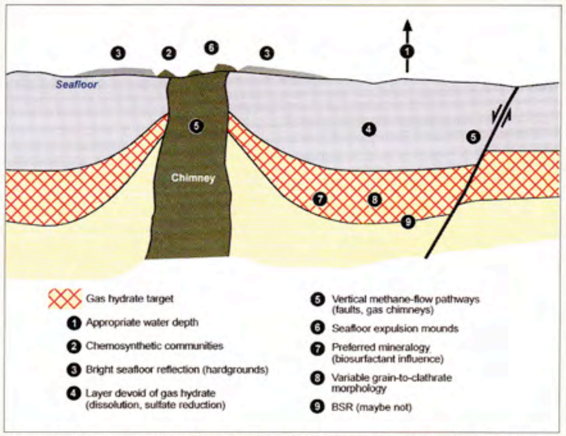

Figure 10. *Seismic identifiers and geologic characteristics of many Gulf of Mexico gas-hydrate seismic targets. Note the distortion of the seismic target in the vicinity of the vertical fluid-expulsion chimney where there is a local alteration of geothermal gradient.*

Based on the evidence of tests such as those done by Rogers, some gas-hydrate researchers consider dirty sand an ideal host medium for gas hydrate. In dirty sand, bacterial surfactin encourages hydrate growth on the clay components, and the sand component provides the desired permeability.

Bottom-simulating reflections. Bottom-simulating reflections (BSRs) are classic seismic identifiers of gas-hydrate accumulations in marine environments. In many gas-hydrate locations, BSRs are bold, obvious events that are easily seen and interpreted in stacked/migrated seismic data. In contrast, BSRs across GoM gas-hydrate systems are subtle, discontinuous, and sometimes just not detectable. Investigators are now documenting more BSR events across the gulf than were previously known, but robust BSRs that extend for great distances, as occurs in some gas-hydrate provinces, are rare. Because of the less-dominant role of BSRs in this area, gas-hydrate target indicators previously mentioned (vertical conduits for fluid flow and bright seafloor reflections at appropriate water depths) are presently the preferred seismic evidence for identifying prime locations for gas hydrate in the GoM. No doubt BSRs will increase in importance as hydrate target indicators as our knowledge of hydrate systems increases and as the study areas expand.

Conclusions. The diagram in Figure 10 brings all of these observations together to create a generalized model of many gas-hydrate systems across the northern shelf of the GoM. The most likely location of a gas-hydrate seismic target relative to the seafloor is identified by the cross-hatched interval. The nine labeled features define important identifiers and characteristics expected to be present for many hydrate targets in this area. The more identifiers that can be recognized at a site, the more likely gas hydrate will be present at that location. We make no claim that these identifiers are associated with gas hydrate in any deepwater environment other than the northern shelf of the GoM.

Identifying and characterizing gas-hydrate accumulations across the GoM will be challenging. Seismic technology will be a key tool in these efforts. The information presented here provides partial answers to the question, "What and where are gas-hydrate seismic targets in the Gulf of Mexico?" and may assist future gas-hydrate investigations.

Not only will such investigations be important for evaluating and quantifying gas-hydrate resources, but they also need to be done to determine if there is a genetic link between gas-hydrate accumulations and shallow water flows that plague deepwater drilling. Shallow water flows are high volume flows of freshwater from intervals that are shallow relative to the seafloor, but the seafloor itself is in water depths capable of sustaining gas hydrate. Once initiated, these intense water flows are capable of destroying drilling or producing wells and eroding the seabed away from seafloor-based facilities. If a well bore penetrates an interval containing gas hydrate, warm drilling mud in exploration wells or deep, hot hydrocarbons passing through production wells can raise the temperature of the interval and cause gas hydrate to dissociate. This dissociation can produce large volumes of freshwater if hydrate concentration is high. There is growing evidence that dissociated gas hydrate is one cause of shallow water flow.

Suggested reading. *Clathrate Hydrates of Natural Gases* by Sloan (Marcel Dekker, 1998). " Introduction, physical properties, and occurrence" by Pellenbarg and Max (in *Natural Gas Hydrate in Oceanic and Permafrost Environments*, Kluwer Academic Publishers, 2003). "A primer on the geological occurrence of gas hydrates" by Kvenvolden (in *Gas hydrates: relevance to world margin stability and climatic change*, Geological Society Special Publication No. 137, 1998). "20 000 microbes under the sea" by Kunzig (*Discover*, 2004). TLE

Acknowledgments: Funding for gas-hydrate research is provided to the authors via DOE NETL Contract DE-PS26-05NT42405 and MMS Contract 1435-01-99-CA-30951.

Corresponding author: bob.hardage@beg.utexas.edu

APPENDIX F

GAS HYDRATE—A SOURCE OF SHALLOW WATER FLOW?

Gas hydrate—a source of shallow water flow?

BOB A. HARDAGE and RANDY REMINGTON, Bureau of Economic Geology, University of Texas at Austin, USA
HARRY H. ROBERTS, Louisiana State University, Baton Rouge, USA

Shallow water flow is a serious drilling hazard encountered across several areas of the Gulf of Mexico (GoM). Numerous incidents have occurred in which intense shallow water flows have disrupted drilling, added millions of dollars to the cost of a well, or caused a well to be abandoned. In one survey of 74 offshore wells, Alberty and colleagues found only 34% of the wells did not encounter problems related to shallow water flow. In separate writings, Holm and Alberty stated that steps taken to prevent or remediate shallow water flow add at least $2 million to the cost of a well.

One interesting aspect of shallow water flow is that a high production rate of water tends to start long after the drill bit has passed the interval where flow originates, implying that a time-delay factor is involved in the genesis of the water production. In one instance, shallow water flow did not initiate beneath a multiwell seafloor template until several strings of 36-in and 30-in casing had been set to depths of several hundred feet below mud line in a batch-drilling approach. Resulting seafloor erosion then caused major damage to the template and its wells. Furlow reported that 10 of 21 well slots were lost in this incident because of severe casing buckling. In short, shallow water flow is a major factor in drilling safety, marine environmental impact, and drilling costs across the GoM, with a time-delay factor usually involved that as one drilling supervisor said "never allows you to be sure the problem is solved."

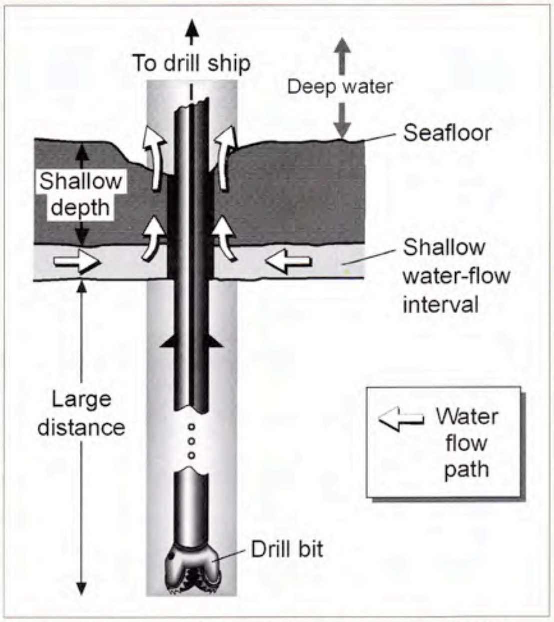

Figure 1. Shallow water flow occurs in deep waters of the Gulf of Mexico at shallow subseafloor depths. Flow often commences long after the flow interval has been penetrated and the drill bit is at a deep depth or even after the well has been placed in production. Flow is outside the outer structural casing and its cement.

Defining "shallow." The term *shallow* used to describe these destructive water flows is somewhat misleading but seems to be fixed terminology. The phenomenon originates in strata that are in water depths of 500 m or more in the GoM, but the water-flow interval is relatively close to the seafloor. Thus the adjective *shallow* in shallow water flow describes the depth where the water flow occurs below the seafloor, not the depth of water at the drill site (Figure 1). A common definition of shallow water flow found in engineering papers is "water flowing on the outside of structural casing to the ocean floor," which is the flow path shown in this figure.

The freshwater conundrum. Since becoming involved in gas-hydrate research, we have had the opportunity to discuss shallow water flow with people who have had to deal with the problem. During these conversations, we have frequently asked the question, "What is the salinity of the water produced by shallow water flow; is it freshwater?" A common answer has been "It's freshwater." The only other reply has been "I don't know." We should exercise caution and not conclude that all shallow water flow involves freshwater, but judging from this modest survey, freshwater is produced in numerous shallow water flows.

The observation that shallow water flow can produce freshwater leads to a puzzling question: "How does freshwater come to be near the seafloor in deepwater areas of the Gulf of Mexico?" Sediment deposited in an offshore basin would ordinarily have connate water with a salt content equal to or greater than the salinity of seawater. To explain this puzzle, some investigators have proposed that rapid and massive fluvial deposition can entrap and transport freshwater into some offshore environments, which may be true in some unique situations. A second group envisions complex freshwater aquifer systems extending from onshore to offshore. This option is not generally accepted by experienced Gulf of Mexico explorationists. Others wonder whether gas hydrate is somehow involved because shallow water flow appears to occur only in water depths and across subseafloor intervals appropriate for hydrate stability. We lean toward this latter hypothesis—that there is a genetic link between deepwater hydrate and some shallow water flows.

Gas hydrate and freshwater. The smallest repeating unit volumes of hydrate structures I, II, and H are shown in Figure 1 of another Special Section paper, "Gas hydrate in the Gulf of Mexico: What and where is the seismic target?" The unit volume of structure I has eight cavities (eight possible gas molecules) and 46 water molecules; structure II's unit volume has 24 cavities (24 possible gas molecules) and 136 water molecules; and the unit volume of structure H has six cavities (six possible gas molecules) and 34 water molecules. Comparing the number of cavities and the number of H_2O molecules defined in the diagrams, one can see that, on average, there are 5.7 molecules of H_2O per cavity in each hydrate structure. In other words, there are more than five molecules of H_2O for each possible molecule of gas. Gas hydrate thus has a great deal of freshwater trapped in its crystalline structure. If this hydrate crystalline structure dissociates, freed H_2O molecules can become a significant source of freshwater.

The dissociation process. For hydrate to dissociate, its crystalline structure must be exposed to an altered environment having increased temperature, or reduced confining pressure, or both. One explanation for a dissociation process that could initiate shallow water flow in deepwater Gulf of Mexico wells is an increase in temperature within a hydrate interval penetrated by a well bore. During drilling, warm circulating drill mud can, over time, raise formation temperature within a hydrate zone and initiate dissociation. During production, warm fluids produced from deep reservoirs can also raise the temperature of a hydrate-bearing interval as fluids flow to the surface. In some instances, the time required for either process to raise the formation temperature to the point of hydrate dissociation may be rather long, explaining why shallow water flow often does not initiate until the drill bit has progressed far beyond the shallow subseafloor depth where flow originates, or until additional wells have been drilled and several warm, closely spaced well bores have sufficient time to affect shallow formation temperatures.

Conclusion. Shallow water flow is not confined to the GoM where we do our hydrate research. Shallow water flow has been reported in wells drilled offshore West Africa, west of Shetland, Borneo, southeast Asia waters, the Norwegian Sea, the North Sea, and the southern Caspian Sea. In the Gulf of Mexico, the Deep Star Drilling and Completions Committee has identified shallow water flow as "one of the most imposing problems encountered in deepwater drilling" (see Snyder). This same conclusion probably applies to the other deepwater areas just named.

Some descriptions of the destructive force of shallow water flow are spectacular. One ROV video showed a plume of sand and debris jetting 60 ft above the seafloor, a true "over the derrick" blowout (see Furlow). Alberty and colleagues described a seafloor fissure extending 300 ft from the well head with a vertical displacement of 7 ft between opposing walls of the trench. Furlow reported an incident where seafloor erosion produced gullylike features large enough for a ROV to enter and traverse the length of the chasm and another where a cementing job had to fill an open hole that had enlarged to an average diameter of 50 in.

Almost all papers in engineering journals and conferences ascribe the source of shallow water flow to overpressured sands. This conclusion is based on hard engineering data amassed over many problem wells. However, these papers do not mention the salinity of the produced water, and therein lies the issue. Is the water produced by shallow water flow fresh (as numerous colleagues have told us), or does its salt content equal or exceed the salinity of seawater? If the water is salty, connate water in shallow overpressured sand is a logical model for the genesis of the shallow water flow. If the water is fresh, then hydrate somehow has to be involved.

The concept discussed here, that there is a genetic link between deepwater gas hydrate and some shallow water flow, is a hypothesis, not a proven fact. The connection seems logical and adds importance and urgency to gas-hydrate research. The possibility introduces a new work area for geoscientists and causes deepwater geophysical imaging and facies-detection technologies to become invaluable to engineers who have to avoid shallow-water-flow complications as they plan and execute drilling and production programs.

Much of the information related to shallow water flow is anecdotal. Some of this unpublished information needs to be made available to gas-hydrate researchers so that the idea proposed here can be investigated on a case-by-case basis. If a shallow water flow incident involves confidential data that cannot be shared with one of the numerous gas-hydrate research efforts now under way in several countries, the operator of the shallow water flow well needs to do an internal postmortem analysis to determine whether there is a plausible link between the shallow water flow and dissociated gas hydrate. A common thread in any of these investigations would be to determine the salinity of the produced water so that a link between shallow water flow and deepwater hydrate can be discounted or supported.

A point worthy of emphasis is that any effort to dissociate methane and other gases from gas hydrate for commercial purposes will involve large volumes of produced water. Managing this produced water will be an important factor in deciding the economic feasibility of methane hydrate production. In some instances, the production of this much water may turn out to be positive because the water is pristine freshwater. In some areas of the world, a prolific supply of freshwater can be valuable.

Suggested reading. Many papers discussing shallow water flow can be found in *Offshore* published by PennWell. "Cost analysis of SWF preventative, remedial measures in deepwater drilling" by Alberty (*Offshore*, 2000). "How one of the biggest fields in the U.S. Gulf almost got away" by Furlow (*Offshore*, 1999). "Shallow water flows: how they develop; what to do about them" by Furlow (*Offshore*, 1998). "Controlling shallow water flows in deepwater drilling" by Holm (*Offshore*, 1998). *World Oil* also has some informative articles. "Industry zeroes in on shallow water flow problems/solutions" by Snyder (*World Oil*, 1997). Numerous papers presented at the Offshore Technology Conference describe experiences with shallow water flow. "Mechanisms of shallow waterflows and drilling practices for intervention" by Alberty et al. (OTC proceedings, 1997). We depended on Sloan's book, *Clathrate Hydrates of Natural Gases* (Dekker Press, 1998) to help us envision the physical architecture of hydrate structures. In addition, the July 2002 issue of *TLE* has several good articles on the topic of shallow water flow. TLE

Corresponding author: bob.hardage@beg.utexas.edu